REMOTE SENSING OF IONOSPHERIC EFFECTS ASSOCIATED WITH LIGHTNING USING VERY LOW FREQUENCY RADIO SIGNALS

A DISSERTATION

SUBMITTED TO THE DEPARTMENT OF ELECTRICAL

ENGINEERING AND THE COMMITTEE ON GRADUATE STUDIES

OF STANFORD UNIVERSITY

IN PARTIAL FULFILLMENT OF THE REQUIREMENTS

FOR THE DEGREE OF

DOCTOR OF PHILOSOPHY

By

Thomas George Wolf

January 1990

I certify that I have read this dissertation and that in my opinion it is fully adequate, in scope and quality, as a dissertation for the degree of Doctor of Philosophy.

Umran S. Inan (Principal Advisor)

I certify that I have read this dissertation and that in my opinion it is fully adequate, in scope and quality, as a dissertation for the degree of Doctor of Philosophy.

Robert A. Helliwell

I certify that I have read this dissertation and that in my opinion it is fully adequate, in scope and quality, as a dissertation for the degree of Doctor of Philosophy.

Gene F. Franklin

Approved for the University Committee on Graduate Studies:

Dean of Graduate Studies

Abstract

A comprehensive investigation of the Trimpi effect has revealed a number of important new properties of this phenomenon. The Trimpi effect consists of transient perturbations, caused by lightning, in the amplitude or phase of VLF (3 - 30 kHz) and LF (30 - 300 kHz) radio signals propagating in the earth - ionosphere waveguide. This research involved the design and development of a new, fast responding, phase sensitive, VLF receiver and the deployment of this receiver at several sites to collect an extensive set of data on the Trimpi effect. This data set consists of simultaneous amplitude and phase measurements on four different signal paths to Stanford University, and four signal paths to Palmer Station, Antarctica.

The new properties that were identified can be summarized as follows. Although both amplitude increases (enhancement) and decreases (attenuation) are possible, specific paths have specific distributions in event polarity. The NPM transmitter (Hawaii) to Palmer and NLK transmitter (Washington) to Stanford paths exhibit almost exclusively attenuation while the NLK to Palmer path has an equally strong tendency toward enhancement. Most of the other paths show tendencies toward either enhancement or attenuation, but not as strongly. Only the NSS transmitter (Maryland) to Stanford path is evenly distributed between enhancement and attenuation. The polarity distribution of phase events is different. With the exception of the 48.5 kHz transmitter (Nebraska) to Stanford path, all other signal paths exhibit a strong tendency toward phase advancement; phase retardation does occur but is not common on these paths. The range of event magnitude, both amplitude and phase, also varies from path to path, but is fairly constant for a given path. The magnitudes of simultaneous changes in amplitude and phase on a given signal are only weakly correlated, and even the time signatures (onset and recovery) of the event amplitude and phase are often independent. While events occur

with no amplitude change ($\Delta A < 0.1$ dB) or no phase change ($\Delta\phi < 0.5°$), the occurrence rates of such events vary with path. Half of the events observed at Stanford had no measurable phase change, while less than 20% of the Palmer events did.

These path dependent properties do not fit simplified models of subionospheric propagation, but agree better with computer models of the earth - ionosphere waveguide. These new properties can be used to guide the further development of these models, and thus enhance the understanding of subionospheric propagation. The range of possible event magnitudes and the relative independence of amplitude and phase changes suggest that a detailed understanding of the profile of the perturbed ionization versus altitude in the ionosphere is necessary in order to accurately model the Trimpi effect. The observed difference between Stanford paths and Palmer paths is not yet understood. Several interesting differences between these paths have been identified, but both more data and more modelling are required before this new result can be explained.

Acknowledgement

This research was supervised by Professors U. S. Inan and R. A. Helliwell. The author is grateful for their support and encouragement. Their interest and advise have helped guide this research, and their critical reading has enhanced the content and readability of this dissertation. Professor G. F. Franklin's efforts in reading and commenting on this dissertation are also appreciated.

I am particularly indebted to Professor John P. Katsufrakis, retired, who introduced me to both Stanford and the Antarctic Research Program. This antarctic research has provided some of the most unique and thrilling experiences in my life. Working with John was one of the highlights of my time at Stanford and was both a pleasure and an education. John was an expert at managing remote field research and taught me many things about research operations that cannot be learned in a classroom. The most valuable of these lessons was the need for awareness of the people that you work with. While it is well known that any research is only as good as the tools used in that research, few engineers realize that the most important tool is the people involved in the research. John possesses an incredible awareness of diverse personalities, and knows how to anticipate and provide for people's needs, and when necessary to provide motivation. I hope that I develop some of that capability as well.

In addition to the technical support, a Ph. D. candidate requires a great deal of emotional support. For that I am grateful to my parents, brother and sisters and my close friends. In particular, Kim Fletcher and David Shafer were always available and encouraging, even when the complaints and frustrations were incessant. As a close friend and professional colleague, David has provided invaluable support in every aspect of this work. He has participated in all aspects of the development of this experiment and the analysis of the

results. He has patiently listened to my ideas, pointed out the ridiculous ones, helped refine the good ones, and suggested some of his own. He was never too busy to discuss my problems or ideas, either personal or technical, and I could not have achieved this without him. I hope that I can return the favor as David finishes his Ph. D.

Financial support for this research was provided by the National Science Foundation, in part through the Division of Polar Programs under grant number NSF-DPP-8611623, and in part through the Division of Atmospheric Sciences under grants NSF-ATM-8415464 and NSF-ATM-8804273.

Table of Contents

List of Tables

List of Illustrations

Chapter 1 - Introduction

In 1963, while conducting research in upper atmospheric physics, Michael Trimpi, a Stanford engineer at Eights Station Antarctica, discovered a surprising correlation between whistlers and changes in the amplitude of subionospheric radio signals. Whistlers are lightning - generated radio impulses that propagate, along magnetic field lines, through the magnetosphere (the rarefied, fully ionized, outermost part of the atmosphere). The subionospheric radio signals are man - made signals propagating between the earth's surface and the lower boundary of the ionosphere (the portion of the atmosphere where ion and electron concentrations are large enough to affect radio propagation). These are both very low frequency radio signals propagating from the northern hemisphere to the southern, but along very different paths through different parts of the atmosphere, and yet changes in the amplitude of the subionospheric signals were simultaneous with the reception of individual whistlers. An example of Trimpi's original data appears in Figure 1-1, where a strong whistler occurs coincident with a sharp increase (64% in 2 sec.) in the strength of the pulses received from the NSS transmitter (22.3 kHz) located at Annapolis, Maryland.

After analysis of one month of data, including approximately 100 events, additional supporting data were collected, and the finding was published along with a description of a possible mechanism [Helliwell et al., 1973]. The physical basis and the background for this mechanism, as well as the terminology used are explained in detail in Chapter 2, but can be summarized as follows.

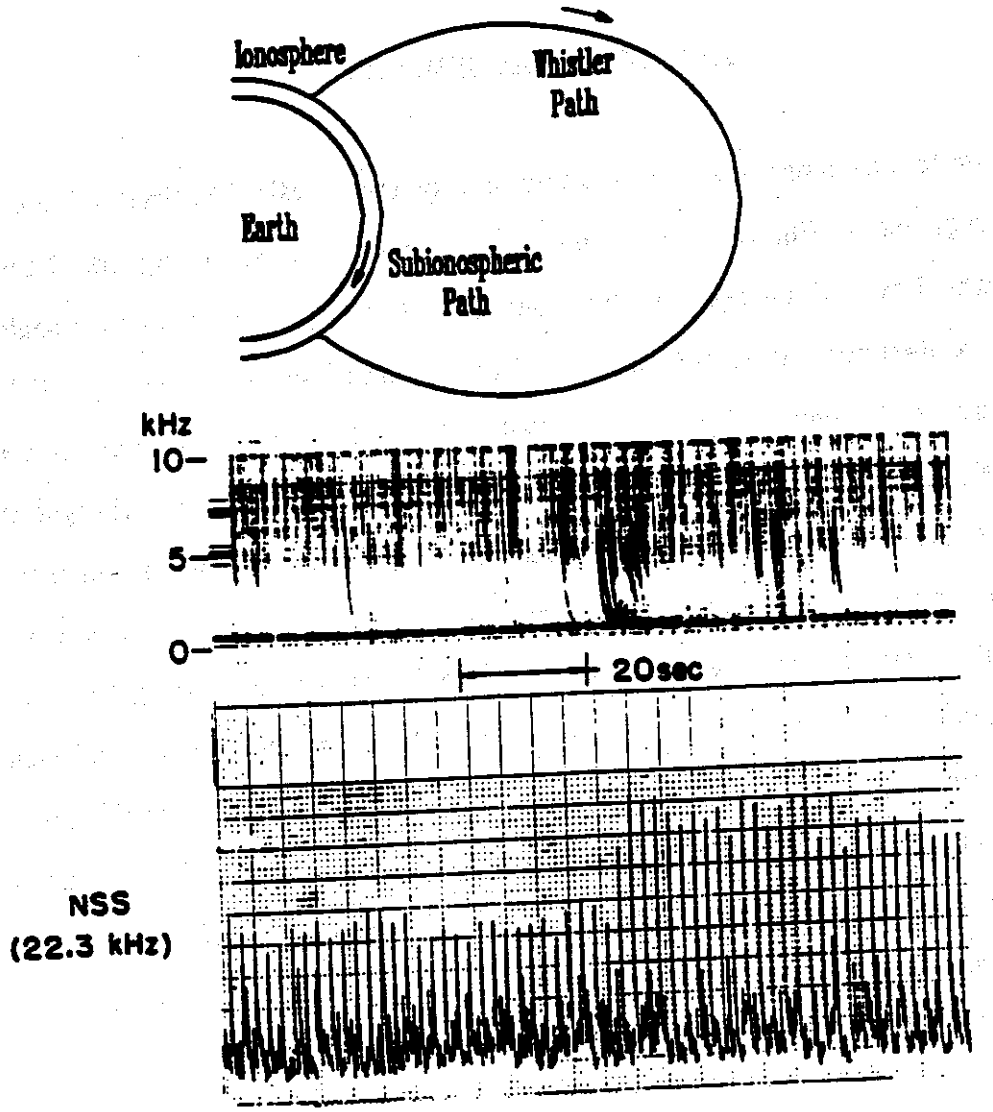

Figure 1-1 First Observations of the Trimpi Effect. The top panel illustrates the different paths followed by the whistler wave (along the magnetic field) and the NSS signal (subionospheric). The middle panel contains a spectrogram, with frequency along the vertical axis and time along the horizontal. Darkness represents signal intensity, so whistlers appear as dark, near - vertical, streaks, curving toward the lower right, since lower frequencies arrive later. The bottom panel contains a narrowband relative amplitude measurement (a linear scale in arbitrary units), centered on the NSS transmitter (Annapolis, Maryland) frequency of 22.3 kHz. In 1963 when this recording was made, the transmitter was pulsed on and off, so the vertical spikes in the amplitude indicate the transmitter signal. There is a clear increase in the NSS signal strength, coincident with a group of strong whistlers in the spectrogram. These data were recorded at Eights Station, Antarctica on 4 October 1963, at about 00:50 UT.

1.1 Mechanism of the Trimpi Effect

In addition to the commonly observed flashes of light, lightning discharges generate radio impulses throughout the electromagnetic spectrum. A fraction of the radio energy in the VLF (Very Low Frequency, 3 - 30 kHz [DeRosa, 1968]) range and below can penetrate through the ionosphere into the magnetosphere, and can propagate in "ducts" of enhanced ionization, along magnetic field lines, from hemisphere to hemisphere. However, due to the dielectric properties of the magnetosphere at VLF frequencies, only one mode of field aligned propagation, right hand circular polarization, is supported, and speed of propagation is a function of frequency. As a result, the lightning - generated radio impulses are dispersed into whistlers, with lower frequencies usually arriving later than higher frequencies [Helliwell, 1965].

The magnetosphere is also populated with high energy electrons constrained to travel, in a spiraling motion, along the magnetic field lines, mirroring, or reversing direction, near the ends of the field lines [Roederer, 1970]. Under the right conditions this gyrating motion of the electrons can match the spiral motion of the fields from the whistler waves, allowing a resonant interaction to occur. In this interaction, the wave can alter the energy and momentum of the electrons, changing the altitude at which they mirror and sometimes resulting in their penetration into the ionosphere. As they enter the increasingly dense ionosphere, these electrons dissipate their high energy by colliding with and ionizing heavy neutral atoms. The result of this "electron precipitation" is a temporary localized increase in the ion and electron concentration of the ionosphere.

VLF radio communication signals can be received over lc · distances because they propagate in the earth - ionosphere waveguide, where the radio signals are guided by the reflective surfaces of the earth and the lower ionosphere. Since this propagation is

dependent upon the electrical properties of the ionosphere, localized perturbations in the lower ionosphere can cause decreases or increases in the amplitude or phase of the received signals.

This mechanism involves both whistler - electron interactions in the magnetosphere and ionization and propagation effects in the ionosphere, so the measurement of the *Trimpi effect* and its analysis is a potentially powerful tool for studying both the ionosphere and the magnetosphere, using only ground - based instruments. In addition, the Trimpi effect is a phenomenon in which lightning discharges in the lower atmosphere lead to energy transfer from the magnetosphere to the lower ionosphere. This represents a potentially important means of coupling between these disparate regions of the atmosphere, and the precipitation of energetic electrons into the ionosphere may be an important loss process for the electron population of the magnetosphere. The occurrence rates and spatial distribution of Trimpi events must be established on a global basis, in order to assess the influence of this phenomenon on the dynamics and energy balance of the atmospheric system.

1.2 Known Properties of the Trimpi Effect

Since its initial discovery, investigations of the Trimpi effect have developed in several different directions. Although initially observed on NSS at 22.3 kHz and NAA (a transmitter located at Cutler, Maine) at 18.6 kHz, Trimpi events have been observed on signals at frequencies as low as 3.79 kHz from the transmitter at Siple Station, Antarctica [Carpenter et al., 1985], and at frequencies as high as 780 kHz from a broadcast transmitter at Santa Cruz, Argentina [Carpenter et al., 1984]. In addition to the changes in amplitude originally observed, advances in the phase of the received signal [Lohrey and Kaiser, 1979] and delays in phase [Inan et al., 1985] have been found, as well as

simultaneous changes in amplitude and phase on a single signal [Inan and Carpenter, 1987; Dowden and Adams, 1988]. Most observations reported involve amplitude changes ranging from 0.04 dB [Carpenter et al., 1984] to 6 dB [Helliwell et al., 1973], and phase changes as large as 12° [Inan and Carpenter, 1987].

Analysis of the time signature of observed events has added support to the mechanism described above [Inan and Carpenter, 1986], as well as revealing additional information. The typical event onset takes 0.1 - 2 sec., and recoveries resemble exponentials and last for 10 - 100 sec. [Carpenter et al., 1984]. Some events have unusually fast initial time signatures, implying a different, as yet undetermined mechanism [Inan et al., 1988c], and other anomalous time signatures on some low latitude events were interpreted as involving particularly high energy electrons (of order 1 MeV) [Inan et al., 1988a]. Analysis of time delays between the lightning discharge and the perturbation revealed the involvement of both northbound and southbound whistlers [Inan and Carpenter, 1986]. Statistical analyses indicate that events occur primarily at night (when most of the signal path is in darkness) and are more common within 1000 km of the receiver (at least when observed at Palmer Station, Antarctica) [Leyser et al., 1984]. Events are more common during equinoctial periods, but occur throughout the year, and seem to occur more frequently at moderate latitudes, where the local magnetic field lines cross the equator at a distance of 2 - 3 earth radii [Carpenter and Inan, 1987].

The vast majority of Trimpi events have been observed in the Antarctic [Hurren et al., 1986; Inan and Carpenter, 1987], but observations have also been reported from New Zealand [Lohrey and Kaiser, 1979; Dowden and Adams, 1988; 1989] and in the northern hemisphere from Stanford University; Lake Misti[illegible], Quebec; Saskatoon, Saskatchewan; and Arecibo, Puerto Rico [Inan et al., 1988a; b; c; d; Burgess and Inan, 1990]. In attempts to localize and estimate the size of the perturbation in the ionosphere,

events have been correlated with detected lightning strokes [Inan et al., 1988b] and simultaneous events on multiple paths (even to different receiving sites) have been identified [Inan et al., 1988d].

Research on the theoretical aspects of this phenomenon has progressed in parallel with experimental results. The whistler - electron interaction in the magnetosphere has been modelled, identifying the energy distribution and flux levels of precipitating electrons [Chang and Inan, 1985b], and these findings have been supported by satellite observations of precipitating electrons correlated with whistlers observed on the ground [Voss et al., 1984; Inan et al., 1989]. The propagation of signals in the earth - ionosphere waveguide including the effect of localized ionospheric perturbations has been modelled [Tolstoy et al., 1982] and the sensitivity of various signal paths to this phenomenon has been explored [Tolstoy et al., 1986]. More recently, perturbations located off the direct signal path have been considered [Dowden and Adams, 1988; 1989], and a full three dimensional model for the perturbation location in the waveguide has been introduced [Poulsen et al., 1990].

1.3 Outstanding Questions

While research on the Trimpi effect progresses, some unanswered questions remain and several new areas of exploration have been identified. Among these new areas are those pertaining to the geographic distribution of Trimpi events, the time evolution of individual events, the relative roles of phase and amplitude measurements, and the variation in event characteristics with location.

1.3.1 Geographic Distribution

Questions of geographic distribution pertain to both the global distribution of event occurrence and the spatial distribution of individual perturbed regions. Events have been observed frequently in the Antarctic, and less often at several sites in North America, but the world - wide extent of this phenomenon remains to be established.

The spatial dimensions of individual ionospheric perturbation regions are not known, and the range of distances over which a given lightning stroke can affect the ionosphere has not been established. It was initially assumed that ionospheric perturbations occur on or very near the great circle (or most direct) path between transmitter and receiver, but more general models of earth - ionosphere waveguide propagation, in combination with new data, can now be used to assess the role of more distant perturbations. The distribution of event locations and occurrence rates is expected to be influenced by the distribution of lightning storms as well as magnetospheric and ionospheric factors, but the relative roles of these various factors has not been established.

This information about the global extent of the Trimpi effect, and the size of individual perturbations is essential in assessing the importance of the effect to global atmospheric dynamics. These questions can be addressed by a distributed network of receiving sites, each monitoring many signal paths, and thus providing simultaneous observations of large portions of the ionosphere.

1.3.2 Time Signature of Trimpi Events

Detailed analysis of the time signature of events should also provide new information about the various physical processes leading to a Trimpi event. The delay between the

causative lightning impulse and the onset of the signal perturbation has been found to be consistent with the wave - particle interaction mechanism described above [Chang and Inan, 1985a], but further quantitative study of variation in this time delay from event to event and day to day is needed. Variations in this delay time have revealed the difference between precipitation events caused by northern and southern hemisphere lightning [Inan and Carpenter, 1986], and might provide evidence for additional perturbation mechanisms [Inan et al., 1988c].

The event rise time has been related to the duration of the precipitation burst triggered by the whistler. This duration would be determined by the whistler and electron travel times, the wave - particle scattering coefficients, and the energetic particle distribution [Inan et al., 1982; Chang and Inan, 1985a]. Accurate measurements of this rise time, in conjunction with theoretical models would yield new information about the physics of the wave - particle interaction and the energetic particle distribution.

The recovery time, the time it takes for the signal to return to pre-event levels, is a measure of ionospheric properties. This quantity would reflect the rate at which the ionospheric density enhancement decays, and thus the rate at which excess electrons recombine with ions, or attach to neutral atoms [Dingle, 1977]. This recovery time is then indicative of the transient response of the ionosphere near the reflection height of the particular signal. Variation of this time with subionospheric signal frequency may be indicative of variation in ionospheric properties with altitude [Carpenter et al., 1984]. Thus, high resolution time measurement of the events could provide quantitative information about the whistler - electron interaction, whistler and electron propagation in the magnetosphere, and the aeronomy of the ionosphere.

1.3.3 Phase and Amplitude Trimpi Events

Both phase and amplitude changes have been observed and it has been suggested that under some conditions, phase should be a more sensitive measure of ionospheric perturbations [Inan and Carpenter, 1987]; however, to date, little data have been available with simultaneous amplitude and phase measurements. Such measurements on a number of signal paths can provide valuable information about the relative sensitivity of amplitude and phase, and would be useful in the interpretation of the observations in terms of the earth - ionosphere waveguide structure. In addition, the relative magnitudes of the amplitude and phase changes could provide insight into the three dimensional shape of the ionospheric perturbation.

1.3.4 Variations in Event Properties

Comparative analysis of event occurrence and characteristics on many paths would identify those properties that are generic to the Trimpi phenomenon and those that are unique to individual paths. The generic properties might be expected to be determined by the basic physics of the phenomenon, such as the wave - particle interaction and the shape of the perturbed ionospheric regions. The path - specific properties are more likely to be controlled by the propagation characteristics of the particular path or the location of the perturbation with respect to the path. Once specific properties are determined, they can be used to refine the models for subionospheric propagation, for wave - particle interaction, and for the precipitation of energetic electrons into the ionosphere.

1.4 Contributions of this Research

This research addresses primarily the questions pertaining to the significance of simultaneous amplitude and phase events, and the comparative analysis of occurrence and characteristics of events on many different paths. The specific contributions of this research as related to these outstanding questions include the following:

- The design and development of a new VLF/LF receiver for high resolution measurements of propagation effects. Capabilities include simultaneous amplitude and phase measurement, tuneable multichannel reception, and high time resolution.
- Analysis of a comprehensive data set of VLF radio signatures of ionospheric perturbations. This data set includes multiple receiving sites, multiple signal paths at each site, and simultaneous amplitude and phase data.
- Identification of several new properties of VLF signal perturbations associated with lightning. Among these are the path dependence of the polarity of amplitude changes, and the predominance of phase advancement independent of path. Another property is that the magnitudes of simultaneous amplitude and phase changes on a given path are only weakly correlated with one another. Also, the distribution in magnitude of simultaneous amplitude and phase events varies with the path, but for a given path, is independent of time. Finally, half of the events observed in the northern hemisphere had no detectable phase change, while less than one fifth of the southern hemisphere events did.

These new properties provide constraints on existing and future theoretical models of the wave - particle interaction and the ionospheric perturbation mechanism, and can be used to refine these models in the future.

The hardware developed to perform these observations is described in Chapter 3, and the results that were obtained are described in the subsequent chapters. Chapter 2 provides the necessary scientific background, describing the terminology, the physics and the processes involved in the perturbation of subionospheric radio propagation associated with lightning.

Chapter 2 - Scientific Background

As introduced above, lightning can perturb the propagation of subionospheric Very Low Frequency (VLF) radio signals through a complex sequence of physical interactions. In order to understand this process, it is necessary to understand the basic properties and interactions of various regions of the earth's atmosphere.

2.1 The Ionosphere

The existence of the ionosphere is a consequence of two commonly known properties of the atmosphere. At any altitude, the density of the air is determined largely by the total weight of the atmosphere above that altitude. This results in the first of these simple properties, which is that the density of the atmosphere decreases with altitude above the earth's surface. The second property of interest, a result of the chemical composition of the atmosphere, is that the atmosphere absorbs much of the Ultraviolet (UV) and higher energy radiation incident upon it, from the sun and other cosmic sources [Ratcliffe, 1972].

The absorption of this energy results in the ionization of atoms and molecules in the atmosphere, but the ions and free electrons thus created are soon absorbed by interaction with other nearby ions and atoms [Ratcliffe, 1972]. As a result, there is a dynamic equilibrium between the production of electrons and their absorption, yielding an average free electron density. As the altitude increases, the intensity of the radiation increases because less radiation has been absorbed above, and so the rate of ionization increases. In addition, since the density of the atmosphere decreases with ' ude, the free electrons that are formed exist longer before they collide with other particles and are absorbed. Thus, as altitude increases, the rate of production of electrons increases, and the rate at

which they recombine decreases, so the equilibrium shifts and the density of free electrons increases. Starting at approximately 60 km altitude, the concentration of free electrons is sufficient to have a significant influence on the dielectric properties of the atmosphere. This forms the lower edge of the *ionosphere*, which is defined as "The part of the atmosphere ... where free electrons exist in numbers sufficient to influence the travel of radio waves" [Ratcliffe, 1972].

Throughout the ionosphere, the total particle concentration continues to decrease with increasing altitude, while the fraction of these particles that is ionized continues to increase. The combination of these two effects causes the ion (and electron) concentrations to reach a maximum near 300 km [Rees, 1989]. Above that peak, the atmosphere is predominantly ionized, and the density decreases monotonically. Finally, at altitudes above approximately 1000 km, the effect of collisions is negligible and the properties of the atmosphere are dominated by the influence of the earth's magnetic field [Park and Carpenter, 1978]. This outer region is named the *magnetosphere*, and is discussed separately below. A typical profile of neutral particle concentration and free electron concentration versus altitude for the ionosphere is shown in Figure 2-1.

The ionosphere is further divided into layers (labelled D, E and F), based upon the radiation absorbed, the types of ions, and the chemical properties prevalent at certain altitudes [Rishbeth and Garriott, 1969]. For the purposes of this research, however, it suffices to note that most of the effects of interest occur in the D region, near the bottom of the ionosphere, between 60 and 100 km altitude.

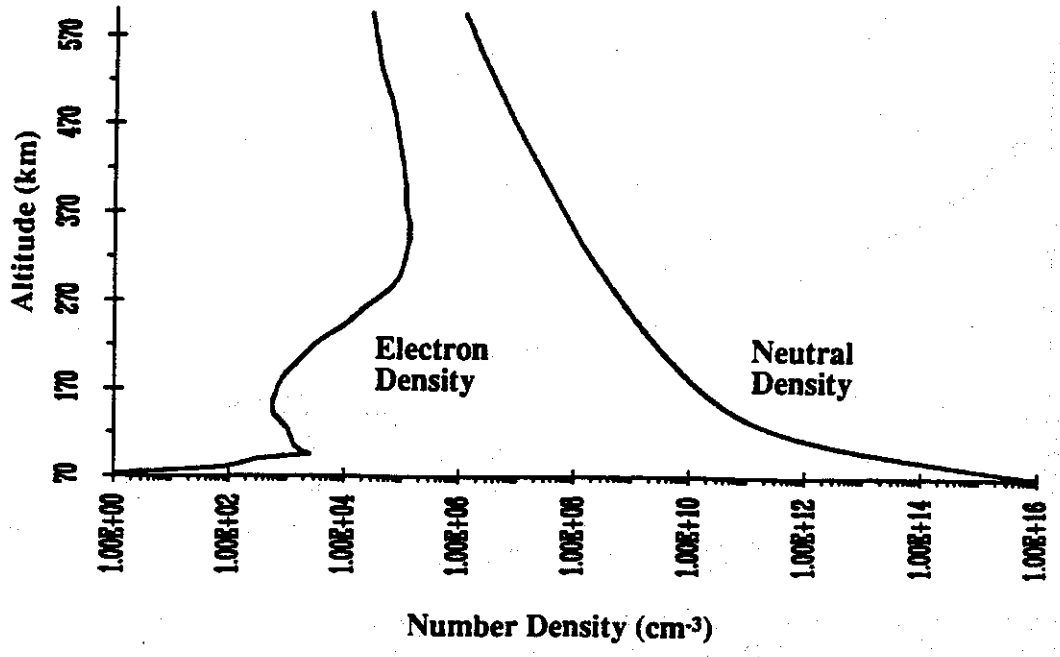

Figure 2-1 Ionospheric Density Profile. The neutral particle density (atoms and molecules) and electron density versus altitude are shown for typical nighttime, quiet sun conditions. Electron data below 100 km are from Poulsen et al. [1990], electron data above 100 km are from Rees [1989], and neutral data are computed from the MSIS-86 model atmosphere for 13 July 1976 [Rees, 1989].

2.1.1 Radio Waves in the Ionosphere

When radio waves are incident upon the ionosphere, they encounter an extremely complicated dielectric, whose properties vary with altitude and direction (inhomogeneous and anisotropic). Detailed analysis of this dielectric has been described in numerous references [Ratcliffe, 1959; Davies, 1965; Budden, 1985], and only some simple properties will be reviewed here. For the VLF frequency range, an incident radio signal undergoes a combination of absorption, reflection off the ionosphere, and transmission through the ionosphere, depending upon the frequency, the angle of incidence, and the electron and ion concentrations in the ionosphere at the time [Helliwell, 1965].

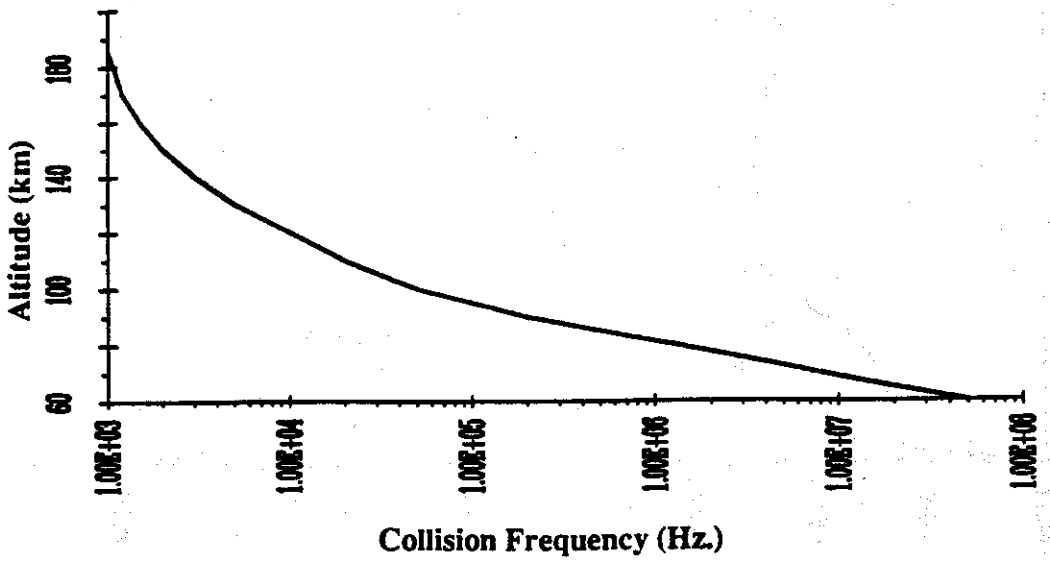

Figure 2-2 Collision Frequency Profile. The effective electron collision frequency versus altitude in the lower ionosphere is shown for temperate latitudes, but is a good estimate for most conditions and locations. Data are from Budden [1985].

Absorption of radio waves in a dielectric is primarily a consequence of collisions between electrons, moving in response to the electromagnetic fields of the waves, and heavier atoms and ions [Ramo et al., 1965]. These collisions in turn transfer the propagating wave energy to thermal energy of the atoms, reducing the wave intensity. The lower regions of the ionosphere, where the density is greatest have the highest rate of occurrence of these collisions, and therefore are the most absorbing [Ratcliffe, 1959]. A typical collision frequency vs. altitude profile is shown in Figure 2-2.

An electromagnetic wave totally reflects from a medium with varying dielectric properties when the refractive index becomes zero [Jackson, 1975]. Although this concept has been successfully applied to some frequencies and certain portions of the ionosphere [Ratcliffe, 1959], it does not generally apply to VLF signals. Instead, the value of the refractive index for VLF signals in the ionosphere is complex (containing both a refractive and an absorptive term) and depends upon local properties of the medium and wave direction (with respect to the earth's magnetic field) in a complicated

manner. Due to the influence of the earth's magnetic field and the presence of absorption, the refractive index never becomes zero [Ratcliffe, 1959], so total reflection does not occur, but substantial partial reflection is possible. The region of the ionosphere where such reflection of the wave occurs can be visualized as a region where the refractive index is changing very rapidly over a distance equal to the wavelength. When this occurs, the region acts like a sharp boundary between two different media and a mixture of transmission and reflection results. Quantitatively, this occurs in the region where the following expression holds [Ratcliffe, 1959]:

$$X = Z, \text{ or equivalently, } \omega = \omega_N^2 / \nu$$

where

$X = \omega_N^2 / \omega^2$

$Z = \nu / \omega$

ω = wave frequency

ν = effective collision frequency of electrons with heavy particles

ω_N = plasma frequency of the medium given by:

$$\omega_N = 4 \pi N e^2 / \varepsilon_0 m$$

with

N = number density of electrons

e = charge of an electron

ε_0 = electric permittivity of free space

m = mass of electron

A more accurate expression for the reflection condition at VLF frequencies, based on empirical measurements and assuming an exponentially varying ionosphere [Wait and

Spies, 1964], is now generally used. Note that this expression is independent of wave frequency:

$$\omega_r = 2.5 \times 10^5 \text{ s}^{-1}$$

where

$\omega_r = \omega_N^2 / \nu$ = the "conductivity parameter"

In the VLF frequency range, during nighttime, reflection generally occurs at altitudes near 85 km [Inan et al., 1985]. As seen in Figures 2-1 and 2-2, at this altitude, N and therefore ω_N increase exponentially and ν decreases rapidly with altitude, so the frequency independence of the reflection height is not surprising, and the two expressions for the reflection condition above are quite similar. Although convenient for describing propagation, the concept of a reflection height is an oversimplification since, as with any dielectric boundary, the characteristics of the reflected wave are influenced by the electromagnetic properties of the media for several wavelengths above and below the boundary [Helliwell, 1965]. The more detailed problem has been treated using computers for a full wave analysis, determining all wave components throughout the ionosphere and the lower atmosphere [Pappert and Snyder, 1972].

2.1.2 The Earth - Ionosphere Waveguide

The surface of the earth is a moderately good conductor of electricity, and can reflect radio signals in the lower frequency ranges, including VLF [Davies, 1965]. Since, as described above, the ionosphere is also a good reflector of these signals, VLF radio signals can propagate over long distances along the surface of the earth by repeated reflections off the earth and the ionosphere, as illustrated in Figure 2-3. In other words, these two essentially parallel surfaces - the ionosphere and the earth's surface - act as a

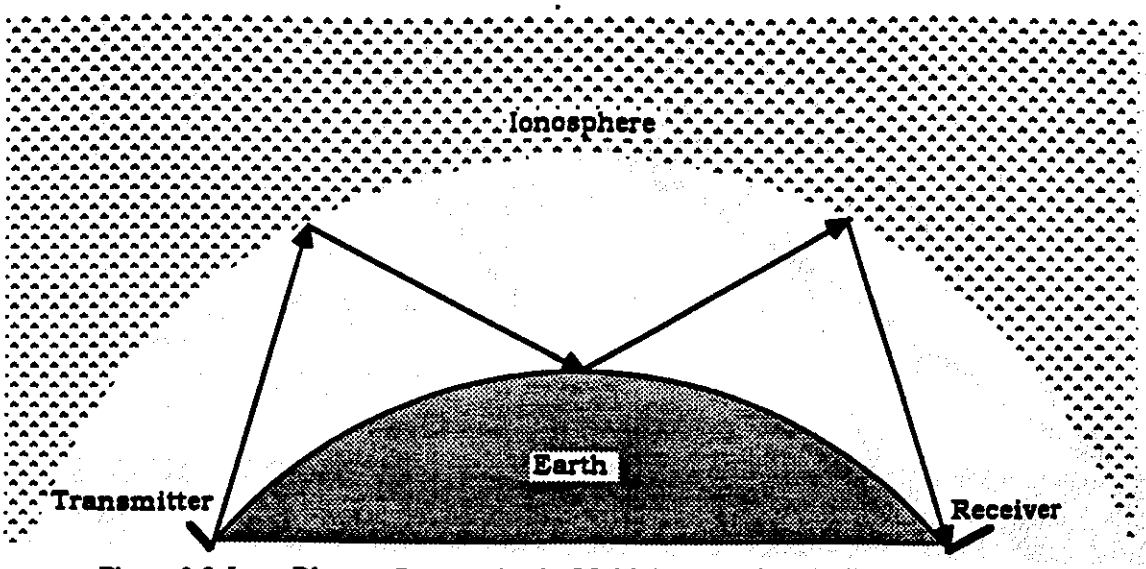

Figure 2-3 Long Distance Propagation by Multiple Reflection. An illustration of long range propagation of VLF signals by repeated reflection from the ionosphere and the earth's surface.

waveguide, keeping the VLF radio wave energy in the lower portions of the atmosphere and guiding it along the earth's surface.

As with any waveguide, there are two equivalent methods of analyzing wave propagation in the earth - ionosphere waveguide [Ramo et al., 1965]. The ray optics approach [Born and Wolf, 1965] is easier to visualize, and sometimes simpler to analyze, and is the one illustrated in Figure 2-3. This approach treats the propagation as a sum of plane waves each with the wave vector along a straight line from the transmitter to the reflector(s) and ultimately to the receiver [Budden, 1985]. These ray paths can be enumerated by the number of reflections required to traverse the region [Davies, 1965]. For example, there may be a direct signal (called the *ground wave*), and, as shown in Figure 2-4, several *sky waves* including a path which reflects off the ionosphere once, a path which reflects off the ionosphere twice, with a reflection off the earth in between, etc.

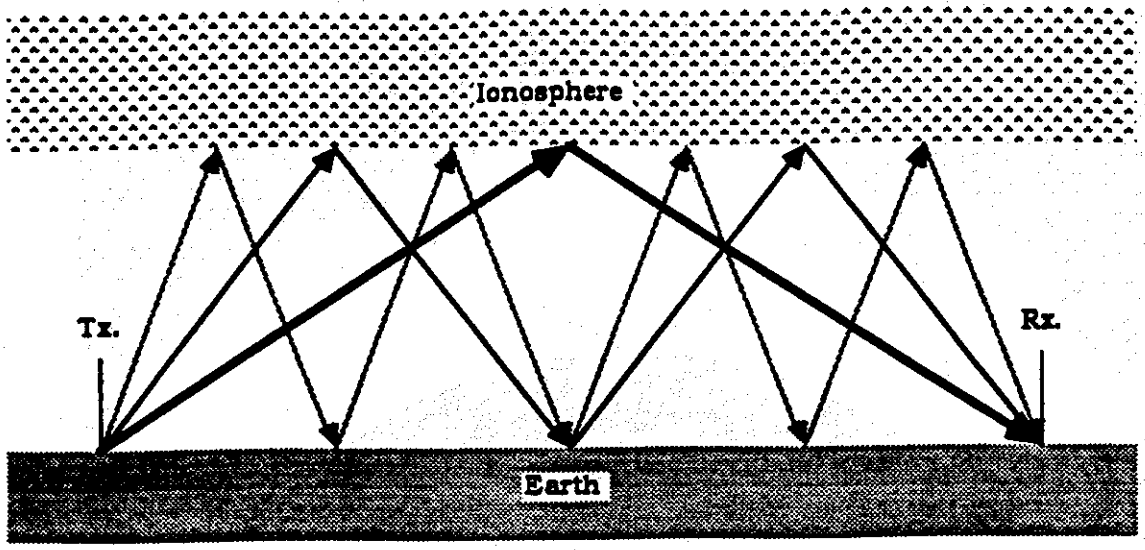

Figure 2-4 Possible Ray Paths from Transmitter to Receiver. The discrete possible ray paths are those that complete an integral number of "hops" from earth to ionosphere and back to earth, between the transmitter (Tx.) and the receiver (Rx.). It can be seen that the paths with more hops have nearer vertical incidence.

Although an infinite number of paths is possible, the number of these discrete paths that contains any appreciable signal is often quite limited. Paths with many reflections and nearer vertical incidence are longer than more direct paths with fewer reflections, and as with any radiating system, field strength falls off with overall path length from transmitter to receiver [[Mallinckrodt, 1949]. Also, neither reflection off the ionosphere nor off the earth is perfect, so some signal strength is lost with each reflection. In addition, the more vertical the incidence of the signal on the boundary, the more of the signal is lost through absorption and transmission into the medium, and thus, the weaker the reflection [Davies, 1965]. The combination of these effects implies that the paths that have many reflections, at near vertical angles of incidence, will rapidly lose signal strength, and generally, only the paths with relatively few reflections and oblique incidence will dominate the received signal.

When the dimensions of the waveguide are smaller than a few wavelengths, it is often more appropriate to use waveguide modes to analyze the propagation of the signal within

the waveguide [Wait, 1962]. As with the ray approach, there are discrete waveguide modes that can be enumerated, and the received signal at any point is a vector sum of signals propagating in each of these modes. The modes are determined by the fact that the component of the wave propagating perpendicular to the waveguide must form a standing wave pattern that continuously satisfies the conditions dictated by the boundaries [Ramo et al., 1965]. Waveguide mode theory is easiest to visualize in the case of parallel, planar, perfectly conducting boundaries. In this simple example, the wave fields at the boundary can have no electric fields parallel to the boundaries ($E_{\parallel}$). Thus the propagating modes would be those where $E_{\parallel}$ completed 1/2, 1, 1-1/2, 2, etc. cycles between the two boundaries [Ramo et al., 1965].

For VLF signals propagating in the earth - ionosphere waveguide, the problem is substantially more complicated. First, the boundaries are not perfect conductors, but instead, lossy dielectrics, requiring the use of complex reflection coefficients and complex angles of incidence [Budden, 1961]. In addition, the ionosphere is not a sharp boundary, but rather a stratified medium that varies with altitude. This is allowed for by either modelling the ionosphere with a sharp boundary of complex impedance at an equivalent reflection height [Wait, 1962] or by using computers to analyze the wave fields throughout the ionosphere, using various models for the ionosphere [Foley et al., 1973]. The curvature of the earth also complicates the waveguide by changing reflection angles, and the presence of the earth's magnetic field introduces anisotropy in the ionosphere [Wait, 1962].

Despite these complications, a series of discrete waveguide modes can be identified [Wait, 1962] and for each one, parameters such as phase velocity, attenuation rate, and excitation factor can be established. Although exact values for these parameters depend upon the ionospheric model used [Foley et al., 1973], typical attenuation rates for the first

mode are 2 - 4 dB / 1000 km during the day and 0.5 - 2 dB / 1000 km at night [Ferguson and Snyder, 1980], and higher order modes generally have higher attenuation [Foley et al., 1973]. One interesting consequence of the anisotropy of the ionosphere is that attenuation is less for east - to - west propagation than for west - to - east propagation [Foley et al., 1973]. The excitation factor is a measure of how efficiently the transmitting and receiving antennas couple into the various modes, and depends upon the size of the antenna, its polarization, and its location in the waveguide. For higher frequency VLF signals, the curvature of the earth causes the lowest order mode to become "earth detached" where it is guided by the curved ionosphere and has minimal signal strength at the earth's surface [Wait, 1962].

For ground based transmitters and receivers, the dominant waveguide modes are primarily TM (Transverse Magnetic) modes although some TE (Transverse Electric) modes do propagate [Ramo et al., 1965; Foley et al., 1973], and may even dominate at higher altitudes [Turtle et al., 1989]. For short paths, five or more modes must be considered, but for long paths (> 3000 km), the variation in attenuation rate usually causes the second or third mode to dominate [Tolstoy et al., 1982; Foley et al., 1973] (the lowest order mode is usually poorly excited because of its earth detached nature [Ferguson and Snyder, 1980]). The waveguide mode picture can be further complicated by irregularities on the surfaces of the waveguide, such as mountains, or sea water to land transitions on the earth, or ionization enhancements, or the day - night terminator on the ionosphere. Such irregularities result in coupling or conversion between the various modes [Tolstoy et al., 1982; Pappert and Snyder, 1972].

When properly analyzed the ray approach and the mode approach are equivalent, and the choice is based primarily upon the ease of analysis and the preference for visualizing the effects. The ray approach is often used for short paths (where only ray paths with few

reflections have angles of incidence far from vertical) and for waveguides with dimensions of many wavelengths (where the exact fields at the boundaries are not as significant). The waveguide approach is more appropriate for small waveguides, and long paths (where high order waveguide modes tend to be attenuated, leaving only a few modes, while many reflecting ray paths are possible). The ray approach is usually easier to visualize and will be used in the qualitative discussion of propagation phenomena here, but due to the complexity of the waveguide boundaries, the waveguide mode approach would be more appropriate for detailed and quantitative analysis of VLF propagation phenomena [Morfitt and Shellman, 1976].

The earth - ionosphere waveguide is used for long distance communication over a wide range of frequencies, extending as high as the HF frequency band (3 to 30 MHz) where it is used by shortwave broadcast stations, amateur radio operators, and others. At lower frequencies the waveguide becomes more reliable (less dependent upon variable ionospheric conditions) and less attenuating (because of the longer wavelength), so in the VLF band, the U. S. Navy uses a variety of transmitters in the 20 to 30 kHz range for reliable world - wide communications. The Omega global navigation system operates at even lower frequencies, in the 10 to 14 kHz range. These VLF transmitters operate very reliably and are powerful (most of the Navy transmitters exceed 1 MW radiated power) and so are extremely useful for ionospheric measurements.

2.1.3 Lightning and Radio Atmospherics

When a lightning discharge occurs, it generates an impulse of electromagnetic energy throughout the frequency spectrum. In addition to the visible [illegible] a burst of appreciable energy is radiated throughout the radio frequency range. Popping and crashing sounds heard on AM broadcast signals are familiar to most people, and this effect is even more

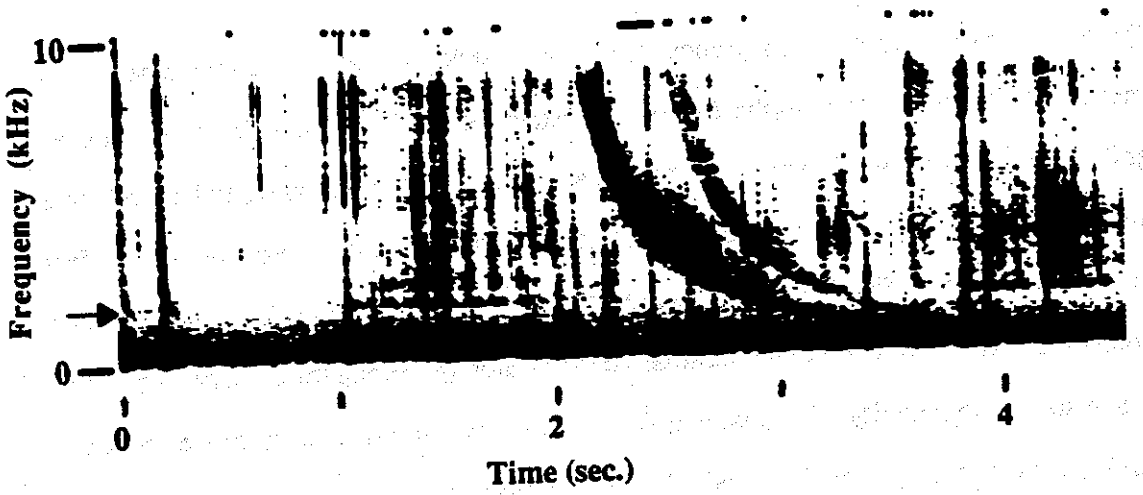

Figure 2-5 Typical Atmospherics and Whistlers. A sample spectrogram of natural signals received at Palmer Station. The vertical axis is frequency, 0 - 10 kHz, the horizontal axis is time, and darkness represents signal strength. Atmospherics appear as vertical dark lines, most of which end at the waveguide cutoff frequency (arrow). Whistlers appear as dark arcs, curving toward the lower right, showing that dispersion delays the lower frequencies. Data are from 30 March 1983, at approximately 05:50 UT.

apparent in the VLF frequency range. The spectrum of the radio frequency output of a lightning stroke shows a strong burst of energy from near DC to 100 kHz and above, with a peak near 5 kHz [Uman, 1969].

These low frequency impulses propagate to long distances in the earth - ionosphere waveguide, because of their long wavelength and their high initial signal strength. With this long range propagation and the high incidence of lightning in the world (~ 100 flashes per second) [Uman, 1983], these impulses are a dominant feature of the atmospheric VLF spectrum and are called radio atmospherics (or spherics for short) [Davies, 1965]. Examples of these atmospherics appear in Figure 2-5.

As with other waveguides, the earth - ionosphere waveguide exhibits a *cutoff frequency*, below which signals do not propagate well. For typical conditions, this cutoff is around 1 - 2 kHz [Helliwell, 1965], so atmospherics that have propagated long distances often do not have significant energy below this frequency. Signals at frequencies just above the

cutoff generally have phase and group velocities much lower than those for signals far from the cutoff [Ramo et al., 1965], so that the radio impulse is distorted. The received atmospheric is then an impulse with a slower low frequency tail. These distorted atmospherics are referred to as *tweeks* because of the way they sound when received through an audio system [Helliwell, 1965].

2.2 The Earth's Magnetic Field

The presence of the earth's magnetic field has a dominant influence on the properties of the magnetosphere, so an understanding of its basic properties is necessary for this study. The magnetic field is essentially dipolar, centered close to the center of the earth and tilted 11° from the rotation axis, as shown in Figure 2-6. The strength of the field is given by [Lyons and Williams, 1984]:

$$B = 0.312\times10^{-4} (R_E / R)^3 (1 + 3 \sin^2 \lambda)^{1/2}$$

where

R_E = mean earth radius = 6370 km

R = distance from the center of the earth

λ = magnetic latitude (0° at magnetic equator)

B = magnetic field strength in wb / m^2

A dipole magnetic field line can be described by the relation:

$$R / \cos^2 \lambda = R_{eq}$$

where R_{eq} is the radius at which the field line crosses the magnetic equator. The field line

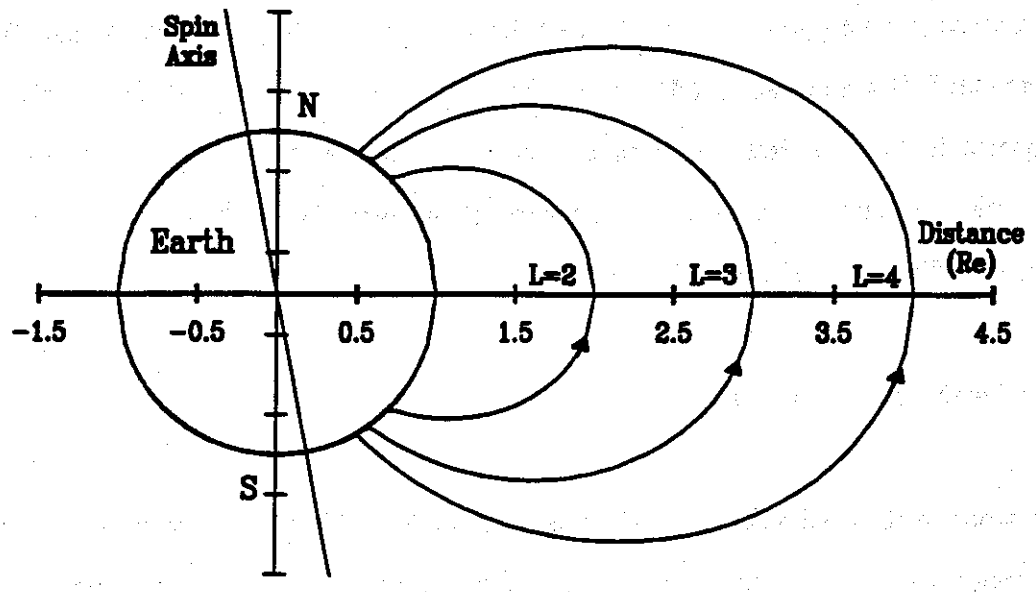

Figure 2-6 Dipole Model of the Earth's Magnetic Field. A diagram of the magnetic field lines corresponding to the centered dipole model of the magnetic field, showing the L parameter used to characterize field lines. The dipole is tilted by 11° from the spin axis.

is usually characterized by its equatorial radius, using the parameter L [Lyons and Williams, 1984] given by:

$$L = R_{eq} / R_E$$

Combining these three relations, the field strength along a field line with a given L value is given by:

$$B = 0.312 \times 10^{-4} (1 + 3 \sin^2 \lambda)^{1/2} / (L \cos^2 \lambda)^3$$

Note that the magnetic field strength is weakest at the magnetic equator, and increases with magnetic latitude along a field line.

This dipole model is generally used to describe the magnetic field, and to define a geomagnetic coordinate system, consisting of L, λ (some texts use the field strength, B, instead of the latitude, λ), and θ (magnetic longitude), but it is not an entirely accurate description of the earth's magnetic field. A more accurate (within 10%) simple model is to displace the dipole ~ 400 km toward the western Pacific from the center of the earth [Fraser - Smith, 1987]. Still more accurate models use multipolar or other high order expansions based upon empirical values [Jensen and Cain, 1962; Olson and Pfitzer, 1974], and accurately reflect a number of anomalies in the shape of the magnetic field. The most significant of these anomalies is the *South Atlantic Anomaly*, a region of extremely weak magnetic field off the coast of Brazil.

The actual field has contributions from currents in the earth's crust, currents in the ionosphere, particle motion in the magnetosphere, and distortion of the magnetic field by the solar wind. The field can be changed by as much as 10^{-6} wb / m^2 by solar magnetic storms, and also experiences weaker fluctuations that range from very rapid (of order seconds) to very slow (of order years) [Jacobs, 1970]. For the purposes of this research, it is sufficient to treat the magnetic field as a constant geocentric dipolar field, with the addition of the South Atlantic Anomaly.

2.3 The Magnetosphere

As mentioned above, the *magnetosphere* is the uppermost region of the earth's atmosphere, above the ionosphere (some texts define the ionosphere as extending further out and including the magnetosphere as the highest portion of the ionosphere), whose properties are dominated by the presence of the earth's magnetic field [Ratcliffe, 1972]. The magnetosphere is a neutral, low density, low energy plasma consisting almost entirely of ionized hydrogen atoms (protons) and free electrons although some oxygen

and helium ions are also present [Ratcliffe, 1972]. At these altitudes (h > 1000 km), there are few neutral atoms so little radiation is absorbed, and the density is low allowing few collisions. As a result, at middle to low latitudes (L < ~ 4) the particle concentration as a function of altitude is determined primarily by *diffusive equilibrium*. Electrons and ions produced in the ionosphere flow upward, along magnetic field lines, driven by diffusion from the high concentrations in the ionosphere, and the density of the magnetosphere is determined by an equilibrium between diffusion and gravity [Ratcliffe, 1972].

On the sunlit side of the earth, electron production in the ionosphere is high, and particles flow into the magnetosphere, while on the night side, ionospheric production is diminished and particles flow down from the magnetosphere, helping to sustain the ionospheric population [Park and Carpenter, 1978]. The particle density continues to decrease with altitude above the earth, until it reaches the level of the interplanetary region, but the shape of this density profile is quite complicated. On the day side, the pressure of the solar wind (a continuous stream of protons and electrons from the sun with a typical density of $\sim 5\,cm^{-3}$ and a velocity of $300\,km/s$) compresses the magnetosphere, forming a sharp boundary between the magnetosphere and the interplanetary medium at $\sim 10\,R_E$ [Ratcliffe, 1972]. The magnetosphere, on the night side, is elongated into the *magnetotail*, pointing away from the sun and stretching out to $100\,R_E$, before joining the interplanetary medium [Ratcliffe, 1972].

Up to an altitude of $4\,R_E$, the solar wind has relatively little influence on the magnetosphere, and the shape of the magnetic field is nearly dipolar. In this inner region, the electron density falls gradually from $\sim 10^4\,cm^{-3}$ at 1000 km to $\sim 10^3\,cm^{-3}$ at $4\,R_E$, but then falls abruptly by up to two orders of magnitude over $0.15\,R_E$ [Park and Carpenter, 1978]. This transition, called the *plasmapause*, is typically at $\sim 4\,R_E$, but may vary between 3 and $7\,R_E$ depending upon solar activity [Carpenter et al., 1971; Ho and

Carpenter, 1976]. The position of the plasmapause is not symmetric around the globe; instead it varies with longitude and is affected by the earth's spin and interaction with the sun [Ho and Carpenter, 1976].

The region inside the plasmapause, known as the *plasmasphere* is the area of interest in this research; in this region all magnetic field lines start at the earth's surface at low to moderate latitudes, extend across the equatorial plane, and end at low to moderate latitudes in the opposite hemisphere. This region is primarily populated by low density, low energy electrons, referred to as the *cold plasma* or the *thermal plasma*, with typical densities of $N = 10^3\ cm^{-3}$ and energies of $E = 0.1\ eV$ [Ratcliffe, 1972]. At VLF frequencies, it is primarily these electrons that determine the electromagnetic wave propagation properties of the plasmasphere.

2.3.1 The Radiation Belts

The magnetosphere is also populated by high energy electrons (with energies of 10 keV to 1 MeV, or more) [Ratcliffe, 1972] which were emitted by the sun, or by high energy collisions in the ionosphere and became trapped by the earth's magnetic field. These energetic electrons exist throughout the magnetosphere, but are concentrated in a toroidal region surrounding the earth (typically at $1.5 < L < 6$). For the highest energy ($E > 500$ keV) particles, this toroid is separated into two *belts*, by a low concentration *slot region* near $L = 3$ [Lyons and Thorne, 1973]. The low density ($N < 1\ cm^{-3}$ [Schulz and Lanzerotti, 1974]) of this *hot plasma*, compared to the cold plasma, implies that it does not affect the dielectric properties of the plasmasphere, but due to their high energy these electrons have other significant interactions.

The motion of these electrons, under the influence of the magnetic field can be separated into three distinct components. Since a charged particle moving in a magnetic field experiences a force perpendicular to the magnetic field and perpendicular to the direction of motion, any motion perpendicular to the field will be converted into a circular motion [Ramo et al., 1965]. The first component of the motion is this *gyration* around the field line, characterized by its rotational frequency or *gyrofrequency* (ω_H), the gyration period (τ_H), and the gyroradius (r_H), given by [Jackson, 1975; Chen, 1984]:

$$\tau_H = 2\pi / \omega_H \text{ where } \omega_H = |e B| / \gamma m \text{ and } r_H = v_\perp / \omega_H$$

with

e = electron charge

m = electron mass

B = magnetic field strength

$\gamma = (1 - (v / c)^2)^{-1/2}$

v = electron speed

c = speed of light

$v_\perp$ = electron speed perpendicular to magnetic field

Note that the particle energy affects only the radius of gyration; the gyrofrequency is independent of energy (for non - relativistic velocities). This circular gyration can be separated from other particle motion provided the magnetic field does not change significantly during one gyration; that is, provided $\tau_H \, dB/dt << B$ and $\tau_H \, v_\parallel \, dB/dz << B$ (where z is the direction along the magnetic field and $v_\parallel$ is the component of the electron motion along the z axis). In the plasmasphere, τ_H is generally of order 1 ms [Lyons and Williams, 1984] and these assumptions are valid. The electron trajectory can then be described as a spiral and its velocity, v, characterized by the two velocity components, $v_\parallel$

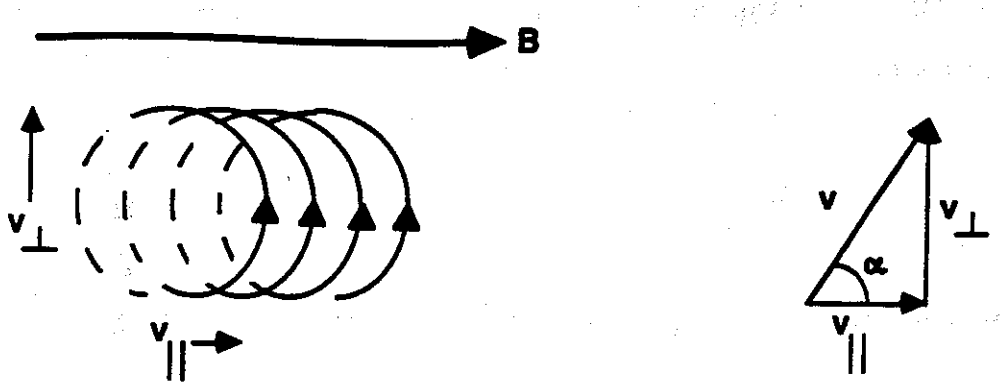

Figure 2-7 Electron Motion in a Magnetic Field. The left panel shows the spiral motion of an electron in the presence of a magnetic field (B). The right panel shows the relationship between the velocity components (v, $v_{||}$, $v_{\perp}$) and the pitch angle (α).

and $v_{\perp}$, as shown in Figure 2-7. These two components are related by the *pitch angle* (α), given by:

$$\tan(\alpha) = v_{\perp} / v_{||}$$

The magnetic field constrains motion across the field to circles, but does not restrict motion along the magnetic field, and since the force is perpendicular to the motion, the field does no work on the electron. Thus, the electron spirals along the magnetic field with a constant kinetic energy. For the field to do no work on the electron when the field strength, B, changes, the total flux through an electron gyration must remain constant [Jackson, 1975], thus:

$$\Phi_M = B \pi r_H^2 = \text{const.}$$

Substituting for r_H and ω_H, and consolidating constants, this becomes (neglecting relativistic effects):

$$v_\perp^2 / B = \text{const.}$$

Now, $v_\perp = v \sin \alpha$, and since energy is conserved, v is constant, so:

$$\mu_B = \sin^2\alpha / B = \text{const.}$$

μ_B is known as the *first adiabatic invariant* and is a property of the electron motion. As the electron moves along the field line, with velocity $v_\parallel$, the magnetic field strength changes, but μ_B does not, so α changes. A changing pitch angle with constant total energy implies that energy must be transferred between $v_\perp$ and $v_\parallel$. This gives rise to the second motion of the electrons, known as *bounce* motion.

Along a magnetic field line, the field is weakest at the equator, as described above, so the pitch angle of a spiraling electron is smallest at the equator. As the electron moves away from the equator, the field strength, and so the pitch angle, increases. If the field becomes large enough to cause the pitch angle to reach 90°, the particle will have no motion along the field, i.e., $v_\parallel = 0$, and all of the energy will be in the gyration. When this happens, the gradient in the magnetic field drives the electron back up the field line toward the equator. This reversal of direction, called *mirroring* [Chen, 1984], causes the electron to bounce back and forth between hemispheres, along the magnetic field. This periodic bounce motion has a period of order 1 sec. [Lyons and Williams, 1984] and thus can generally be treated separately from the gyration. These electrons are then *trapped* in the magnetosphere, gyrating and bouncing along the magnetic field line [Roederer, 1970]. If the pitch angle is low enough at the equator, the electron will follow the field line all the

way down to the ionosphere before mirroring. In the ionosphere, the electron will most likely collide with heavy particles, giving up its energy, and thus be removed from the radiation belt [Rees, 1969]. Not all electrons that collide in the ionosphere are lost. Some of them (up to 90% depending upon pitch angle and energy) may be *backscattered* by the ionosphere and return to the magnetosphere, on the same or nearby field lines, but with altered energies or pitch angles [Berger et al., 1974].

An energetic electron can be characterized by its energy (E) and its equatorial pitch angle (α_{eq}) and has two possible destinations, depending only upon α_{eq} and not E. For a given magnetic field line (determined by L value and longitude) there is a critical equatorial pitch angle called the loss cone angle (α_{lc}). Electrons with $\alpha_{eq} > \alpha_{lc}$ will be trapped, and remain in the magnetosphere for extended periods, while electrons with $\alpha_{eq} < \alpha_{lc}$ will be lost to the ionosphere, in a process called *precipitation*, giving up some of their energy by locally increasing the ionization in the ionosphere [Roederer, 1970; Rees, 1969].

This process of mirroring and precipitating is further complicated by the anomalies in the earth's magnetic field [Schulz and Lanzerotti, 1974]. These asymmetries in the magnetic field mean that it is possible to have different loss cone angles for northbound and southbound electrons on the same field line. Thus, it is possible to have an electron mirror in the north, and then precipitate in the south (or vice versa), depending upon the detailed structure of the magnetic field [Barish and Wiley, 1970]. This is particularly apparent over the eastern United States and the Atlantic ocean, due to the particularly weak magnetic field near the South Atlantic Anomaly.

Electrons also experience a third motion called *drift*, in the longitudinal direction (ie. east - west). This motion, driven by electric fields and gradients in the magnetic field is much slower, with orbital periods around the earth of order hours [Lyons and Williams,

1984] and may affect diurnal variations in Trimpi event occurrence rates, but is not significant for the analysis performed here. It is, however, important in the overall trapping process, and the long term characteristics of the radiation belts [Schulz and Lanzerotti, 1974].

2.3.2 Wave Propagation in the Magnetosphere

As mentioned above, the dielectric properties of the plasmasphere are determined by the cold plasma. The wave refractive index for this medium is described by the Appleton - Hartree equation [Budden, 1985], and generally is complex, with both a propagating and an absorbing term. In addition, the anisotropy introduced by the earth's magnetic field results in there being two characteristic waves with different refractive indices [Helliwell, 1965]. The value of the refractive index depends upon the electron density, the magnetic field strength (usually expressed in terms of the electron gyrofrequency), the collision frequency (usually negligible in the magnetosphere), the wave frequency, and the angle between the wave normal and the direction of the magnetic field [Helliwell, 1965].

Analysis of the Appleton - Hartree equation reveals several important properties of the magnetosphere. First, at VLF frequencies, the only mode that can propagate is known as the *whistler mode*, and has right - hand circular polarization when viewed in the direction of the magnetic field [Helliwell, 1965]. The whistler mode has a relatively high refractive index ($n = 10 - 100$), so whistler mode waves have low group and phase velocities ($v = 0.01 - 0.1\ c$). In addition, these velocities are functions of wave frequency, resulting in *dispersion*, where different frequencies are received with different delays [Helliwell, 1965]. For the whistler mode in the magnetosphere, there is a frequency of minimum time delay, known as the *nose frequency* (typically ~ 14 kHz for $L = 2.5$), and signals at frequencies above or below the nose frequency are delayed relative to those nearer the

nose frequency. Impulses generated by lightning which penetrate the ionosphere and propagate through the magnetosphere (as well as propagating in the earth - ionosphere waveguide) are distorted as a result of dispersion. Frequencies below the nose frequency are delayed, with the lower frequencies experiencing longer delays, so that an impulse received after propagation through the magnetosphere sounds like a whistling tone, falling in frequency, and is therefore called a *whistler* [Helliwell, 1965]. Figure 2-5 is a spectrogram (frequency versus time plot) showing a received whistler, as well as the subionospherically propagating radio atmospherics.

As with the energetic electrons, cold plasma electrons can move easily along the magnetic field lines, but cannot readily move across them, since any perpendicular motion is converted into a spiral around the field line. Therefore, any local irregularity in the electron density is spread out into a field aligned irregularity along the magnetic field line. These field aligned irregularities, whether enhancements or depletions, then form cylindrical tubes that can act as waveguides to steer VLF signals along the magnetic field. These waveguide structures, called *ducts*, guide a VLF signal along the magnetic field, allowing it to propagate efficiently from hemisphere to hemisphere [Helliwell, 1965]. As a signal exits a duct in the opposite hemisphere from which it entered, it can pass through the ionosphere and be received on the ground. It can also reflect from the lower boundary of the ionosphere and reenter the duct (or another one nearby) and return to the source hemisphere. This process of reflection, called *echoing* can be repeated over and over in each hemisphere, resulting in a received signal followed by one or more echoes. Each echo is delayed by several seconds (depending upon frequency) from the one before, and has greater dispersion, since the delays are compounded with each "hop" through the magnetosphere [Helliwell, 1965]. Whistler energy from lightning also propagates in the magnetosphere in the *non - ducted* mode [Edgar, 1976]; however generally, only ducted waves are observed with receivers on the ground, since

non - ducted ones usually have high wave normal angles and do not penetrate the ionosphere, to reach the ground [Helliwell, 1965].

2.3.3 Wave - Particle Interactions

Both the whistler mode radio signals and the energetic electrons follow paths along the magnetic field lines in the magnetosphere. Much of the time, the waves and particles pass through each other with no noticeable effect, but the wave is circularly polarized, and the electron follows a helical path, so under certain conditions, the direction of the electromagnetic fields (from the wave) relative to the electron velocity ($v_{\perp}$) can be constant for an appreciable period. When this occurs, the condition is called *cyclotron resonance*, and energy can be transferred from the wave to the electrons or from the electrons to the wave [Helliwell et al., 1980; Lyons and Williams, 1984]. Cyclotron resonance is generally described as occurring when the doppler shifted wave frequency equals the gyrofrequency of the electrons [Schulz and Lanzerotti, 1974]. The doppler shift is necessary because the electrons are moving along the magnetic field line with a velocity $v_{\parallel}$. An alternative derivation of the first order cyclotron resonant condition (neglecting relativistic effects) begins by considering the classic expression for the field of a propagating wave:

$$E = E_0 \sin (\omega t - k z)$$

where

ω = wave frequency

t = time

k = wave number

z = position

The electron's position can be described by its position z, along the field line, and its position in orbit around the field line given by:

$$x = r_H \cos(\omega_H t)$$

$$y = r_H \sin(\omega_H t)$$

$$z = v_{\|} t$$

There will be appreciable interaction between the particle and wave only if the phase of the particle in its orbit stays constant relative to the phase of the wave for an extended period, thus:

$$d/dt [\omega_H t - (\omega t - k z)] = 0$$

Assuming ω_H and k are changing only slowly, this reduces to:

$$\omega_H - (\omega - k\, dz/dt) = 0$$

but now, the electron is moving along the field line (z axis) at a velocity $v_{\|}$, so:

$$dz/dt = v_{\|}$$

This then yields the first order cyclotron resonant condition:

$$\omega_H = \omega - k v_{\|}$$

For the whistler mode of propagation, $\omega < \omega_H$, so for cyclotron resonance to occur, $v_\parallel$ must be negative [Inan, 1977], meaning that the wave and particle are moving toward each other, in opposite directions along the field line.

When cyclotron resonance occurs, there are a number of different possible outcomes [Brice, 1964]. It is possible for the electrons to give up energy to the wave, amplifying the intensity of the wave [Chang and Helliwell, 1980]. The wave can also trigger an instability in the electron motion causing them to radiate signals at frequencies near the wave frequency (called *triggered emissions*) [Helliwell, 1971], and in the mechanism of interest here, the wave can alter the momentum of the electrons, changing their trajectories, or *scattering* them [Inan, 1977].

The condition for resonance is a function of magnetic field strength (through ω_H), particle energy (through $v_\parallel$), and wave frequency (ω), so the likelihood of resonance occurring varies throughout the magnetosphere. Since the density of energetic electrons usually decreases with increasing energy [Chang and Inan, 1985a], the optimum conditions for efficient scattering, for a given wave frequency, are those where the magnetic field is weakest (at the equator for a given field line), allowing resonance with lower energy, higher density electrons. Interaction with electrons is also most efficient when the resonant condition is satisfied for an appreciable time, so resonant interaction is most significant where the magnetic field strength is changing slowly (also at the equator) [Carlson et al., 1985]. In cases where the wave frequency is changing with time, such as whistlers, all three quantities (ω, ω_H, and $v_\parallel$) are changing with time, and it is possible for the interaction to extend far from the equator as well [Inan et al., 1989]. Near L = 2.5, typical whistler frequencies (0.5 kHz to 6 kHz) can reso[illegible] with high energy electrons in the 40 - 400 keV range [Helliwell et al., 1976]. In whistler - mode gyroresonance interactions, electron scattering generally involves primarily a change in

electron momentum. The energy transfer from the wave to the particle is small, but the electron motion is changed by transferring energy between $v_{\parallel}$ and $v_{\perp}$. This results in a change in pitch angle (α), and a subsequent change in the mirror height for the electron [Inan, 1977].

2.3.4 Electron Precipitation

The cyclotron resonant interaction between whistlers and energetic electrons can alter the pitch angle of the electrons by as much as ±2° [Inan et al., 1989], so if the electron pitch angle was just above the loss cone angle (typically ~ 13° at L = 2.5) and the electron is scattered toward lower pitch angles, the electron can be scattered into the loss cone. When this occurs, the electron precipitates into the ionosphere, as a result of interaction with the wave.

In geographic regions where most existing observations of the Trimpi effect have been conducted, lightning activity is much more prevalent in the northern hemisphere, so that the majority of precipitation events involve southbound whistlers interacting with northbound energetic electrons [Inan and Carpenter, 1986]. When these electrons then precipitate in the northern hemisphere ionosphere, the process is known as *direct precipitation* [Chang and Inan, 1983]. In longitudes where the magnetic field is asymmetric, such as near the South Atlantic Anomaly, it is possible for electrons to be scattered into the southern hemisphere loss cone, but not into the northern hemisphere loss cone [Inan et al., 1988c]. When this occurs, it is still southbound whistlers resonating with northbound electrons, but now, the electrons mirror in the north, above the ionosphere, and then precipitate in the south [Chang and Inan, 1983], as shown in Figure 2-8. This process is called *mirrored precipitation* and is the one most frequently observed in the Antarctic.

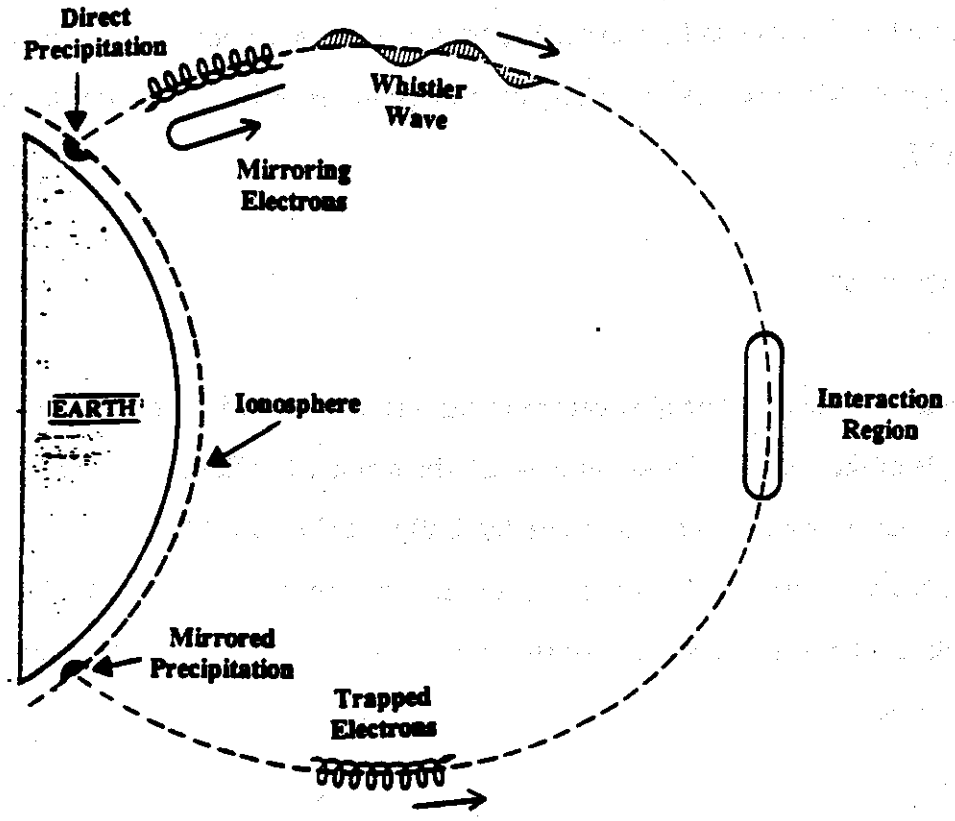

Figure 2-8 Direct and Mirrored Precipitation. Illustration of a southbound whistler interacting with northbound electrons, causing precipitation in the north (direct) and precipitation in the south (mirrored).

When the energetic electrons precipitate into the ionosphere, they sometimes give up their energy by colliding with atoms and molecules in the ionosphere. The energy thus transferred to the atoms and molecules can result in the production of X-rays [Rosenberg et al., 1980], optical emissions [Helliwell and Mende, 1980], and increased ionization [Helliwell et al., 1973]. The excess ions and electrons that are generated slowly recombine in accordance with the normal chemical processes of the ionosphere, including attachment to neutral atoms or molecules and recombination with ions [Dingle, 1977]. As described above, the precipitating electrons can be characterized by their pitch angle and their energy. The pitch angle determines whether the electron will precipitate after scattering, i.e., was it scattered into the loss cone?, but the energy will determine the

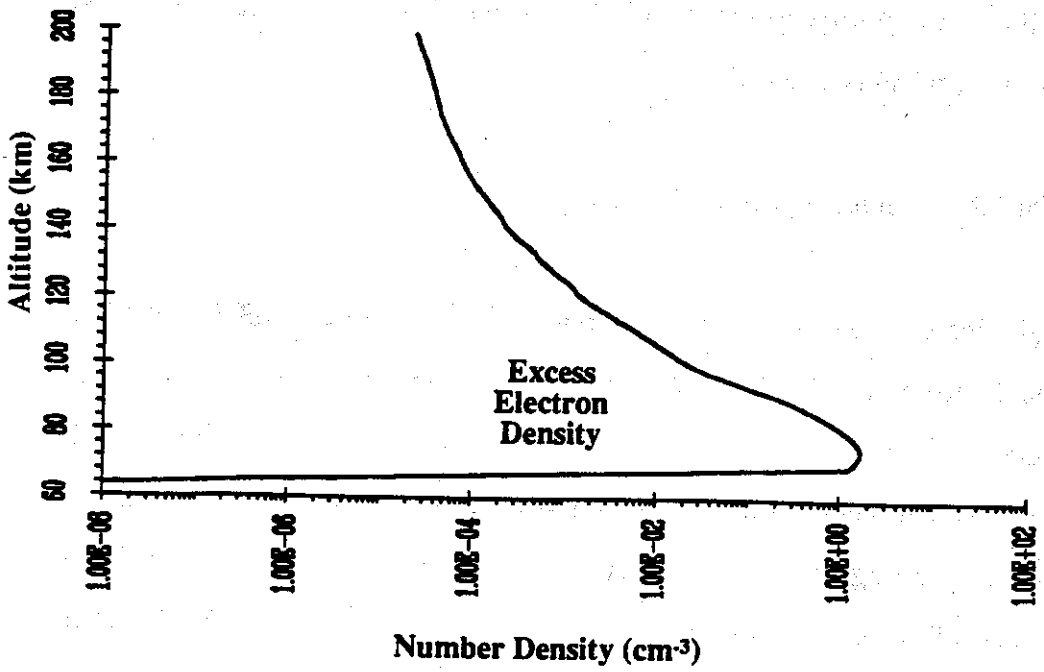

Figure 2-9 Typical Whistler Induced Excess Ionization. The excess electron density caused by a whistler induced precipitation event is shown as a function of altitude. The excess electron density is obtained using Rees [1963], assuming an isotropic distribution of 300 keV electrons with a flux of 10^{-3} erg cm^{-2} s^{-1}, lasting for 0.2 sec.

effect of the precipitation. Higher energy electrons will penetrate deeper into the ionosphere when they precipitate, and will cause more ionization as their energy is absorbed [Berger et al., 1974].

As a population of energetic electrons penetrates deeper into the ionosphere, it encounters an increasing density of atoms and molecules, and so deposits more energy (creating more electron - ion pairs) per unit altitude change. Once a critical density is reached, the bulk of the energy is deposited over a small range of altitude. This altitude for maximum ionization varies with electron energy, ranging from 150 km for 1 keV electrons to 60 km for 1 MeV electrons [Rees, 1969]. At the typical night time VLF reflection height of 85 km [Inan et al., 1985], 40 keV electrons will provide maximum ionization, but electrons of higher energy will also cause substantial ionization [Rees, 1969]. A typical example of excess electron concentration versus altitude is shown in

Figure 2-9. For this simplified example a 0.2 sec. burst of isotropic 300 keV electrons at a flux of 10^{-3} erg cm^{-2} s^{-1} is assumed.

2.4 Perturbation of Subionospheric Wave Propagation

If the precipitating electrons have enough energy (E > 40 keV [Rees, 1969]), and a large enough flux (~ 10^{-3} ergs cm^{-2} s^{-1} [Inan et al., 1985]), they can cause an appreciable change in the local electron concentration in the vicinity of the VLF reflection height. When this occurs, the boundary conditions in this reflection region are altered, and any VLF signal propagating in the earth - ionosphere waveguide under this region is perturbed. Depending upon the resulting electron density versus altitude profile in the ionosphere, and the waveguide modes that are significant, both the amplitude and the phase of the signal can be changed [Tolstoy et al., 1982].

A typical profile of electron density versus altitude is shown in Figure 2-10, where the effect of a 0.2 sec. burst of 300 keV electrons has been added. Although the excess electrons are distributed over a range of altitude, in a complicated fashion that depends upon electron energy distribution, pitch angle distribution, and ionospheric properties, a number of simplified models for the consequences of this perturbation have been used. These models were created to explain specific observations and are extremely useful for a conceptual understanding of the Trimpi phenomenon, but as they are applied to larger sets of data, their limitations become apparent. These models are described here, and comparison of them to recent observations is discussed in Chapter 5.

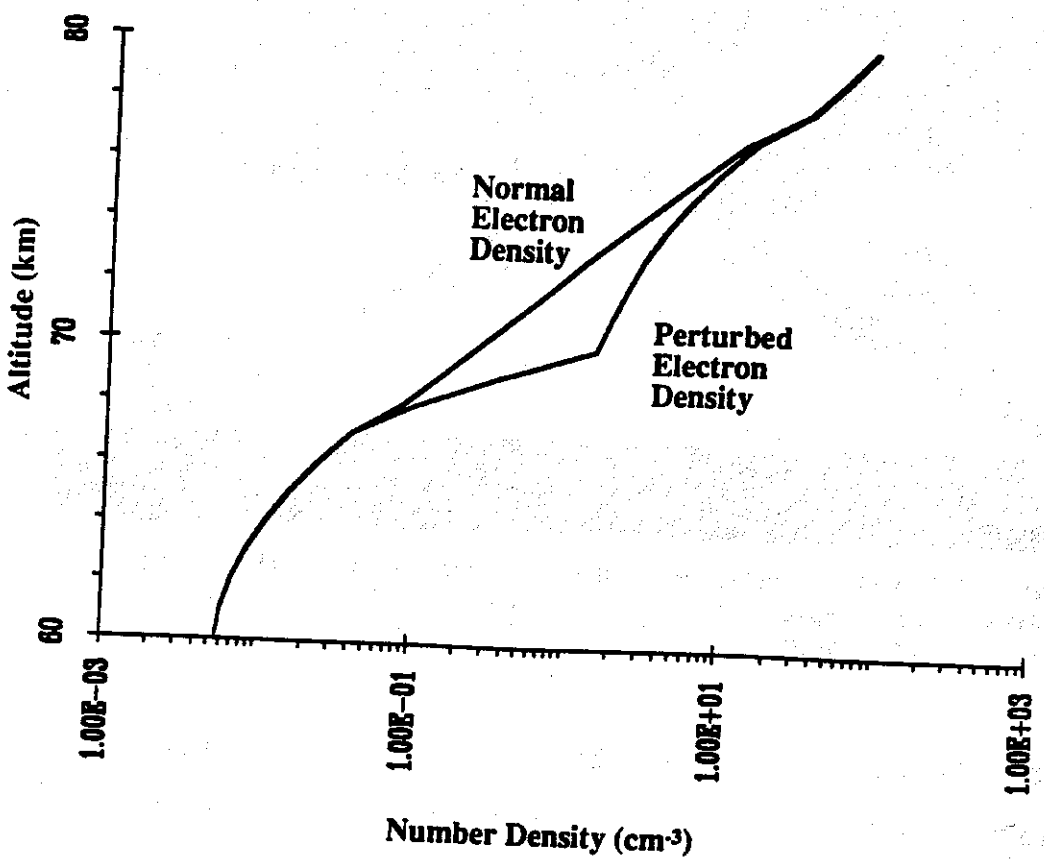

Figure 2-10 Typical Whistler Induced Ionospheric Perturbation. The affect of the typical excess ionization shown in Figure 2-9 on the ionospheric electron density shown in Figure 2-1 is illustrated. The slight increase in electron density in the lower ionosphere can also be viewed as a lowering of the lower ionosphere by ~ 2 km.

2.4.1 Reflection Height Lowering

The simplest model for perturbing a subionospheric signal was used for many years [Helliwell et al., 1973] and is known as Reflection Height Lowering (RHL). This model makes several simplifying assumptions about the waveguide and the perturbation. The first assumption is that of horizontal symmetry in all features perpendicular to the direction of propagation. This reduces the model to two dimensions, one horizontal direction along the line between the transmitter and receiver, and one vertical dimension between the earth's surface and the ionosphere. This assumption is equivalent to

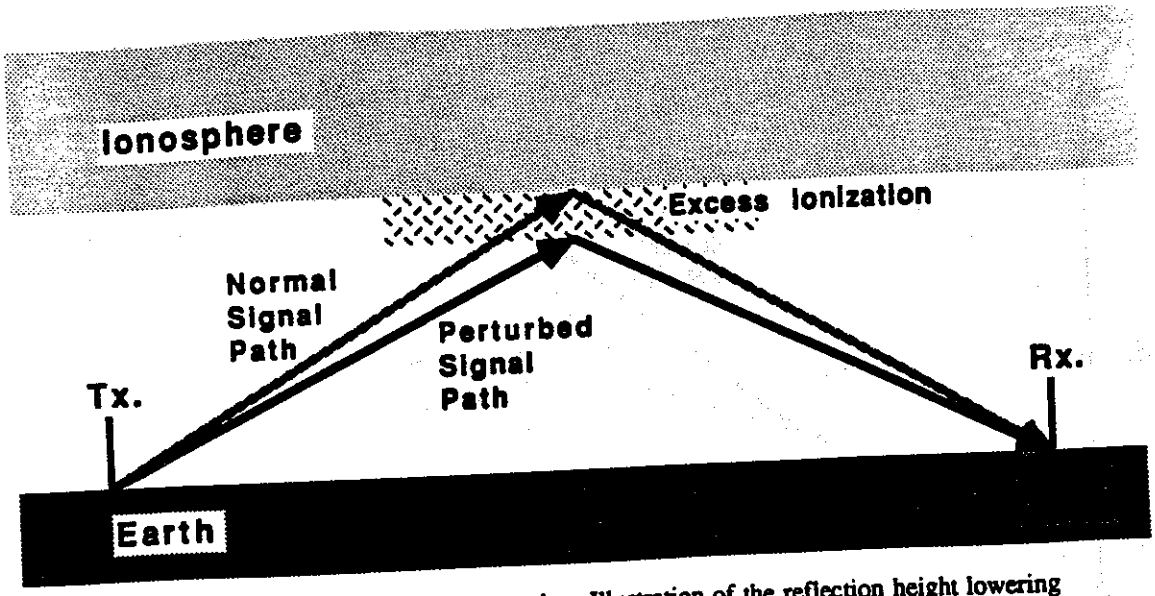

Figure 2-11 Reflection Height Lowering. Illustration of the reflection height lowering mechanism, where precipitation lowers the altitude at which the VLF signal reflects off the ionosphere, shortening the signal path, from transmitter to receiver.

assuming that all perturbations in the ionosphere occur right on the signal path, between receiver and transmitter, and extend far off the path in the perpendicular direction.

A second simplification is that reflection occurs at a specific altitude determined by the electron concentration. If the precipitation event causes an increase in the electron concentration in the vicinity of this altitude, the altitude at which the electron concentration reaches the level required for reflection is lowered (typically by 1 - 2 km [Inan et al., 1985]), as illustrated in Figure 2-11. When the subionospheric wave reflects at a lower altitude, the total path length from transmitter to receiver is shortened, which appears as a slight decrease in propagation time to the receiver. Thus, a lowering of the reflection height appears as an advancement in the phase of the received signal. The increase in electron concentration in the lower ionosphere also increases the absorption coefficient, making the ionosphere more absorbing, so the RHL concept implies that signals would experience an attenuation as well as a phase advancement [Helliwell et al., 1973].

2.4.2 Off Axis Scattering

Recently, a new model, known as Off Axis Scattering (OAS), has been suggested [Dowden and Adams, 1988]. This model assumes that the signal propagating along the great circle path from transmitter to receiver remains undisturbed. Instead, the precipitation event causes a localized patch of excess ionization at the bottom of the ionosphere, near but not on this direct path. This patch then acts as a scattering center, deflecting a portion of the signal it receives from the transmitter back toward the receiver. In its simplest form, this model is not concerned with the vertical dimension of the waveguide and can be illustrated as in Figure 2-12.

The direct signal path from transmitter to receiver is the shortest possible path, so any signal on a scattered path will arrive slightly later than the direct signal. If the total scattered path length were more than 1/2 wavelength longer than the direct path (or if the scattering center introduces an arbitrary phase shift), the resulting signal can experience both phase advancement and retardation. If the model assumes, as Dowden and Adams [1988] do, that the magnitude of the scattering does not vary significantly with distance from the direct path, then phase advancement and retardation should be equally likely, as should amplitude enhancement and attenuation. This is an obvious consequence of the fact that the scattered signal will have an arbitrary phase relative to the direct one. This assumption does, however, imply in general that large phase changes should be associated with small amplitude changes and vice versa, and that simultaneous large amplitude and large phase changes should be rare.

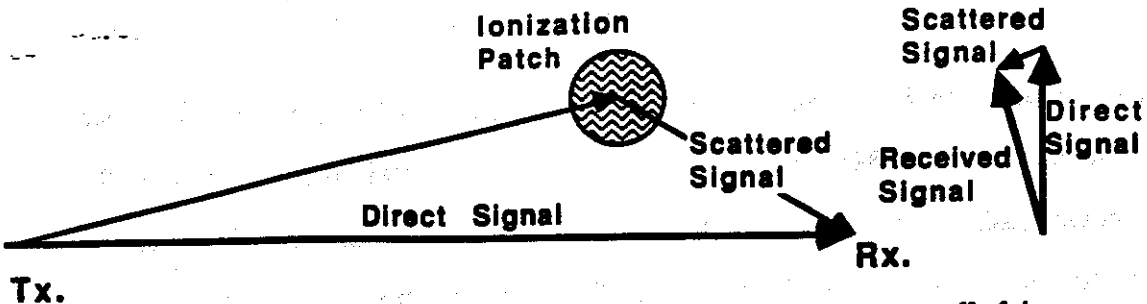

Figure 2-12 Off Axis Scattering. An illustration of how a scattering center off of the path from the transmitter to the receiver, could introduce a second signal path that interferes with the direct signal. Note that this is a top view, the vertical dimension is not shown. The right panel uses a vector to represent the signal amplitude and phase, and shows that adding, to the direct signal, a small scattered signal with different phase will change the amplitude and phase of the received signal.

2.4.3 Waveguide Models

Both of the perturbation models above use the ray approach to understanding the waveguide, making it easy to visualize the perturbation and its effect. An alternative approach is to analyze the waveguide in terms of propagating modes as discussed above. Tolstoy et al. [1982] used a computer simulation to analyze the ionosphere and propagation in the waveguide, and to determine the effect of localized changes in the ionosphere. Initially, 10 - 20 km sections of the ionosphere were simply displaced vertically downward by 3 - 4 km, but later studies used estimated precipitating electron fluxes and energies to better represent the perturbation [Tolstoy et al., 1986], and obtain agreement with observed signal perturbations. In addition, the relative magnitudes of the various waveguide modes have been established [Tolstoy et al., 1982; 1986], and allowance has been made for conversion between waveguide modes by irregularities in the ionosphere [Pappert and Snyder, 1972].

An even more sophisticated waveguide model is being developed [Poulsen et al., 1990], which considers all three dimensions. This model utilizes the two dimensional waveguide

Figure 2-13 Vector Sum of Propagating Modes. Vectors (A and B) representing the amplitude and phase of received signals propagating in two different modes can each experience a phase advancement (from the original grey vector to the new black vector), and yet the resultant sum may experience a phase advancement (left panel) or a retardation (right panel), as well as an amplitude enhancement or attenuation.

described above, including full analysis of the wave in the ionosphere, and realistic estimates of enhanced ionization versus altitude profiles in the perturbed region. This new model includes the treatment of perturbations displaced from the direct (great circle) path, and has revealed a wide range of possible amplitude and phase changes, in agreement with recent observations.

2.4.4 Multiple Mode Propagation

Since the earth - ionosphere waveguide supports an infinite number of propagating waveguide modes (or ray paths), it is necessary to consider the possibility that the received signal is a sum of several modes [Lohrey and Kaiser, 1979]. A perturbation in the ionosphere is likely to have a different effect on each mode, so that the vector sum of the modes immediately after the perturbation of the ionosphere can be quite different from the original sum. Figure 2-13 illustrates the fact that two modes, each experiencing a phase advancement can result in a net phase advancement or retardation, depending upon the relative phases of the two modes. Similarly, amplitude enhancement and attenuation are possible. This is particularly significant if the phases of the modes are such that the sum of all of the modes is small, even though the individual modes are large in magnitude [Lohrey and Kaiser, 1979], as shown in Figure 2-14. Under these

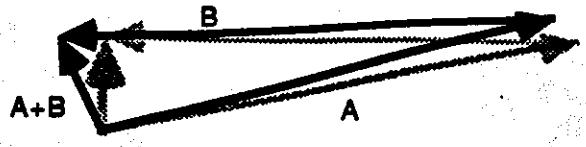

Figure 2-14 Large Perturbations Caused by Destructive Modal Interference. When two strong signals propagating in different modes (represented by vectors A and B) combine in a destructive manner (i.e., a small difference between large values), small changes in each mode (from the original grey vector to the new black vector) can result in large phase changes and large relative amplitude changes in the sum.

conditions, it is possible to have a large change in the relative amplitude or phase of the resultant vector, even though each individual mode changes by a small amount.

This multiple mode concept can be applied to any of the perturbation models described above, and will complicate all of them. Fortunately, detailed analysis of the earth - ionosphere waveguide has shown that for most paths, only a few modes are significant [Tolstoy et al., 1986]. In particular for long paths (> 10000 km) over sea water, a single mode will dominate (by ~ 9 dB), making the models more tractable [Inan and Carpenter, 1987].

2.5 Time Signature of Electron Precipitation Events

The mechanism for the Trimpi effect is a sequence of discrete steps. The whistlers propagate up the field line, and then resonate with energetic electrons. The scattered electrons continue down the field line, sometimes mirror, and some of them ultimately penetrate into the ionosphere. In the ionosphere these electrons generate excess ionization, enhancing the local electron density, thus perturbing the subionospheric VLF radio signals. The electron density then slowly decays back to the normal concentration, by typical ionospheric processes of recombination and attachment. This sequence of physical steps leads to a characteristic time signature for the Trimpi effect.

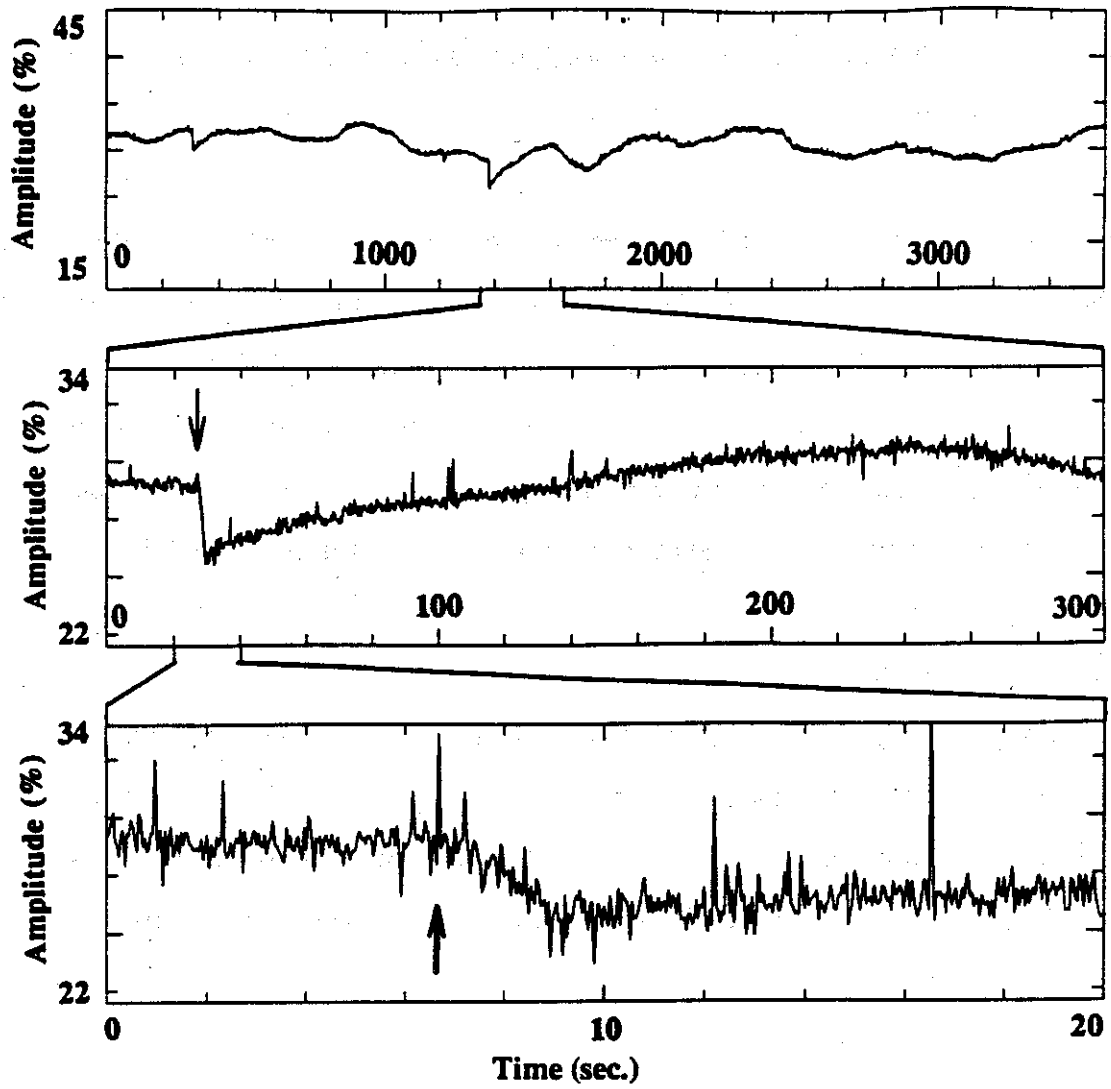

Figure 2-15 Typical Trimpi Event Characteristics. A typical event shown at different time scales, revealing the time characteristics. The top panel reveals the sharp onset and slow recovery. The second panel shows the nearly exponential recovery, taking approximately 150 sec. The final panel reveals the event rise time of approximately 2 sec., and the onset delay of approximately 0.5 sec. measured from the strong atmospheric generated by the causative lightning discharge. This causative atmospheric can be recognized as a spike on top of the received signal (arrows on the lower panels). Data are from the NSS transmitter, received at Stanford University, on 16 March 1987. The three panels start at 05:00:01 UT, 05:22:30 UT, and 05:22:50 UT, respectively.

A typical Trimpi event is shown in Figure 2-15, where the characteristic time signatures are apparent. The onset of the event is rapid, of order 0.1 - 2 sec., and is typical of the wave - particle interaction time in the magnetosphere [Chang and Inan, 1985b]. After its

peak, the signal slowly returns to its pre-event level, over a period of 10 - 100 sec., which is typical of the recombination time in the lower ionosphere [Dingle, 1977].

In addition to the typical perturbation events described above, a number of unusual events have been identified, with different time signatures. There are two time parameters that are characteristic of the commencement of a typical perturbation. The first of these, called the *onset delay* time is the interval between the atmospheric generated by the causative lightning discharge, and the start of the perturbation. This time, of order 0.5 sec., is determined by the time it takes for the impulse to propagate up the field line, interact with the energetic electrons, and for the perturbed electrons to travel down the field line to the ionosphere, and therefore depends upon wave frequency, electron density, electron energy and magnetic field strength. The second characteristic commencement time is the *rise time* mentioned above, which corresponds to the duration of the electron precipitation burst. This time depends upon the duration of the wave - particle interaction and the electron bounce period, if some perturbed electrons precipitate after one or more bounces.

"Early events" have been observed with unusually short onset delay times (less than 0.1 sec.), and "fast events" with extremely fast rise times (less than 0.05 sec.) have also been reported [Inan et al., 1988c]. Casual review of the data collected shows that the vast majority of events have the typical event time signature, and atypical events such as these will be left for consideration in future research.

Chapter 3 - Experimental Apparatus

New high resolution, simultaneous amplitude and phase data on a number of subionospheric VLF signals were necessary in order to investigate the unanswered questions discussed in Section 1.3. This need dictated specific requirements for the data collection apparatus, and new equipment was designed and developed for that purpose. Among the requirements for the new hardware were that it be easy to manufacture, install, and operate, so that many systems could be built and deployed at a variety of receiving sites. In addition, the receivers were required to be tuneable and capable of measuring both amplitude and phase, in order to maximize the variety of data collected at each site. Finally, in anticipation of the large quantities of data to be collected, it was necessary that the new hardware collect the data in a form that would expedite the subsequent analysis of the data.

3.1 Prior VLF Research Equipment

Prior to this experiment, measurements of perturbations in subionospheric VLF signals were performed using several types of commercially available VLF receivers, but these receivers had significant performance limitations. Most of the amplitude measurements were obtained with six-channel fixed frequency receivers built in the early 1960's by Develco, Inc. Although these receivers have proven to be excellent and durable, they are based on discrete Germanium transistor technology, are becoming unreliable with age, and spare parts are no longer readily available. In addition, a serious limitation of these Develco receivers is their fixed frequency design. It was impossible to retune a channel to another transmitter frequency without modifying filters (replacing inductors and capacitors) and replacing the crystal, a time consuming process.

The few existing phase measurements were obtained from slightly newer receivers built by Tracor, Inc. Although tuneable, these receivers were extremely complicated due to their age (mostly discrete transistor technology) and their intended purpose (long term frequency drift measurements, with rapid retuning to other signals). They were also failure prone, being old and having been modified and repaired many times over the years. In addition, since they were designed for long term drift measurements, as opposed to the measurement of fast perturbations in phase as required for Trimpi event studies, they required modification in a variety of ways in order to obtain higher time resolution phase data. Unfortunately, the modifications affected the stability and accuracy of the measurements, limiting the usefulness of the data collected.

An even greater limitation in the previously available VLF data sets was the means by which the data were collected and recorded. Amplitudes and phases were plotted on real-time analog charts. When interesting events were observed in real time, the operator would increase the speed and amplitude gain of the charts, but the charts were generally not monitored continuously, and this magnification could not be performed later. The quantity of higher resolution data was also affected by the subjective evaluation of the operator as to whether events were interesting enough. Higher resolution data were also obtained, in an intermittent manner, by recording the IF output of the receivers on analog recording tape, or by using detected amplitude and phase levels to drive VCO's (Voltage Controlled Oscillators) which were then recorded on analog tapes. These recordings were limited by the stability of analog tape recordings, and as with the higher chart resolution, tape recordings were performed only when the operator decided that the data merited recording.

Thus, the receivers in use lacked the flexibility to make amplitude and phase measurements on many different paths at many different sites. In addition, they required

a skilled technician capable of maintaining them on a regular basis. The recording systems in use provided only low resolution data on an automatic basis, and required continuous monitoring by a knowledgeable operator in order to obtain higher resolution information when interesting data were being received.

3.2 Digital Data Collection System

In order to address the requirements of flexibility, stability, high resolution, automatic operation, and easy post processing of the data, a new digital data collection system was developed by D. Shafer et al., at Stanford. This system was designed to collect a variety of analog signals, sample them at high resolution in both magnitude and time, and store the results in an easily analyzed digital form. Although the details of the design of this system are described elsewhere [Shafer, 1988], an overview is provided here.

The block diagram in Figure 3-1 provides an overall view of the data collection system. The first block in the system, contained in the A/D Interface, standardizes the incoming analog signals, so that all channels are presented to the computer in the same form. This circuit, repeated for each of the 16 channels supported by the data collection system, provides the following capabilities:

- Gain. The analog signal is scaled so that all channels provide the same level of output, between -5 V and +5 V.
- Detection. The amplitude of an AC signal, such as the IF output from a radio receiver, is detected, so that a slowly varying signal, proportional to the average amplitude of the IF signal is provided.
- Antialiasing. The signal is filtered so that variations in signal that occur rapidly compared to the digital sampling rate do not distort the recorded results.

- Offsets. A constant DC offset is added to shift the signal so that it can cover the entire available range of -5 V to +5 V.

Each of these capabilities can be selected or bypassed, to match the characteristics of each individual signal.

The A/D Interface also contains a timing circuit that generates the clock signal used to control the sampling of the data signals. This clock signal is derived from an external, stable frequency reference, and is synchronized to Universal Time (UT) using a signal received from the National Bureau of Standards (NBS), via the GOES satellite.

The 16 standardized analog signals and the sampling clock are then sent to the Analog to Digital Converter in the computer. This circuit, under the control of the computer, samples the analog signals, one at a time, and stores the result as a 12 - bit digital value in the range 0 to 4095, representing -5 V to +5 V. Each of the 16 channels is sampled 100 times per second, but the sampling is not uniformly distributed over each hundredth of a second. Instead, to maximize the simultaneity of the samples, once every 10 msec., all sixteen channels are sampled as quickly as possible, taking less than 160 μsec. to collect the samples. The remainder of the time is used to process and store the samples. The individual samples for each channel are averaged in programmable amounts yielding data collection rates between one and 100 Hz.

The computer then labels the data with precise time information (typically < 1 ms error) obtained via satellite from the NBS, and stores the result on digital recording tapes. The 1600 bpi, 2400 ft. tapes can typically store between eight and 24 hours of data, depending upon averaging rates selected. These tapes contain all of the data collected, with high resolution in both magnitude and time, and are used for subsequent analysis.

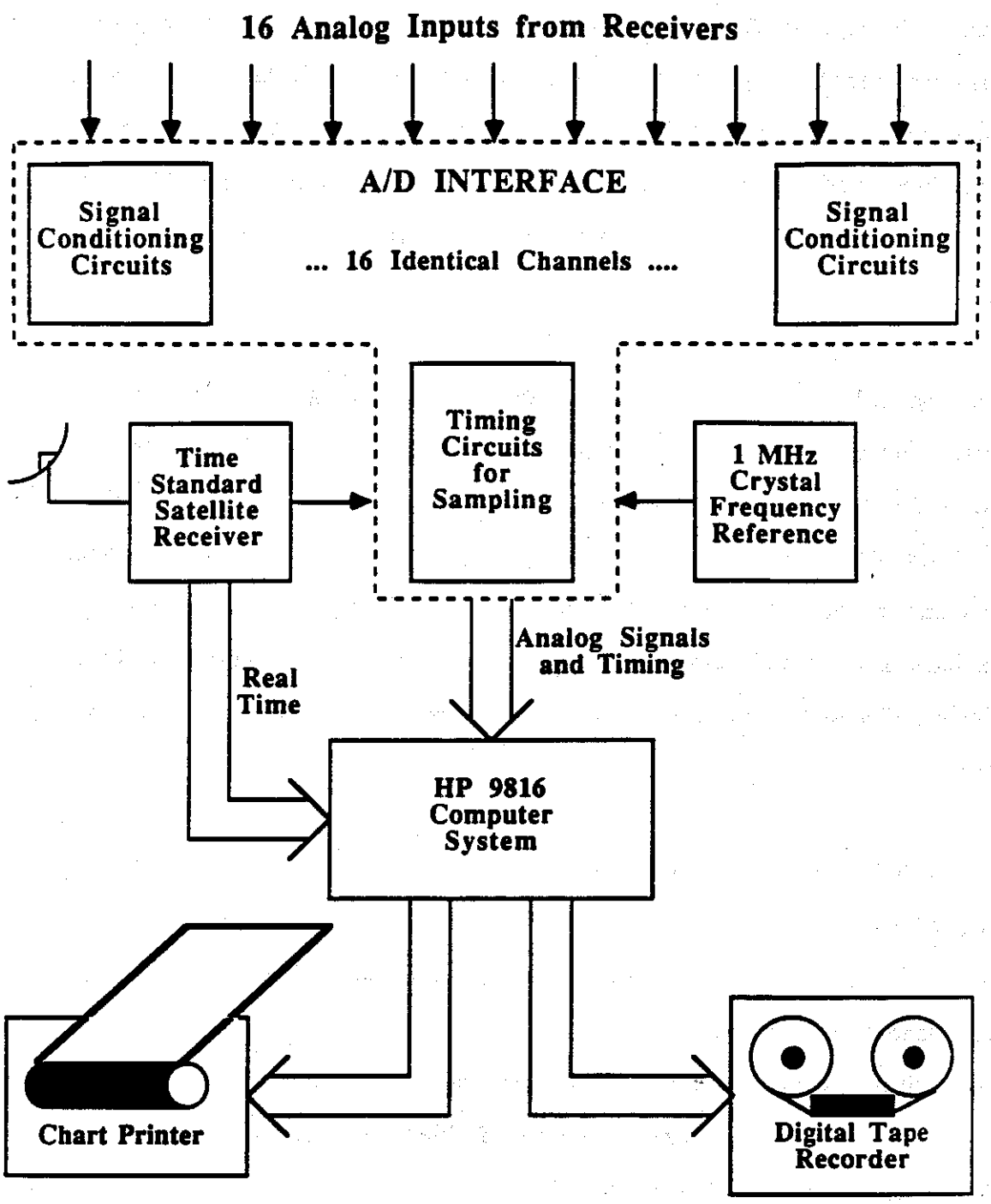

Figure 3-1 Digital Data Collection System. A block diagram of the data collection system, showing key features. The A/D Interface contains circuits to standardize the incoming analog signals and provide timing for the digital sampling. The computer samples the 16 signals, and stores the results on magnetic tape, as well as low resolution plots. Precise timing is obtained from a satellite receiver.

Because of the large volumes of data that can be collected in this manner, two additional features were added to the computer system. One of these is a scheduler built into the software for the computer allowing it to be programmed to collect data only during selected time periods. At most sites, this feature was used to limit the data collection to nighttime periods when perturbations are known to be more common [Leyser et al., 1984].

The second additional feature was the capability of generating low time resolution summary plots of the recorded data on the computer printer. To do this, software was generated that would simulate an analog strip chart recorder output on the printer. Each channel was further averaged to approximately 8 seconds per data point, and plotted with several channels per page. These charts, typically 15 to 20 pages per night, provide a visual index into the high resolution data stored on tape. Periods of interest could be readily identified on the summary plots and then analyzed in detail, using the data stored on tape.

Thus, this digital data collection system, developed by Shafer, provides the following new capabilities:

- Data collection at high resolution - one part in 4096 in magnitude and up to one hundredth of a second in time.
- Simultaneous measurements on up to 16 channels.
- Data storage in a computer readable form to facilitate subsequent processing.
- Low resolution summary plots of the data.
- Reliability, ease of operation, and minimal operator intervention.

3.3 Typical Radio Receiver

In addition to the improved data collection system, this experiment required the development of an improved VLF receiver that was tuneable, reliable, and capable of measuring both amplitude and phase on a variety of signals. In order to maximize the maintainability, and minimize the design effort, this new VLF receiver design was based upon standard radio receiver designs, but was adapted to meet the specific requirements of subionospheric VLF propagation research. The basic function of any radio receiver is to isolate one single signal from a large band of similar signals, and to detect the desired information contained in that signal. To accomplish this a typical modern radio receiver is built as shown in the block diagram in Figure 3-2, and functions as described below [Smith, 1986].

Starting at the antenna, the signal is first amplified by the preamplifier, so that the signals of interest are substantially stronger than any noise introduced by the receiver. Then all frequencies received that are not of interest are attenuated using a band pass filter. It is important that this filtering be performed as early in the receiver as possible, in order to minimize the possibility of strong undesired signals saturating (or overloading) the receiver and causing intermodulation or distortion. To further suppress undesired signals and other distorting effects, this filter is usually tuneable and is made just wide enough to pass the desired signal with its modulation sidebands, but not so narrow that precise tuning is required. Once the signals have been limited to a narrow band around the desired signal, further amplification is performed by the RF (Radio Frequency) Amplifier, in order to boost the desired signal to the level required by the next stage.

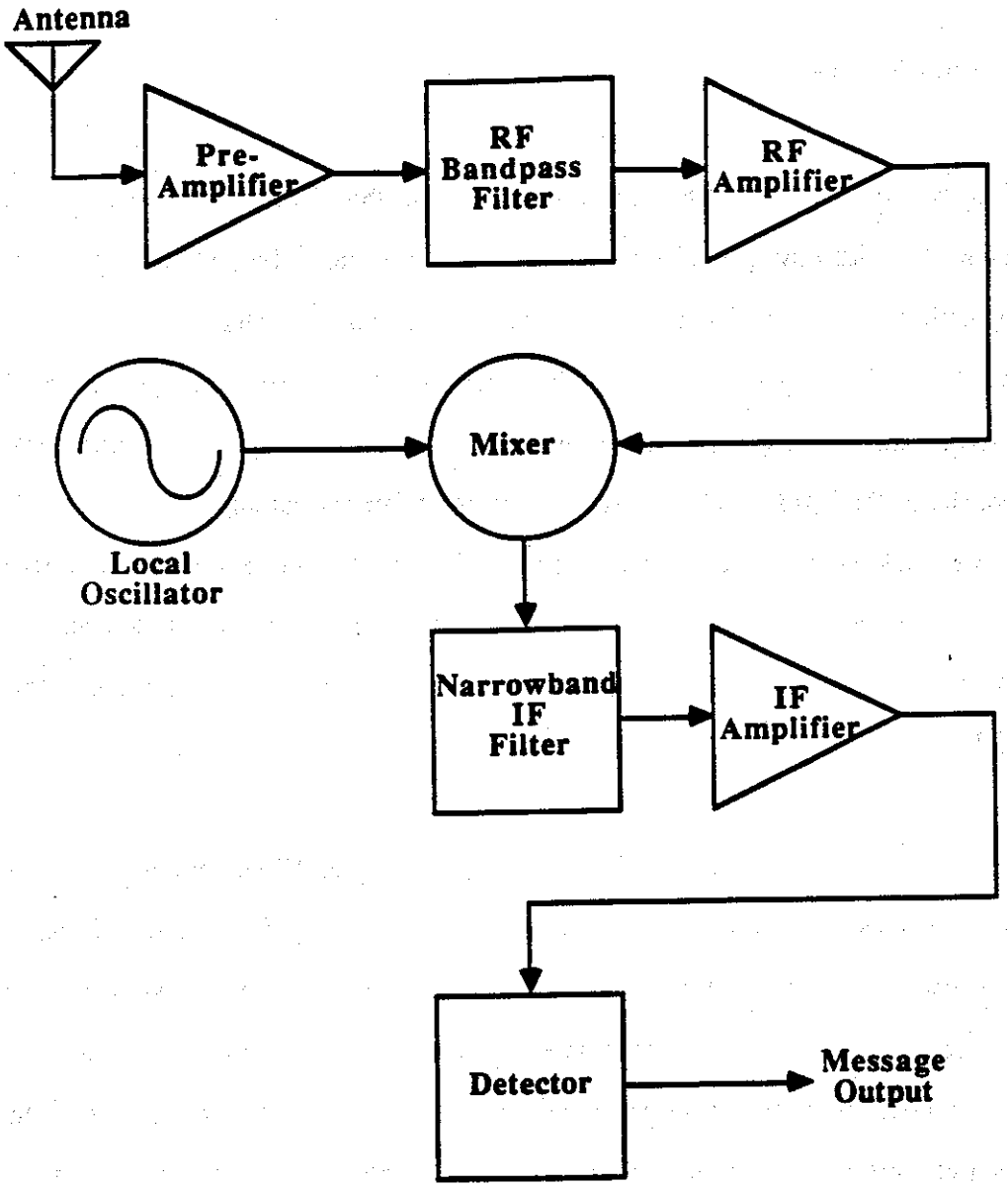

Figure 3-2 Block Diagram of a Typical Radio Receiver. The major components in the design of a typical radio receiver are shown [Smith, 1986].

Early low frequency receivers stopped at this point, but modern receivers use a design called superheterodyne to improve the performance of the receiver and allow much higher frequency capability. The performance of the RF stages described above is limited by the wide frequency range required. The RF filter must be tuneable over the entire frequency range of the receiver, so it is difficult to make the filter stable, narrow enough,

and sharp enough to successfully select a single signal in a crowded radio band. The RF Amplifier performance is also limited by the requirement that it operate stably over the entire frequency range of the receiver. To avoid these limitations, a superheterodyne receiver translates the desired signal to a fixed (usually lower) frequency, called the Intermediate Frequency. This translated signal is then filtered and amplified further using the fixed frequency Intermediate Frequency (IF) Amplifier and IF Filter.

Frequency translation is accomplished by utilizing the trigonometric identity that the product of two sinusoids of different frequencies has two frequency components; one at the difference between the two frequencies and one at the sum of them. Also, if the first of these sinusoids is constant in amplitude and phase, then the sum and difference signals will have amplitudes and phases that track the amplitude and phase of the second sinusoid. Thus, a superheterodyne receiver has a tuneable Local Oscillator (LO) that generates a signal at a frequency (ω_{LO}) which is offset from the incoming desired signal by the fixed IF frequency (ω_{IF}). This local oscillator signal is then mixed (multiplied) with the incoming signal (ω_{RF}), after the RF stage, and the result is two signals, one at the IF frequency ($\omega_{RF} - \omega_{LO} = \omega_{IF}$), and the other at approximately twice the incoming signal frequency ($\omega_{RF} + \omega_{LO} = 2\omega_{RF} + \omega_{IF}$). This sum signal, and any residual portion of the original RF signal that leaks through the mixer, are rejected by the IF filter, so that only the desired signal, shifted to the IF frequency is left for subsequent processing.

While this superheterodyne technique improves the receiver performance by allowing fixed, low frequency filtering and amplification at the IF stage, it does introduce several complications. The first of these is that the local oscillator must be extremely stable. Any noise, or fluctuations in the amplitude, frequency, or phase of the LO will appear as noise in the received signal. In addition, the LO usually does not generate a pure sinusoid, but instead produces some harmonics, or multiples, of the desired frequency as well. These

harmonics can mix with other signals coming from the antenna (at frequencies of $N \times \omega_{LO} \pm \omega_{IF}$), causing additional undesired signals at the IF frequency. Finally, the mixing and IF filtering is insensitive to the polarity of the frequency difference, so the LO signal, when mixed with the incoming signals, will select not only the desired signal at $\omega_{LO} + \omega_{IF}$, but also any undesired signal at $\omega_{LO} - \omega_{IF}$. This undesired signal is referred to as the image signal, and can be minimized by using more sophisticated mixer designs. Interference from both the image signal and any undesired harmonic signals can be further reduced by a well designed RF filter stage which prevents these signals from reaching the mixer. A more effective method of eliminating interference from both the image and the harmonics of the LO is to use an IF frequency that is higher than the highest desired RF signal frequency. This means that both the image frequency and the harmonics are outside the desired tuning range of the RF system, so the RF filter need not be tuneable, and the LO signal need not be spectrally pure. The drawback of this approach is that the IF system must operate at a much higher frequency, and therefore requires more expensive components, more careful design, and more sophisticated test equipment.

Once the desired signal has been isolated from the rest of the frequency spectrum, the final task of the receiver is to detect or demodulate the signal. This involves extracting the desired information, which is slowly varying compared to the radio signal, from the carrier signal itself. For communication purposes, the information can be contained in the variation of amplitude (AM), frequency (FM) or phase (PM) of the signal, and which of these modulation schemes is used will determine what type of detector is required.

3.4 Tuneable VLF Research Receiver

Although this superheterodyne receiver design was used for the new VLF research receiver, there are a number of unique considerations that enter into the design of a receiver for VLF propagation research instead of for communication or navigation purposes. These considerations impose different requirements on some of the components in the block diagram of the receiver.

The first of these considerations is the wide tuning range desired for the receiver. Trimpi events have been regularly observed on signals ranging from the Omega transmitters near 10 kHz [Leyser et al., 1984] up to AM broadcast band signals near 1 MHz [Carpenter et al., 1984]. Many receivers are commercially available for the more common communication frequencies above 200 kHz, so this receiver was designed to cover the range of 10 - 100 kHz, with the possibility of operating as low as 2 kHz, in order to accommodate the research transmitter at Siple Station, Antarctica. The additional requirement that the receiver be capable of accurately measuring phase, suggested that the tuning be performed digitally for better precision. This combination of digital tuning and wide tuning range, implied that it was not practical to design a tuneable RF filter to cover the range, and still reject strong out of band signals such as LORAN navigation transmitters at 100 kHz and nearby AM broadcast stations starting at 540 kHz. Instead, the RF filter was designed as a fixed bandpass filter, passing the entire range of interest (10 - 90 kHz), and suppressing all signals outside this range. To accomplish this, a 2 - pole high pass filter at 10 kHz is used to reduce signals at 1 kHz by 40 dB, and a 6 - pole low pass Bessel filter at 90 kHz attenuates 100 kHz signals by 60 dB, and all higher frequencies by at least 40 dB.

This decision to simplify the RF filter imposed further constraints on the LO, since the RF filter did not limit the presence of signals near harmonics of the LO frequency. One solution, as described earlier, would have been to place the IF frequency above the desired RF range, but this was rejected in favor of simplicity. An IF stage above 100 kHz would have required custom passive IF filters instead of simple active filters, and would have required a second mixer and IF filter stage to translate the frequency down to a low frequency for phase measurement. The alternative was to design the Local Oscillator so that its harmonic content was minimal. In order to maximize the phase resolution, while keeping the IF frequency well outside the RF signal band, an IF frequency of 1 kHz was chosen. Clearly, for RF signals near 100 kHz, the harmonic content of the LO would not be a problem since the second harmonic of the LO (at 99 kHz) would be at 198 kHz, well outside the RF pass band. However, if the desired signal were at 10 kHz, the LO would be at 9 kHz. Under these conditions, an LO harmonic at 18 kHz, for example, could mix with 19 kHz or 17 kHz signals (which would pass through the RF filter), causing additional interfering signals at the IF frequency of 1 kHz. Since the 12th harmonic of the lowest LO frequency (9 kHz) is outside the pass band of the RF filter, it was necessary that the LO substantially suppress at least the first 11 harmonics of its signal.

The desire to make high time resolution phase measurements imposed a second requirement on the Local Oscillator. The frequency to which the LO was tuned would have to be precise, or the slight difference in frequency between the LO and the received signal would appear as a rapid drift in the phase measurement. In addition, the LO would have to have very low phase noise, to avoid introducing noise into the phase measurements. In order to address all of these requirements, a unique Local Oscillator was designed, as shown in Figure 3-3. The precision frequency requirement was met by using a Phase Locked Loop (PLL) circuit to lock the LO signal to an external 1 MHz frequency reference. The frequency reference was obtained from an ovenized crystal oscillator that was periodically (a few times per month) adjusted to the precise frequency.

The PLL circuit uses a Voltage Controlled Oscillator (VCO) to generate a signal at 200 times the desired LO frequency. This VCO frequency is divided by a variable amount to obtain a fixed frequency of 5 kHz. The external reference is also divided down to 5 kHz and the two 5 kHz signals are compared. Any difference in frequency or phase between the two signals causes an error voltage which is used to correct the voltage to the VCO.

Thus, once the loop stabilizes, the VCO runs at a constant frequency and phase, where the frequency is determined by the divider ratio between the VCO and the 5 kHz comparison frequency. The ratios were chosen so that the LO could be tuned precisely over the frequency range 9 to 101 kHz in 25 Hz increments. Further detail on the operation of this Local Oscillator is available in the *VLF Phase Receiver Preliminary Operating and Service Manual* [Wolf, 1988].

To solve the additional problems of low phase noise and low harmonic content, the VCO operates at 200 times the desired LO frequency. This division by 200 automatically reduces the phase noise of the VCO by a factor of 200 [Smith, 1986], yielding typical peak phase noise of less than 0.2° (comparable to the resolution of the 12 - bit analog to digital converter). The division by 200 is implemented as a divide by 8 followed by a divide by 25 so that this last division can be used to generate a 25 point digitally synthesized sinusoid. This 25 - point per cycle synthesis, using 8 - bit resolution decreases the first 11 harmonics by at least 58 dB.

To simplify the circuitry, the functions of the digital sinusoid synthesis and the mixing with the RF signal are combined in a Multiplying Digital to A[illegible]og Converter (MDAC). This single integrated circuit scales an analog input (the RF signal) by a fraction, determined by the digital inputs (in this case the values of the LO sinusoid), yielding an analog signal that contains the product signal. This simple mixer does not perform any

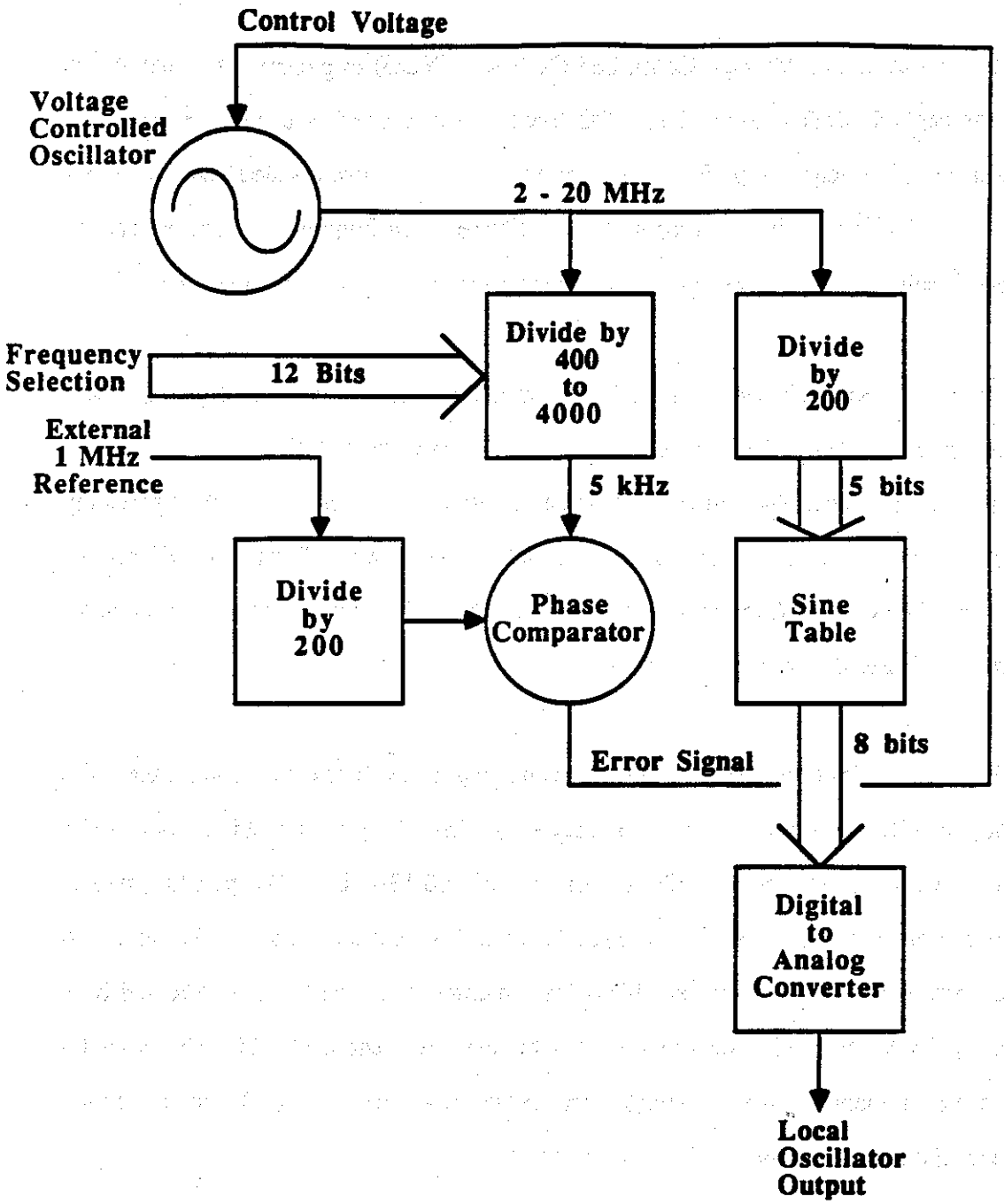

Figure 3-3 Block Diagram of the Local Oscillator. A simplified block diagram of the Local Oscillator portion of the new VLF Research Receiver. The PLL locks the oscillator to an external precise 1 MHz reference for high stability. Phase stability and low harmonic content are achieved, as explained in the text, by operating the oscillator at 200 times the desired frequency.

image rejection, but the VLF band of interest is not crowded with transmitter signals, so interfering images were not expected to be a problem. Instead, the LO was designed so that the operator could select whether the LO was above or below the desired signal, on the assumption that at least one of the two choices would generally not have an interfering image signal. While these assumptions about the VLF band are valid, they did not allow for the possibility of locally generated interference. Electronic equipment such as computers, and especially video terminals generate many weak coherent signals in the VLF band, and if located near the experimental receiver, these signals can interfere with reception. These local signals tended to cause an interfering image problem at some receiving sites using high technology equipment such as Stanford University. To solve this problem, a modified mixer was developed that suppresses image signals by up to 40 dB. The original receivers were deployed at sites such as Palmer Station, Antarctica that do not have a significant interference problem.

After the Local Oscillator signal is mixed with the RF signal, a narrow IF filter, with a 3 dB bandwidth of 500 Hz, is used to isolate the desired IF signal, and reject all other mixer products. This bandwidth is chosen so that it passes the entire spectrum of the modulation on the VLF signals with constant amplitude. The IF signal is amplified further, and then directed to the A/D Interface, described above, for amplitude detection. This IF signal is also supplied to the Phase Detector circuitry shown in Figure 3-4 and described below.

Most of the signals being studied are modulated using a digital frequency modulation scheme called Minimum Shift Keying (MSK) [Carlson, 19[illegible] MSK is derived from the more familiar FSK (Frequency Shift Keying), where two different frequencies are used to represent the two digital bits. To minimize the transmission of spurious signals, and the stress on the transmitter, FSK signals usually switch frequencies only on zero crossings

in the RF signal; thus, each of the two frequencies completes an integral number of cycles in one bit time. As a result, if one of the frequencies completes N cycles in a bit time, the narrowest bandwidth FSK signal would have the other frequency complete N + 1 cycles in one bit time. MSK further reduces the signal bandwidth by completing N and N + 1/2 cycles per bit time in the two frequencies. This still allows switching bits on zero crossings, but now, in order to maintain phase continuity, each of the two frequencies must be available at two phases 180° apart. As a result, when MSK signals are received, there are two possible frequencies, and each frequency has two possible phases, depending upon the message in the signal [Carlson, 1986].

To eliminate this 180° phase ambiguity in the received signal, the IF signal is multiplied by itself in a second mixer, doubling the frequency to 2 kHz. After doubling, the signal will alternate between two nearby frequencies, typically 100 Hz apart, with typical bit durations of 5 msec., representing the binary data being sent in the message. At this point, in order to perform phase measurements, the signal must be demodulated and the phase measured separately on each of these two frequencies.

For simplicity, this receiver selects just one of these two frequencies and measures the phase on it using a very narrow filter (3 dB bandwidth of 60 Hz). A Phase Locked Loop is used to further filter and average this one frequency, and also to act as a "flywheel", maintaining the phase measurement when the received signal is momentarily on the other frequency. This averaged 2 kHz signal is then compared in phase to a 2 kHz reference derived from the external 1 MHz signal, yielding the desired slowly varying signal proportional to the phase difference between the incoming signal and the reference.

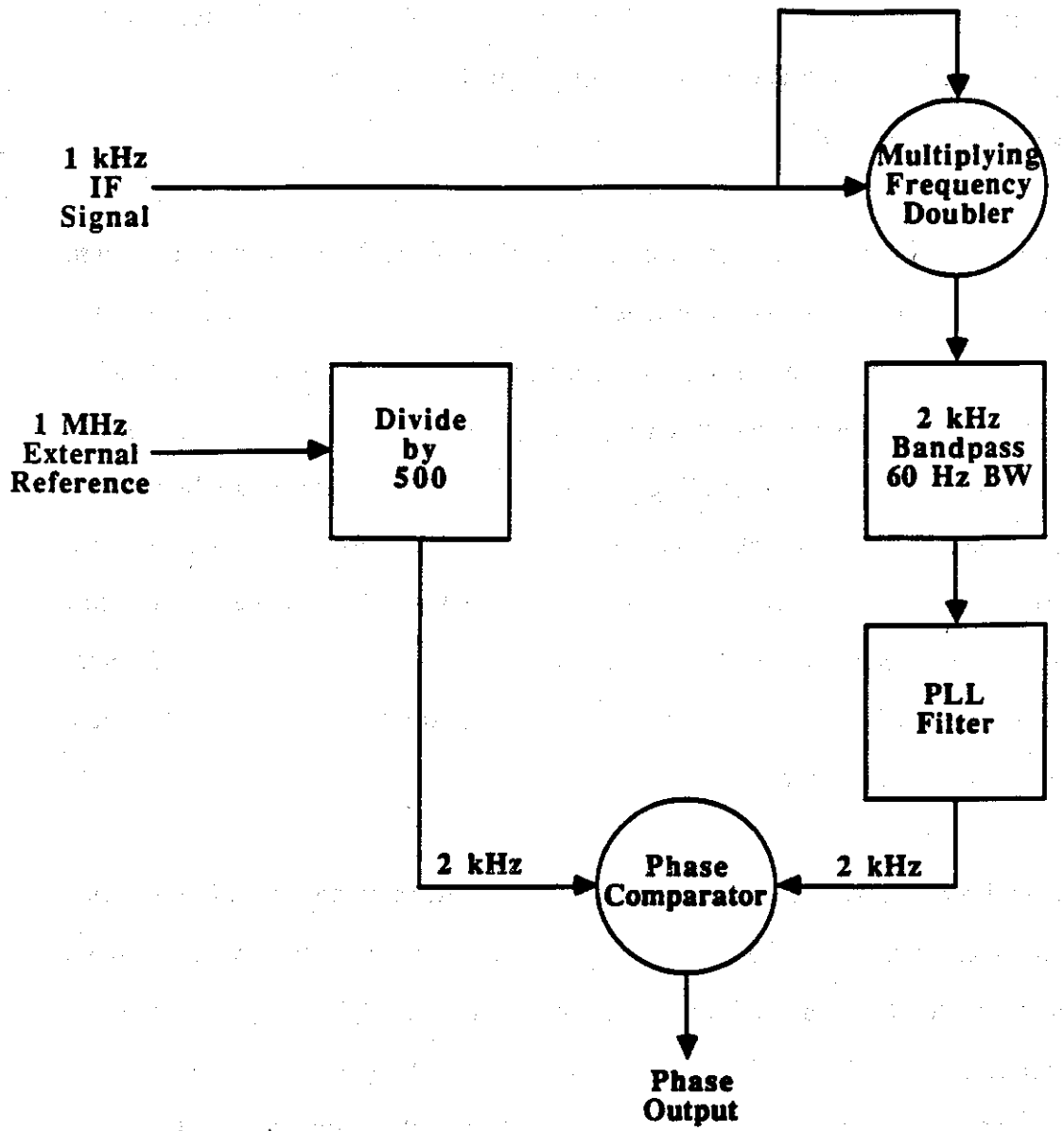

Figure 3-4 Block Diagram of the Phase Detector. A simplified block diagram of the Phase Detector portion of the new VLF Research Receiver. The narrow band filter and PLL isolate and track a single side band of the modulated signal, doubled in frequency. The phase of this signal is then compared to a reference 2 kHz signal derived from the external 1 MHz oscillator.

The step response of the phase detector is determined by the integration time in the PLL and represents a compromise between the ability to track the phase of a weak, noisy signal, and the desire to measure the detailed timing of Trimpi events. To maximize the flexibility of this compromise, this integration time is manually adjustable between 20

and 100 msec. This permits the operator to set the receiver for the maximum step response possible while still tracking the received signal. All step responses are specified as 10% - 90% rise times, and have less than 5% overshoot.

Another aspect of the design that is unique to VLF research receivers is the noise performance. For most communication receivers, low noise design is required, so that the receiver does not generate noise that would overwhelm a weak signal of interest. For subionospheric VLF research, this is not a severe constraint; experience has shown that, in general, many VLF signals exceeding the noise (within 200 Hz signal bandwidths) by 20 to 30 dB can be found at each observing site. In addition, atmospheric noise external to the receiver is strong, implying that even a moderately low noise receiver design, when used with a low noise preamplifier, can render receiver noise insignificant. Another factor affecting receiver noise performance is that the atmospheric noise in the VLF range is not Gaussian in nature [Field and Lewinstein, 1978].

The external noise at VLF frequencies consists of two strong components. One of these components is man - made coherent signals. This interference can be other radio transmitters in the band, or accidental transmitters such as high voltage power lines, video terminals, computers, and other electronic equipment that inadvertently radiate in this frequency range. These signals can be very strong, but are typically confined to a limited band of frequencies, so while they may overwhelm one desired signal, they are not likely to affect other nearby signals of interest.

The other dominant noise component is radio atmospherics, as described in Section 2.1.3. These lightning - generated radio frequency impulses can be much stronger than the desired signal, but are very short in duration [Field and Lewinstein, 1978]. In some areas, such as the eastern United States in summertime, these atmospherics can occur tens or hundreds of times per second, nearly continuously obscuring the desired signals. Because

the atmospherics are so strong, suppression of them must be built into the receiver. A receiver that does not carefully limit the effect of atmospherics will most likely experience saturation and other nonlinear effects when strong impulses are received. These nonlinear effects can then cause intermodulation or other subtle forms of distortion on received signals of interest. Eliminating such distortion is particularly important in studying transient phenomena such as Trimpi events. Intermodulation could cause an event at one frequency to couple into a second frequency, yielding a false correlation between events at two frequencies. Saturation could result in a temporary alteration of the receiver gain, causing a false Trimpi event, or distorting the temporal signature of the recovery of an actual event. Thus, while low noise performance is not critical for a VLF receiver, atmospheric impulse suppression is very important. To achieve this, fast responding clipper circuits (turn on time < 1 μsec.) were employed to limit the impulsive energy reaching the detectors.

An overall block diagram of the tuneable VLF receiver described above is shown in Figure 3-5, and the performance specifications of this new receiver are listed in Table 1. The features that make it uniquely suitable for subionospheric VLF propagation research are as follows:

- The Receiver is tuneable over a wide frequency range.
- The Local Oscillator is phase stable and has low harmonic content, allowing accurate phase measurements.
- The IF filter is wide enough to minimize feedthrough of modulation into amplitude measurements.
- The Phase Detector filter has a narrow enough bandwidth to select a single sideband component for phase measurement.
- Fast responding clipper circuits minimize overloads caused by impulsive noise such as atmospherics.

- The construction is modular to provide a multichannel, low cost unit that is reliable and easy to operate and maintain.

Table 1 - Receiver Performance Specifications

Frequency Range:

3 dB Response:	10 - 90 kHz
20 dB Response:	2 - 98 kHz

Receiver Bandwidth (3 dB):

Amplitude Measurement (IF):	500 Hz
(6-Pole, 0.1 dB Chebyshev Filter)	
Phase Measurement:	60 Hz
(4-Pole, Butterworth Filter)	

Dynamic Range:

Adjustable RF Stage Gain:	58 dB
Adjustable IF Stage Gain:	70 dB
No Automatic Gain Control at IF Stage	
20 dB Automatic Gain Control in Phase Detector	

Transient Response (10-90% rise time):

Amplitude (typical):	10 ms
(depends upon external detector)	
Phase (typical):	20 ms
(adjustable up to 100 ms)	

Phase Tracking Performance:

Minimum SNR in 300 Hz BW:	16 dB
Tracking on One Side Band Only	

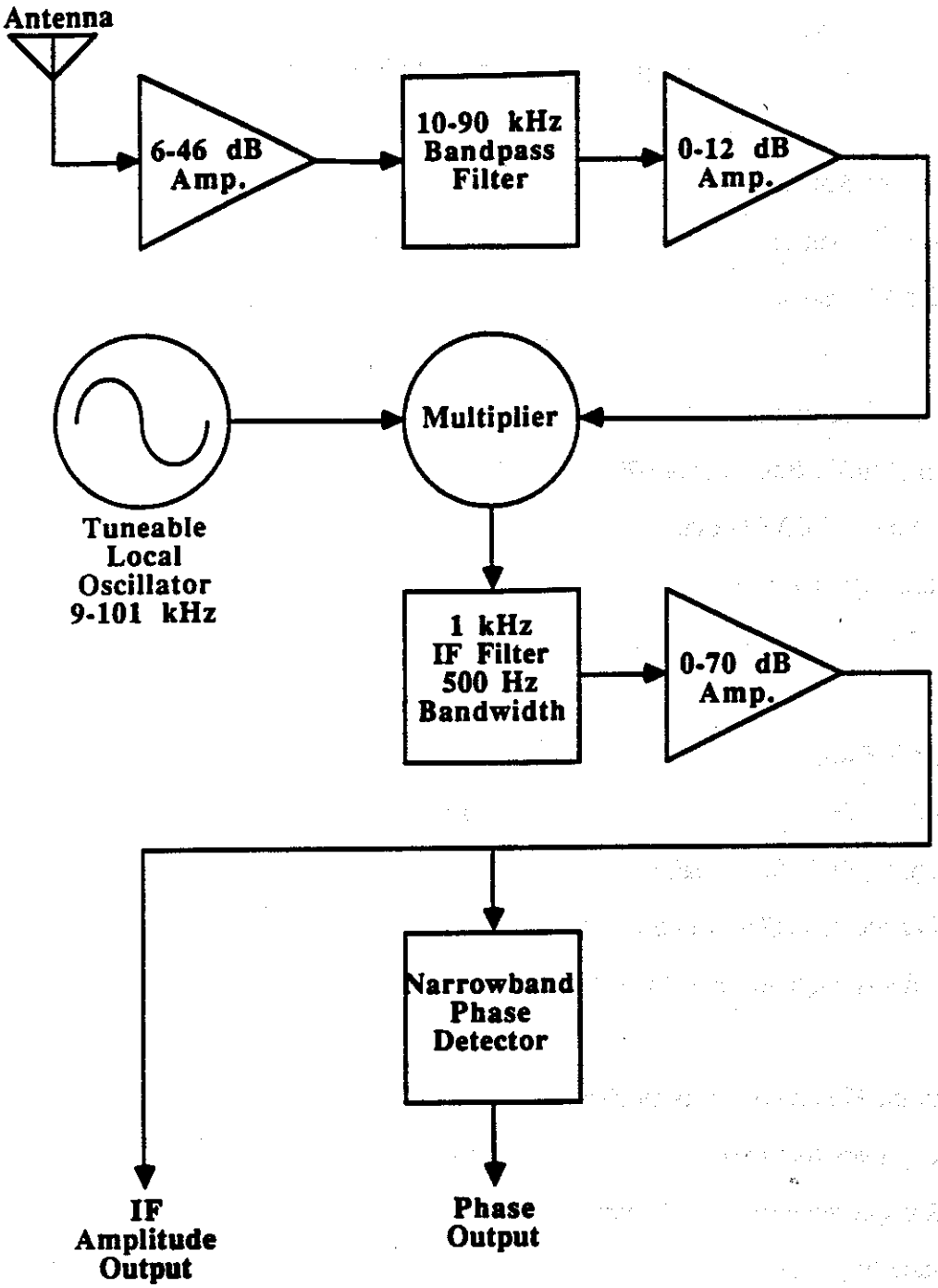

Figure 3-5 Block Diagram of the VLF Receiver. A simplified block diagram of the new VLF Research Receiver. Similarity to the typical receiver shown in Figure 3-2 is obvious. Some of the unique features of this receiver are described in the text.

Chapter 4 - Data Analysis

One of the objectives of this experiment was to compare occurrence rates and magnitudes of perturbations (both in amplitude and phase) in propagation data collected from several sites over extended periods of time. Therefore, it was imperative that a procedure be developed that would identify and measure perturbations in a consistent manner. The procedure developed to provide reliable results involved a number of separate steps, beginning with recognizing and correcting known instrumental errors, and ending with the measurement of the size and temporal signature of each event.

4.1 Instrumental Effects

The limited accessibility of the Antarctic dictated a rapid development schedule, so final testing of the new hardware was left until after field deployment. Once data collection began, it became apparent that the phase data contained several instrumental effects (such as rapid excursions in the measured phase through a full cycle before returning to the measured value) which had not been visible in laboratory tests of the phase receiver. While improvements in the design were being developed, the already deployed receivers were being used to collect research data, despite the instrumental effects. These effects have been attributed to two factors that were expected to complicate phase data, but could not be adequately simulated in the laboratory during system development, without specialized test equipment.

The first of these complications is the presence of modulation on the received signal. The VLF communication signals being measured typically convey binary information by switching between two different near-by frequencies using MSK (Minimum Shift Keying) modulation. However, to avoid the complication of demodulating the signal, the

phase receiver was designed to track the phase of only one of these frequencies at a time. To measure the effect of this rapid switching to a near-by, undesired frequency during receiver development would have required the purchase of an expensive MSK modulated synthesizer, or the development of specialized test equipment, neither of which was possible within the constraints of this project. Thus, it was not until complete system integration after field deployment that the consequence of this switching was fully realized.

The effect of impulsive atmospheric noise on phase measurements was the second complicating factor which was not fully realized before deployment. These impulses, or atmospherics, described in Section 2.1.3, are the radio signatures of lightning strokes and can have broadband intensities that are substantially stronger than the signal being investigated. The time signature of these impulses is variable and difficult to simulate, but receiver circuitry was designed to limit the magnitude of these impulses, as discussed in Section 3.4.

Both of these complications appear as sudden large changes in the incoming signal, which might momentarily obscure the phase of the desired signal. The phase measurements are obtained using an extremely narrow band (60 Hz) Phase Locked Loop circuit, as described in Chapter 3. In order to achieve the desired high time resolution, this loop was only marginally stable, and so could momentarily lose the signal when sudden changes in the signal occurred. To minimize these effects in the future, portions of the receiver have been redesigned to further reduce the influence of both modulation and atmospherics. However, a large and important database has been collected containing these instrumental effects, so software was developed that could scan the collected phase data, recognize and isolate instrumental effects, and where possible correct them.

4.1.1 Phase Switching

The instrumental effects that obscure the phase data fall into two general categories: cycle slipping, and phase switching. Phase switching is a consequence of the use of a dual range in the phase output. The phase receiver resolves phase only over a half cycle (180°) range, but phase data are inherently cyclic in nature, and as the phase reference drifts with time, the measured signal phase drifts through 180° and back to 0°. The measured data have noise superimposed on them, causing them to fluctuate around the true phase value. As a result, when the data get near 180°, they can fluctuate rapidly between near 0° and near 180°. This rapid switching across the full measurement range would obscure any useful information in the data, so a technique was required that would minimize this switching. The solution was to have the phase receiver provide the measurement over a full cycle range, -180° to 180°, with the two half cycles being equivalent. As above, the first time the measurement exceeds 180°, it will switch to the equivalent point near 0°. Now, however, this point is in the middle of the measurement range, so the measurements can fluctuate around 0° without switching back to 180°. Thus, a single smooth transition is made from 180° to 0°, even in the presence of noise.

This dual range capability in the phase output leads to occasional phase switching. Every measured phase value now has two points in the output range that correspond to the measurement, and the selection of which of these two points is used is based upon the history of the data, as stored in the circuitry. Sudden changes in the signal, such as strong bursts of noise or switching to the other modulation frequency, can obscure this stored history, causing the output value to abruptly switch to its equivalent point, differing by 180°. Thus, the dual range capability is a compromise that avoids rapid full scale swings when the data are near the extremes, but allows occasional rapid half scale swings elsewhere in the data, triggered by random, sudden changes in the received signal. Although possible at any point in the data, phase switching is most common with weak

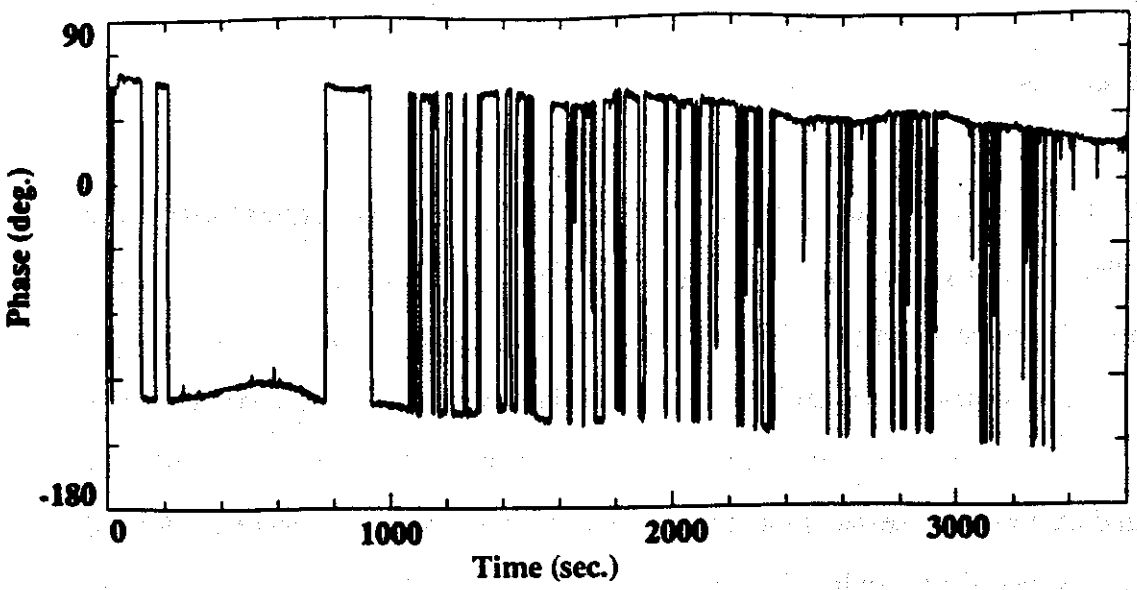

Figure 4-1 An Example of Phase Switching. Phase data (plotted as 1.28 sec. averages of 50 Hz samples) containing an example of the instrumental effect called phase switching, where the phase measurement abruptly jumps from one value to an equivalent one 180° away. These data are from the NSS to Stanford path, starting at 08:00:01 UT on 16 March 1987.

signals, and near the extremes of the measurement range (-180° and 180°). An example of this phase switching found in the data is shown in Figure 4-1.

4.1.2 Cycle Slipping

Cycle slipping is a result of using a Phase Locked Loop (PLL) circuit to track the phase of the incoming signal. A PLL has an internal oscillator that is continually adjusted to keep it synchronized (or locked) with the incoming signal. This locking to the signal allows some filtering and averaging to be performed on the phase of the incoming signal, by limiting the rate at which the PLL can respond to rapid changes in phase caused by noise. The PLL oscillator also serves as a storage element, maintaining the phase of the desired incoming frequency component when the modulation causes the signal to switch momentarily to the other frequency.

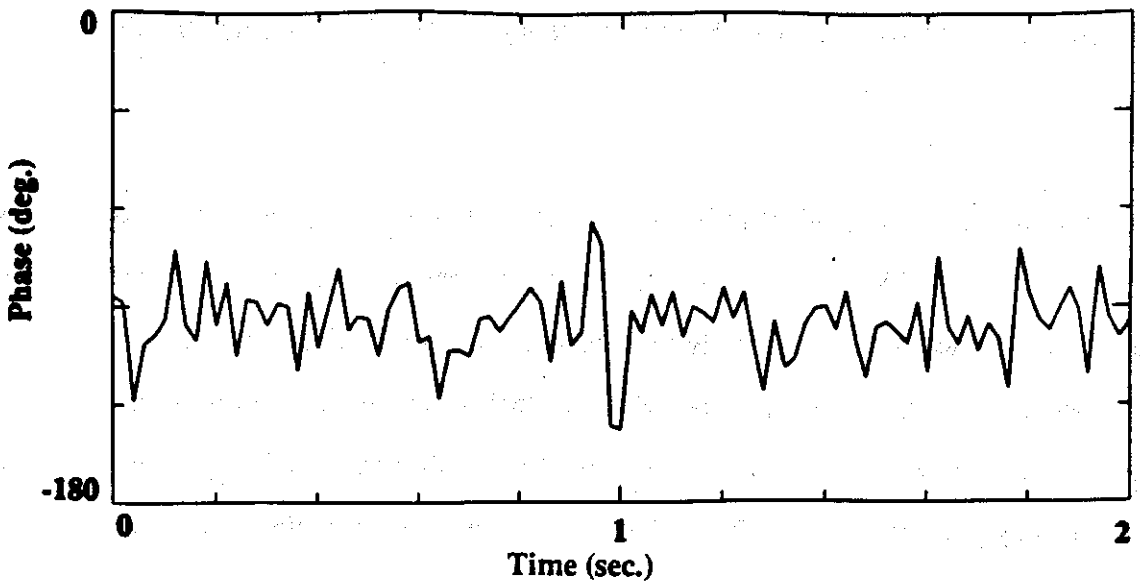

Figure 4-2 An Example of Cycle Slipping. Phase data containing an example of the instrumental effect called cycle slipping, where the phase measurement abruptly loses lock on the signal and drifts through one cycle before locking onto the signal again. At 0.9 sec. after the beginning of this graph, the phase measurement suddenly advances rapidly to 0°, switches to -180°, and continues advancing through one cycle, returning to the correct phase measurement when again locked onto the signal. Note that the fast slipping of the phase compared to the data sampling rate of 50 Hz prevents the recorded data from reaching to the extremes of 0° and -180°. These data are from the NPM to Palmer path, starting at 04:01:18 UT on 12 May 1988. Individual 20 ms data samples are plotted.

While improving the phase tracking capability of the receiver, the PLL introduces the complication of cycle slipping. Since phase is measured on the PLL oscillator which is locked to the incoming signal, it is possible for the circuit to momentarily lose lock, allowing the oscillator to drift off in frequency, thereby causing the phase measurement to drift. This can be caused by a brief loss of the incoming signal, a burst of noise that alters the averaging information stored in the loop filter, or by an input data stream that keeps the modulated signal on the untracked frequency for an extended period of time. When the loop loses lock, it rapidly drifts through one or several complete cycles of phase before it relocks to the signal. It is also possible for the loop to start to drift out of

lock, and then quickly recover and lock back onto the signal after drifting only 20 - 30° off in phase.

As with phase switching, cycle slipping is most common with weak signals (such as at dawn and dusk), but unlike phase switching, it is frequently not apparent in low resolution data. The measurement typically loses lock, drifts through a full cycle or two and relocks within 0.1 sec., and remains locked at least half of the time. As a result, low resolution plots of the averaged data show a smooth and steady line resembling correct data. Unfortunately, this average is shifted off of the true value by the cycle slipping and so is affected by the duty cycle of the locked versus unlocked times. At high resolution, cycle slipping is readily recognized by its high slope (change in phase with time), and by the fact that it always completes an integral number of cycles and returns to the previously measured phase value. When observed in real time, cycle slipping can be eliminated by adjusting the receiver gain to boost the signal strength into the phase detector, proving that it is an instrumental effect. An example of cycle slipping found in the received data is shown in Figure 4-2.

4.2 Correcting Instrumental Effects

The software developed to correct these instrumental effects does so by performing several tests on the data. First and most importantly, it recognizes and corrects the phase switching, by selectively translating data points up or down by 180°, to maintain the continuity of the averaged phase record. In addition, the software identifies individual data samples that are part of patterns that match the instrumental effects (and that therefore are likely to be erroneous samples), and excludes them from any data analysis. Finally, it uses nonlinear filtering techniques to recognize and eliminate any incorrect

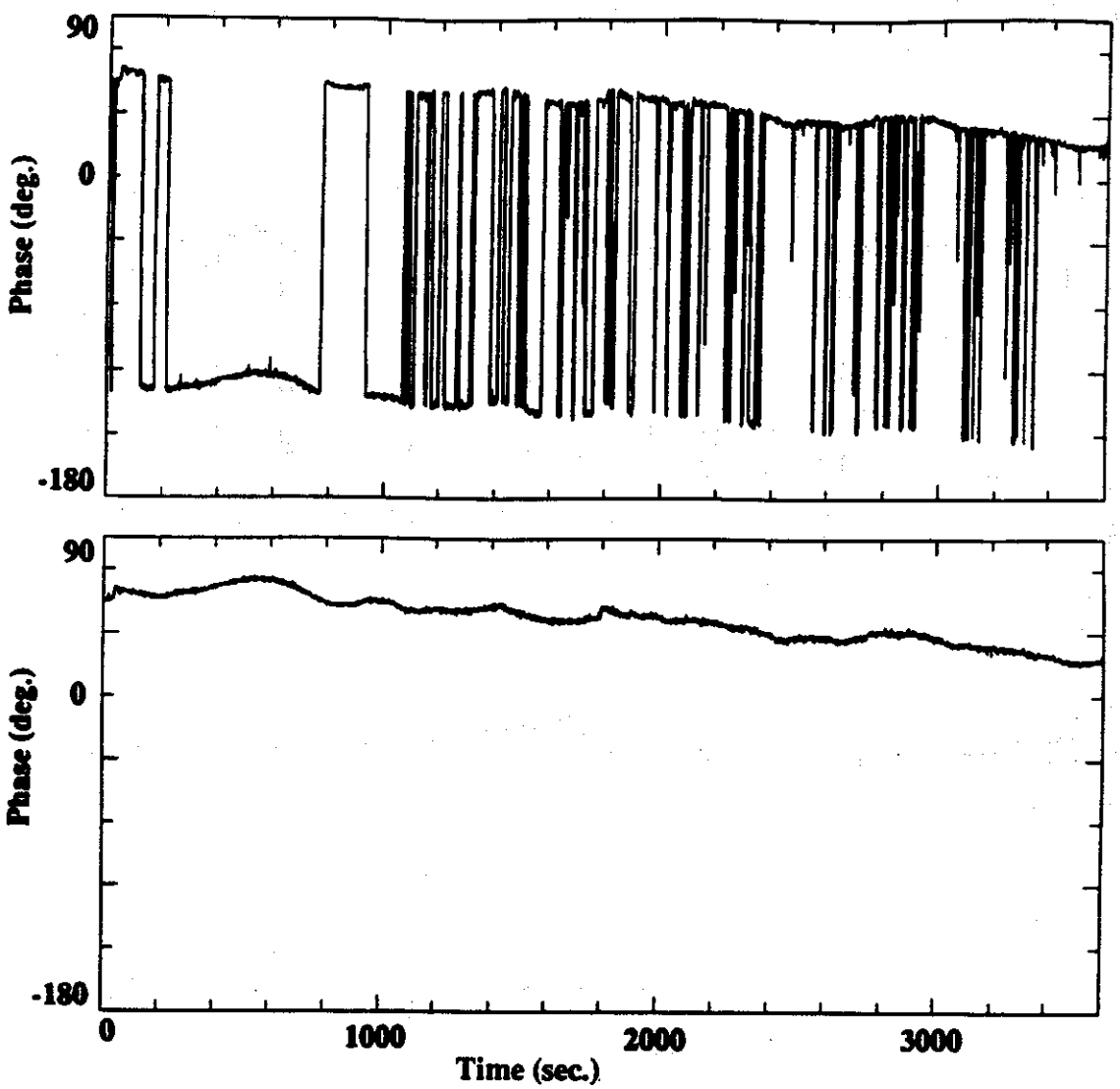

Figure 4-3 Correction of Phase Switching in the Phase Data. A demonstration of the ability of this software to correct the instrumental effect called phase switching, and improve the continuity of the phase data. The top panel contains phase data as recorded. The lower panel shows the same data after phase switching and other instrumental effects are eliminated. These data are from the NSS transmitter, as received at Stanford University, starting at 08:00:01 UT on 16 March 1987. In both panels, 1.28 sec. averages of 50 Hz data samples are plotted.

samples that are the result of cycle slipping. The recognition of these instrumental effects is complicated by the filtering and averaging of the measurements that is performed by

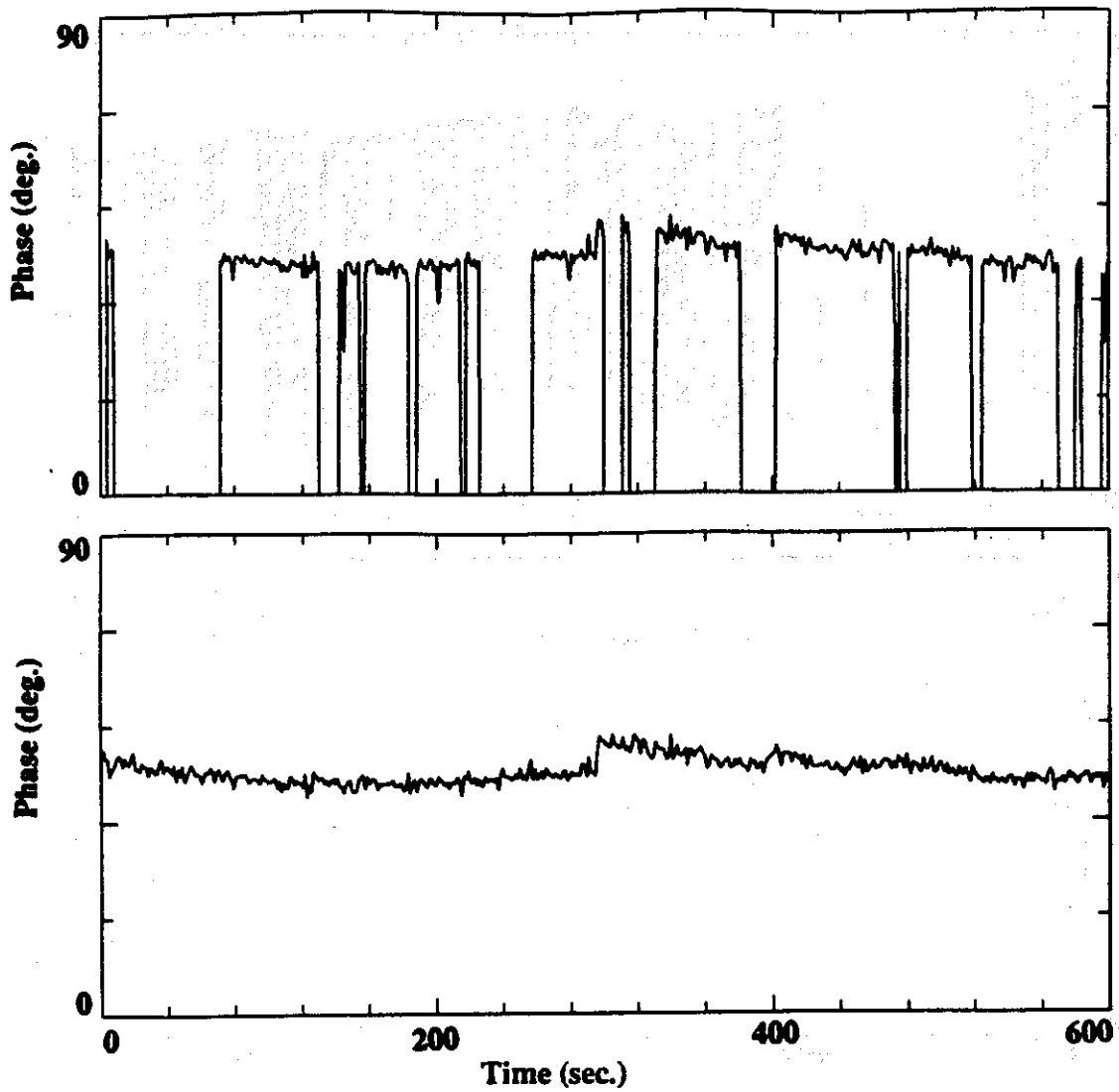

Figure 4-4 Ability of Data Correction to Reveal Events. An enlargement of the central portion (near 1800 sec.) of the plots in Figure 4-3. Even at this higher resolution, the event at ~ 300 sec. is hard to recognize in the uncorrected data (top panel), but is clearly visible in the corrected data (lower panel). These data are from the NSS transmitter, as received at Stanford University, starting at 08:25 UT on 16 March 1987. In both panels, 1.28 sec. averages of 50 Hz data samples are plotted.

the data sampling system before the data are recorded. Both the phase switching and cycle slipping occur rapidly (large phase swings at rates of 1000° / sec. lasting for

~ 0.1 sec.) in comparison to real data changes, but these effects are slowed down by averaging in the recording system, and may not be apparent at all in low resolution plotted data.

The software recognizes phase switching by creating two consecutive one second windows and then scanning these windows through the data. The data points in each of the windows are averaged together and the two averages are compared. If the two averages differ by at least 150°, all subsequent data, starting with the second window is translated up or down by 180° to provide for more continuous data. These phase switches typically occur almost instantly (within a few milliseconds), but the averaging in the sampling system causes them to take approximately 0.1 sec. in the recorded data. As a result, the data samples collected during this transition have erroneous values between the two equivalent phase values. The presence of these intermediate values complicates the detection of phase switches because adjacent windows will not differ by 180°, but instead will differ by a lesser amount depending upon the number of erroneous intermediate values present in each window. To avoid this problem, the two windows used for averaging were separated by a gap of 0.1 sec. When a phase switch was located, the points within this gap were then marked as erroneous and unusable points, since they lay between the two possible correct phase values and their correct value could not be determined. An example of the effectiveness of correcting phase switching is shown in Figures 4-3 and 4-4.

Two different limiting techniques were employed to minimize the distortion of averaged data by both cycle slipping and impulsive noise. First a dynamic limiter was developed that would maintain a running five minute average of the data samples, and limit any individual data samples to less than 20° (the largest phase event found in this analysis was 16° and events larger than 10° are rare) on either side of this average (any samples

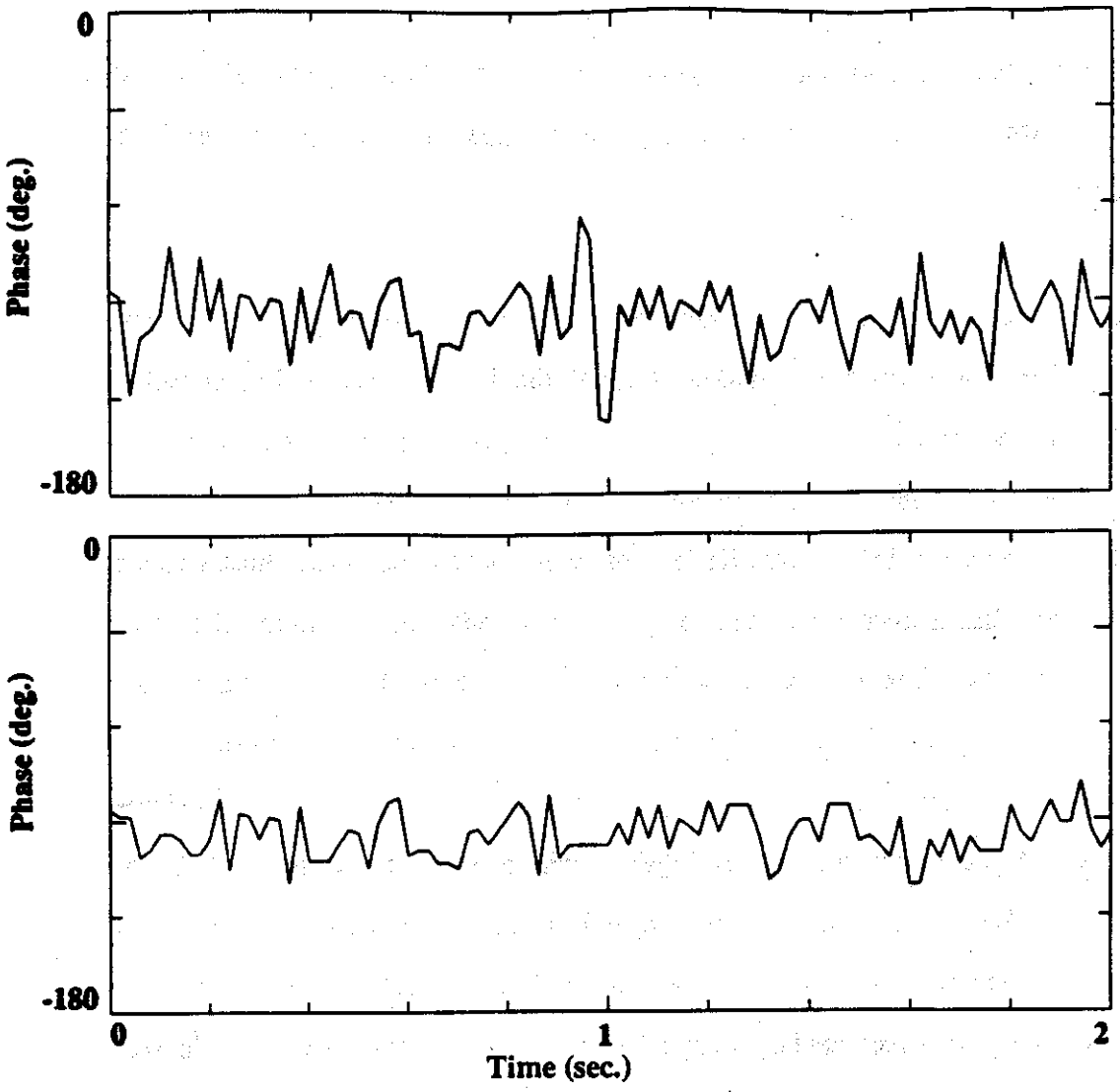

Figure 4-5 Correction of Cycle Slipping in the Phase Data. An example of the ability of this software to correct the instrumental effect called cycle slipping, and improve the continuity of the phase data. The top panel contains phase data as recorded. The lower panel shows the same data after correction of instrumental effects. Note that the correcting program simply marks suspicious data samples with a flag. How this information is utilized is up to the user. This particular plotting program replaces the suspicious samples with the last acceptable sample value (so suspicious areas become horizontal line segments). These data are from the NPM transmitter, as received at Palmer Station, starting at 04:01:18 UT on 12 May 1988. Individual 20 ms data samples are plotted in both panels.

outside this range were limited to ±20°, and marked as erroneous). The second limiter is a slope limiter. The cycle slipping was found to have a substantially greater slope than any

real data effects, so the software recognizes any sudden steep slopes (slopes in excess of 600° / sec.) and marks all points on the steep slope as erroneous.

Note that this program only marks suspicious data with a flag; it does not replace them with other values or alter them in any way. For this analysis, data were generally plotted at relatively low resolution, with many data samples averaged together. In this application, the averaging program was written to exclude any suspicious samples from the average, providing a more accurate average. When data were examined at high resolution, the suspicious points were plotted in a different color, making it clear that they were suspect, but allowing the user to decide how to use the information. The ability of this program to identify cycle slipping is illustrated in Figure 4-5.

This series of tests and corrections was found to successfully improve the detection of VLF phase perturbation events without causing any false perturbations. As further protection against inadvertently creating false events, all data samples that were corrected by the software were marked with identification flags so that the original data could be recovered if necessary. The corrected data set could then be averaged and plotted instead of the original data providing a substantially clearer view of the phase data, as seen in Figures 4-3, 4-4, and 4-5. A listing of the program that achieves this appears in Appendix B.

4.3 Event Recognition

Once the technique for correcting instrumental effects in the phase data had been developed, it was possible to analyze all of the amplitude and phase data in a systematic and consistent manner. It was not practical to correct and replot all of the phase data collected, but cycle slipping typically would not obscure event occurrence, it would only

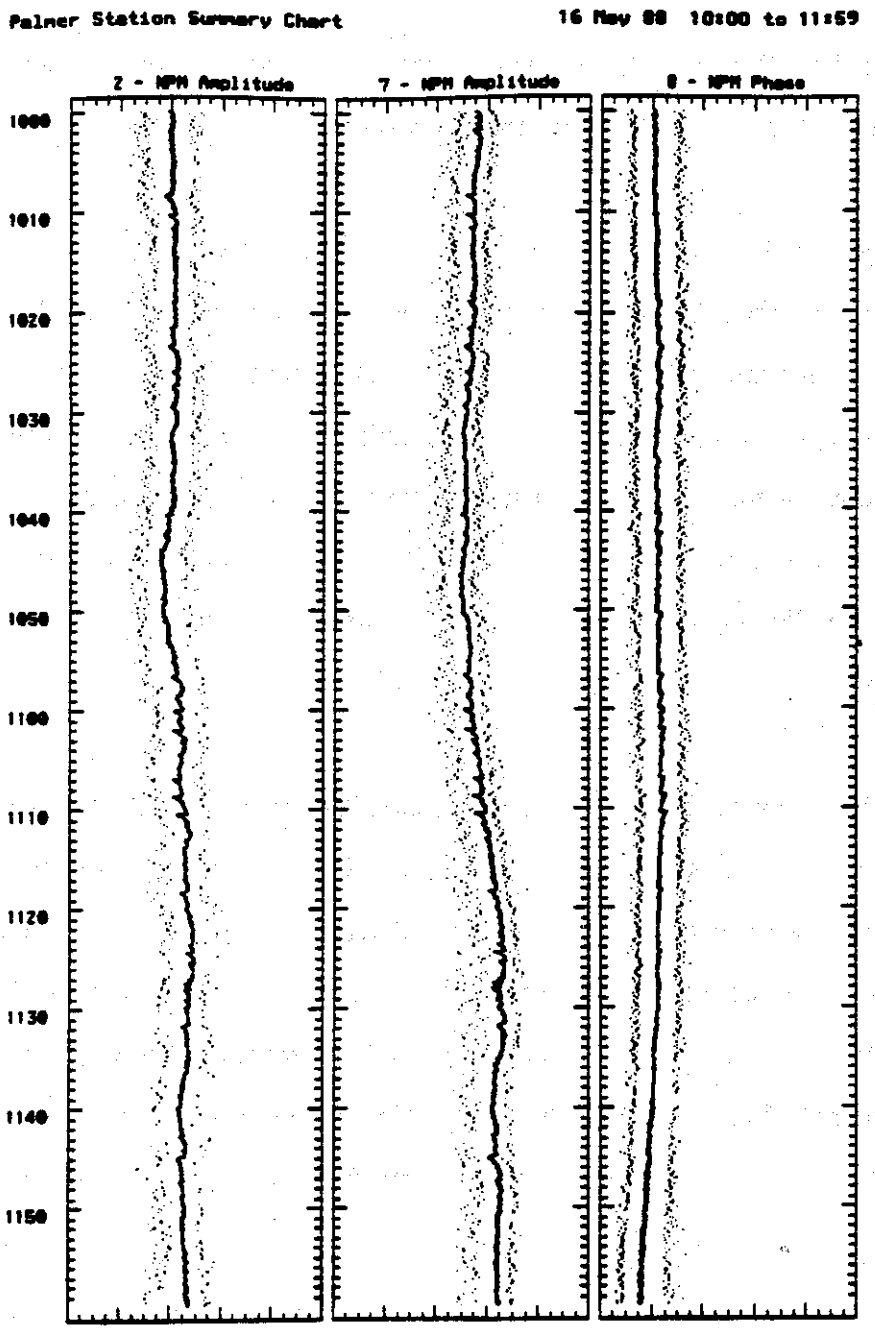

Figure 4-6 Example of Low Resolution Data. Low resolution digital plots (resembling analog charts) such as this are generated when the data are collected, as a graphical index into the data. The right panel contains the phase of NPM as received at Palmer, and the left two panels contain the corresponding amplitude (from two different receivers). In each panel, the solid line represents 1 sec. averages of the sampled data (50 Hz sampling on the right two panels and 20 Hz sampling on the left panel). At this scale, events can be recognized but not measured. These data start at 10:00 UT on 16 May 1988. For publication here, the original chart was reduced to 68% of full size.

distort the event magnitude. Phase switching could obscure events, as demonstrated in Figures 4-3 and 4-4, but occurs relatively infrequently, and typically lasts for less than 15 min. at a time. Thus, the procedure used for event recognition was as follows:

First, all of the low resolution summary plots, generated by the data collection system, such as that shown in Figure 4-6 were reviewed, and periods of time (typically several hours long) that appeared to have characteristic perturbations (the specific criteria are defined below) in either amplitude or phase were identified. Since the majority of these events were very small perturbations and the low resolution graphs were printed with several channels per page, it was difficult to resolve the magnitude and the characteristic shape on these graphs. Instead all of the time periods identified as having possible activity in this first step were processed by the phase correcting program and then replotted at much higher resolution, using the high resolution data recorded on the magnetic tapes. The replotted data used an amplitude range of 15 - 25% of the full scale range used on the original graphs, and a typical phase range of 72°, as compared to 360° on the original graphs. In addition, the time axis was expanded by a factor of two, to one hour per page, and only a single receiver (one amplitude and one phase channel) were plotted on each page. This replotting effectively magnified the plotted area by a factor of 15 to 20, making it possible to consistently recognize events and measure them with a resolution of 0.1 dB in amplitude and 0.5° in phase. 0.64 sec. time averaging was used in the replotted data, in order to provide smoothing of the data and to maximize the consistency of the perturbation magnitude measurements. An example of these replotted data is shown in Figure 4-7.

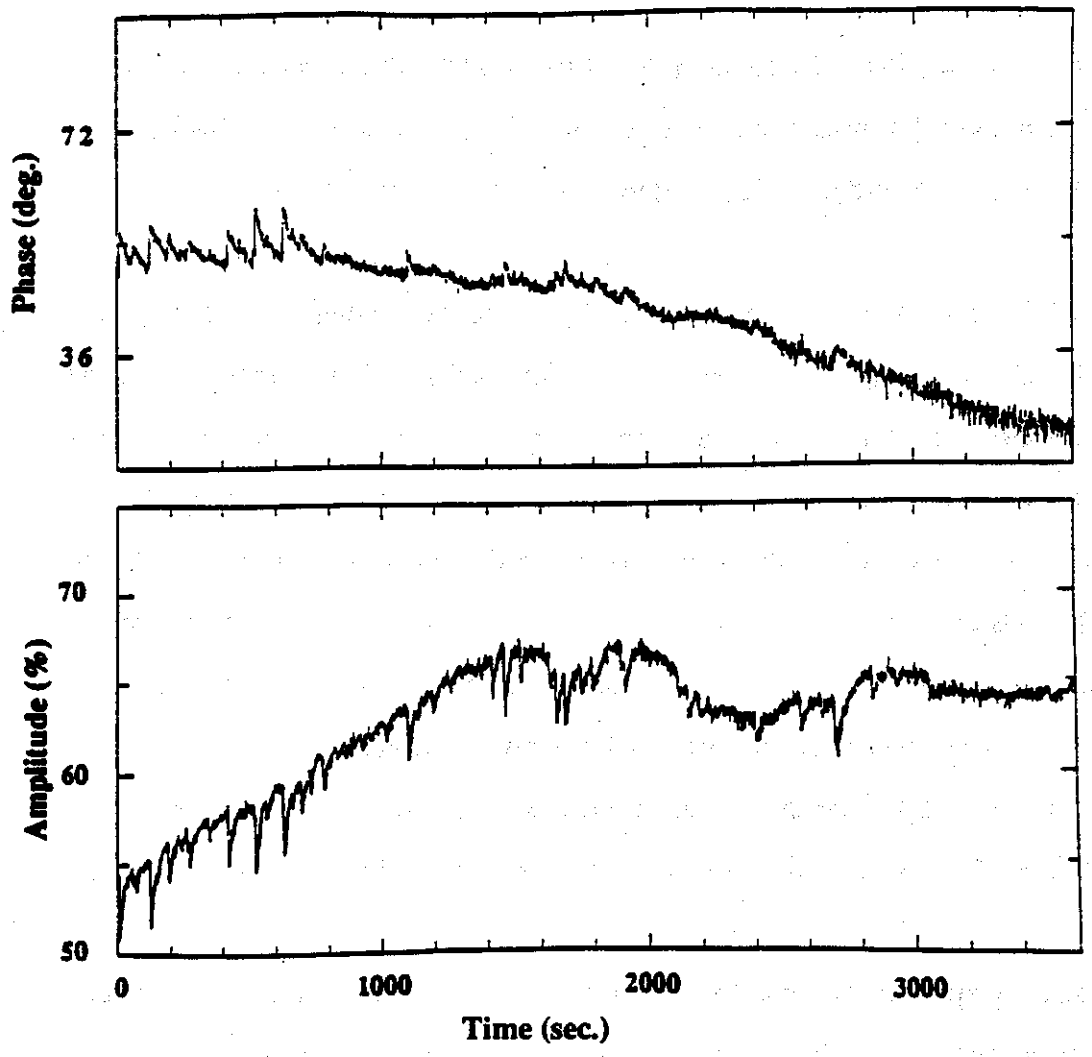

Figure 4-7 Example of High Resolution Replotted Data. The second hour of the data shown in Figure 4-6 is replotted here at higher resolution; using 0.64 sec. averaging of the 50 Hz samples. On this scale, events and their magnitudes are clearly recognizable. These data start at 11:00 UT on 16 May 1988. For publication here, the original plot, used for measuring events, was reduced to 85% of full size.

After the data were plotted in this manner, the next step was to identify all events. As described in Chapter 2, the classic Trimpi event involves an abrupt change in amplitude or phase occurring over a period of approximately 0.1 to 2 second, fo ed by the signal recovering to pre-event levels in 10 to 100 seconds [Inan and Carpenter, 1986]. In typical received data, other, longer term ionospheric and magnetospheric effects cause changes

in the measured amplitude and phase of VLF signals. Thus, most events do not return to the actual pre-event levels, but instead to a projected level the signal would have reached at that time if the event had not occurred. Taking this character of the signals into account, the criteria for recognizing an event were formulated as follows:

- Either the amplitude or the phase of the signal has an abrupt change, of at least 0.1 dB or 0.5°, occurring within two seconds.
- The signal returns to a subjective visually extrapolated pre-event level over a time of 10 to 200 seconds.

These criteria were found to consistently identify characteristic events, but probably allowed a small fraction of poorly defined events to pass undetected and not be included in the data analyzed. In particular, during periods when the signals exhibited other rapid fluctuations, it was often impossible to recognize a return to pre-event levels. It should be noted, however, that these occurrences were uncommon and appeared with equal frequency on amplitude and phase and on all channels analyzed, so that the statistical results comparing the behavior of different signals would not be expected to be altered, by the omission of these questionable events.

The size of each of the identified events was determined by manually measuring the magnitude and polarity of the change in both amplitude and phase. It was found that measuring the pre-event and post-event levels and then taking the difference introduced substantial errors, while measuring the pre-event level and the magnitude of the change provided consistent results. Thus, for each event, five quantities were tabulated: the time of occurrence, the pre-event amplitude, the change in amplitude, the pre-event phase, and the change in phase. This table of events was subsequently analyzed for patterns in the relative occurrence of amplitude and phase events on different paths.

4.4 Description of Data Coverage

The data used in this analysis were limited to that collected with the phase receiver described in Section 3.4, in order to assure the consistency of the results. Prior to July 1988, when this analysis began, the receiver design had been deployed at various times at four different sites: Lake Mistissini, Quebec; Stanford University, California; Wallops Island, Virginia; and Palmer Station, Antarctica. Of these four sites, however, the deployment at Wallops Island was brief, and data collection at Lake Mistissini was limited by hardware difficulties, so only Stanford and Palmer provided substantial data sets suitable for statistical analysis. As a result, the data base for this analysis consists of all data that were collected using the new phase receiver at these two sites through July 1988. The characteristics of this set of transmitters and receivers is listed in Table 2 and their locations and propagation paths are illustrated in Figure 4-8. The specific properties of the paths analyzed are described below.

4.4.1 Data Acquired at Palmer Station, Antarctica

Due to Antarctic logistics constraints for data retrograde, the only data available from Palmer Station were from April and May 1988. However, since Palmer Station (at 65° S, 64° W, and L = 2.4) is in a region of very high event activity [Carpenter and LaBelle, 1982] these two months provided substantial quantities of usable data. At Palmer Station, simultaneous amplitude and phase data were collected on four different signal paths and all of them were analyzed. These paths were selected for monitoring on the basis of their known characteristics, such as adequate signal strength and substantial perturbation activity.

The first two of these paths to Palmer Station are quite similar in many ways. The signals originate at the NSS transmitter in Annapolis, Maryland (transmitting at 21.4 kHz), and the NAA transmitter in Cutler, Maine (transmitting at 24.0 kHz), so the paths will be referred to as NSS - PA and NAA - PA, respectively. Both of these signal paths start on the east coast of the U.S., and travel south over the Atlantic ocean and the Caribbean sea. From there, they cross the length of the South American continent, including much of the Andes. These are both long paths, 11579 km and 12161 km, respectively, with the first third over water and the remaining two thirds over rough land. Both paths were monitored for eleven days in April, and there were a total of 22 events on NAA and 28 events on NSS.

During the month of May, two paths from the western United States were monitored. The first of these, referred to as NLK - PA, originates at the NLK transmitter in Jim Creek, Washington (transmitting at 24.8 kHz). This path crosses the western states, including the mountains and deserts, and then enters the Pacific ocean off the coast of Mexico. From there, the path stays over the Pacific all the way to Palmer Station. Thus, the first third of this 13506 km path is over rough land, and the remainder is over ocean. This path yielded 33 events during the 18 days it was monitored.

The fourth path to Palmer Station, also monitored during this 18 day period in May, originates at the NPM transmitter in Lualualei, Hawaii (transmitting at 23.4 kHz). This path, referred to as NPM - PA, traverses the Pacific ocean for 12335 km to Palmer Station, entirely over sea water. The NPM - PA path had been found to be quite active in the past [Inan and Carpenter, 1987], and exhibited 578 events during the 18 days that it was monitored. Because of this high number of events, this path was used to study some of the finer details of event characteristics, for example the variation of characteristics with time, and the variation of amplitude events with corresponding phase events.

4.4.2 Data Acquired at Stanford University

Data have been collected with systems at Stanford (37° N, 122° W, L = 1.8) since November 1986, but on a sporadic basis, whenever field systems were being developed or tested. The majority of the data collected would come from the period between the completion of a system development and its deployment at a remote field site. As a result, there are many gaps in the collection schedule, but over the year and half that systems were being developed (November 1986 to July 1988), a reasonable quantity of data had been collected on four signal paths.

Of these four paths to Stanford, the highest frequency one is at 48.5 kHz, and originates at an Air Force transmitter located in Silver Creek, Nebraska, whose call sign is unknown. This path (48.5 - SU) covers a rather short, 2160 km path over rough mountainous terrain, and was monitored only infrequently. It was observed for a total of 8 days during November 1986, and July 1988, and only 15 events were observed.

A second short mountainous path (NLK - SU) that was monitored at Stanford was the one that originates at the NLK transmitter in Jim Creek, Washington (transmitting at 24.8 kHz). This path is only 1220 km long and was monitored in June and July of 1988. During this 44 day period, 61 events were found.

A longer path received at Stanford was the one originating at the NAU transmitter (transmitting at 28.5 kHz), in Aguadilla, Puerto Rico. This path (NAU - SU) was monitored for 57 days in March through May, 1988, and produced 92 events. The path is 5726 km long and crosses the Gulf of Mexico, and then the southwestern United States, and so is lying above about half water and half land.

Table 2 - Characteristics of the Signal Paths Analyzed

Transmitter	Freq. (kHz)	Receiver	Distance (km.)	Months Analyzed	Total Days	Active Days	Number Events
NSS	21.4	Stanford	3964	Nov-May	136	9	141
NAU	28.5	Stanford	5726	Mar-May	57	5	92
NLK	24.8	Stanford	1220	Jun-Jul	44	4	61
"48.5"	48.5	Stanford	2160	Nov,Jul	8	1	15
NPM	23.4	Palmer	12335	May	18	11	578
NLK	24.8	Palmer	13506	May	18	1	33
NSS	21.4	Palmer	11579	April	11	2	28
NAA	24.0	Palmer	12161	April	11	4	22

The path monitored at Stanford that provided the most events was the one that originates at the NSS transmitter (21.4 kHz) in Annapolis, Maryland. This path (NSS - SU) traverses the entire United States, from coast to coast and is 3964 km long. It was monitored for 136 days from November 1986 to May 1987, and yielded 141 events.

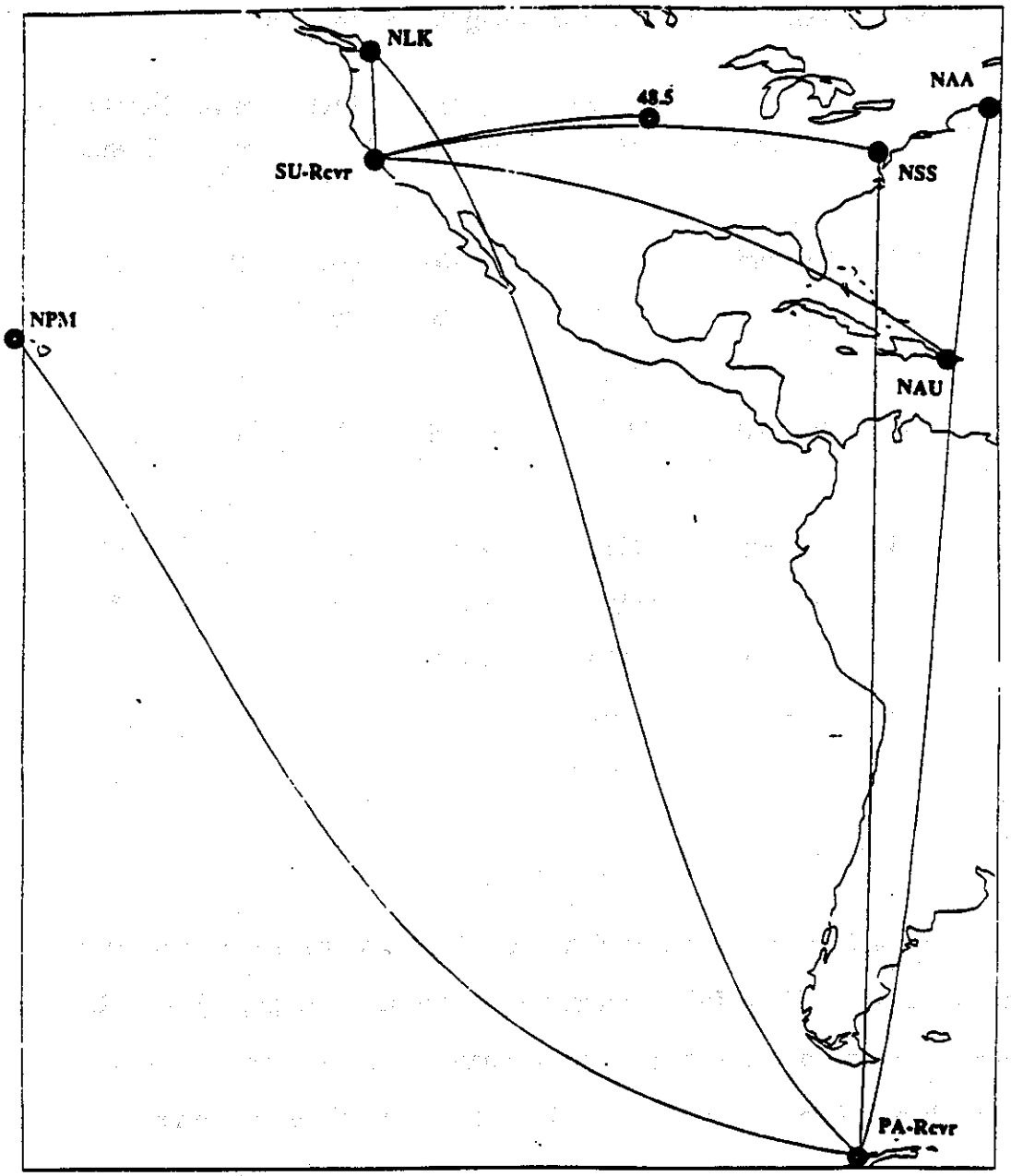

Figure 4-8 Map of the Signal Paths Analyzed. A map of the western hemisphere, showing the eight signal paths used for data collection in this analysis. Four signals were received at Palmer Station Antarctica (PA-Rcvr), and four were received at Stanford University, California (SU-Rcvr).

Chapter 5 - Results and Interpretation

Once the individual events had been identified and measured, the data were sorted by path (transmitter to receiver) and examined in a number of different ways, to investigate properties or consistent characteristics. The distributions of event polarity and event magnitude as a function of path were investigated, as well as the relative occurrence properties of amplitude and phase changes. Some characteristics were found to be consistent for a given path, but varied from one path to another. Other properties were consistent for all of the paths analyzed.

5.1 Distribution of Changes in Amplitude and Phase

5.1.1 Polarity of Perturbation Events

For each path, the polarity distribution (amplitude enhancement versus attenuation and phase advancement versus retardation) is plotted in Figures 5-1 (amplitude changes) and 5-2 (phase changes). From Figure 5-1, it is clear that different paths have quite different amplitude polarity distributions. The NPM - PA and NLK - SU paths show a strong preference for amplitude attenuation, while NLK - PA data have an equally strong tendency toward amplitude enhancement. For the other paths, tendencies were not as strong, but attenuation is more prevalent on NAU - SU, NSS - SU is evenly distributed, and enhancement is more common on 48.5 - SU, NSS - PA, and NAA - PA.

The distribution of phase perturbations shown in Figure 5-2 exhibits a striking asymmetry in the polarity of phase changes. With the exception of 48.5 - SU, all of the other seven paths exhibit a strong preference for phase advancement (or no phase change). The 48.5 - SU path is comparatively short and crosses only mountainous land, and the signal has a substantially higher frequency than the others analyzed; all facts that

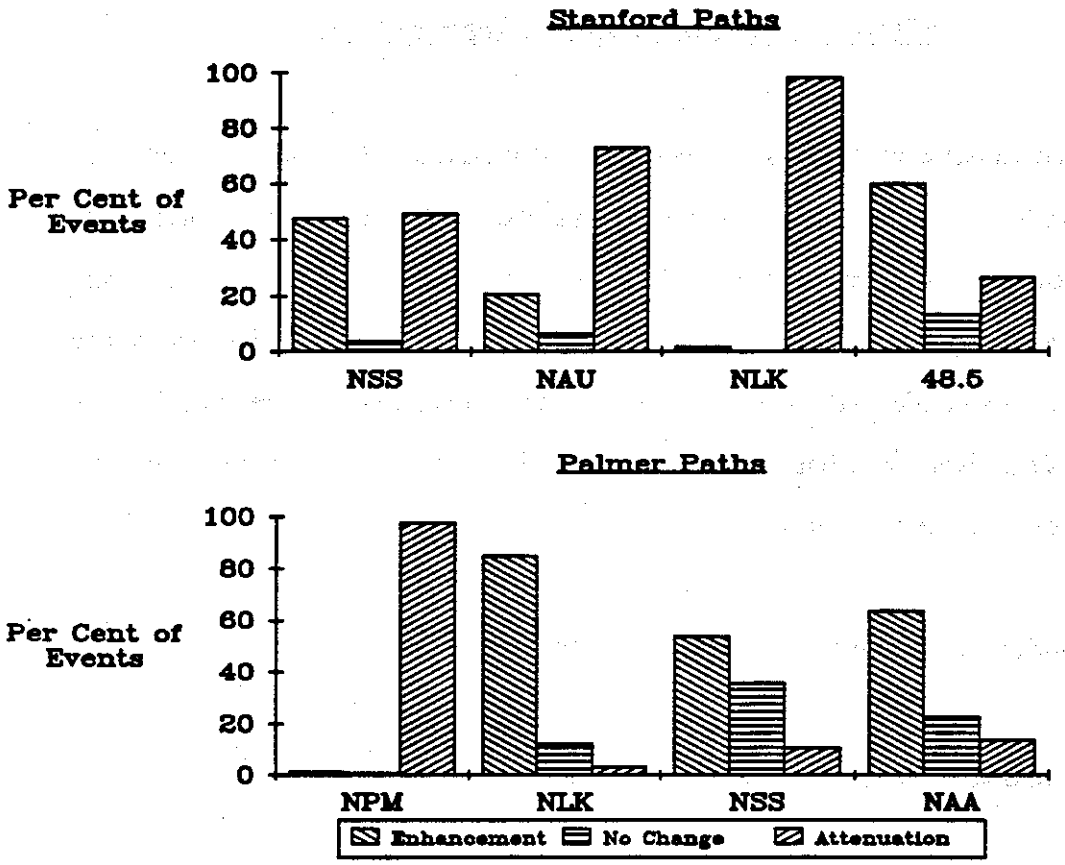

Figure 5-1 Polarity of Amplitude Events. The top panel contains the signals observed at Stanford and the bottom panel contains the signals observed at Palmer Station. For each path, the percent of events that had amplitude enhancement, amplitude attenuation and no amplitude change (only a phase change), are shown.

would be expected to complicate the path properties. In addition, only a small set of events was available on this path (15 events), so results must be considered preliminary. The substantially more common occurrence of phase advancement on all the other paths, despite the differences between these paths appears to be an important property of the Trimpi phenomenon.

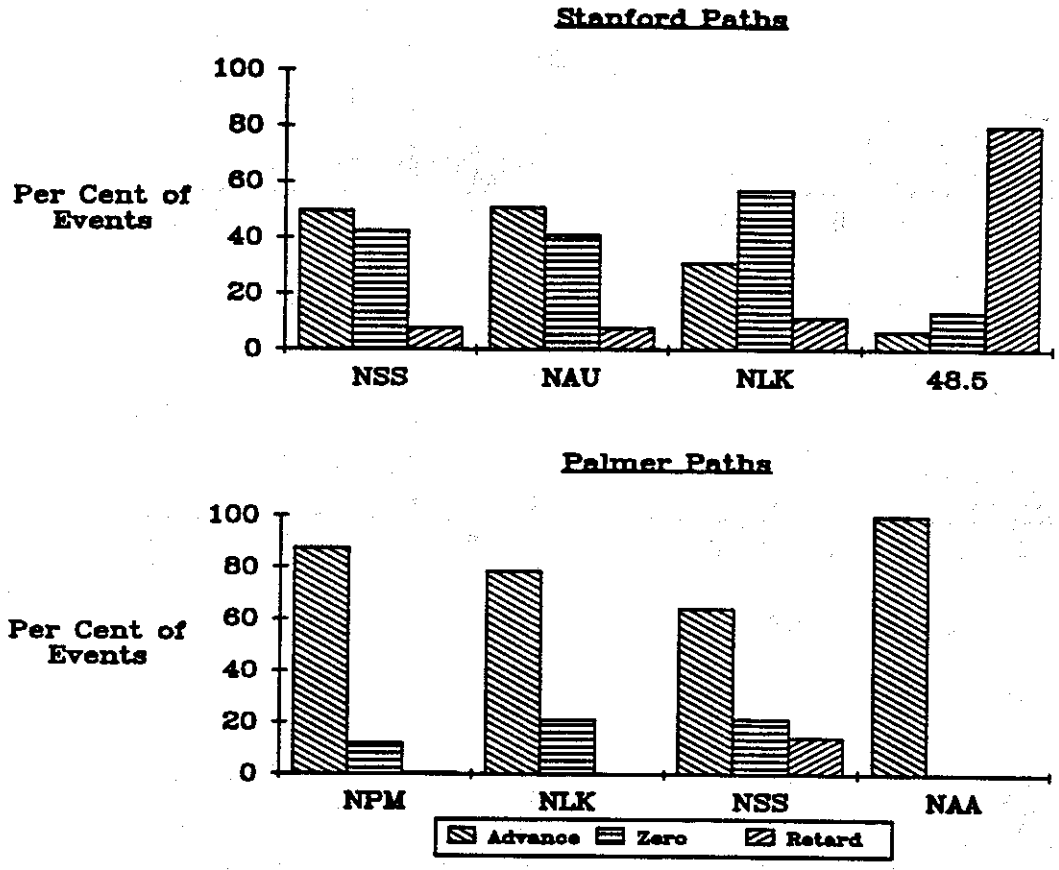

Figure 5-2 Polarity of Phase Events. The top panel contains the signals observed at Stanford and the bottom panel contains the signals observed at Palmer Station. For each path, the percent of events that had phase advancement, phase retardation and no phase change (only an amplitude change), are shown.

5.1.2 Event Magnitude as a Property of the Path

Another important parameter in characterizing the mechanism of the Trimpi effect is the relative magnitude of simultaneous amplitude and phase events. As discussed in Chapter 2, some models suggest that there should be a direct relationship between the size of the phase change ($\Delta\phi$) and the size of the amplitude change (ΔA), while others suggest that large phase changes should coincide with small amplitude changes and vice versa.

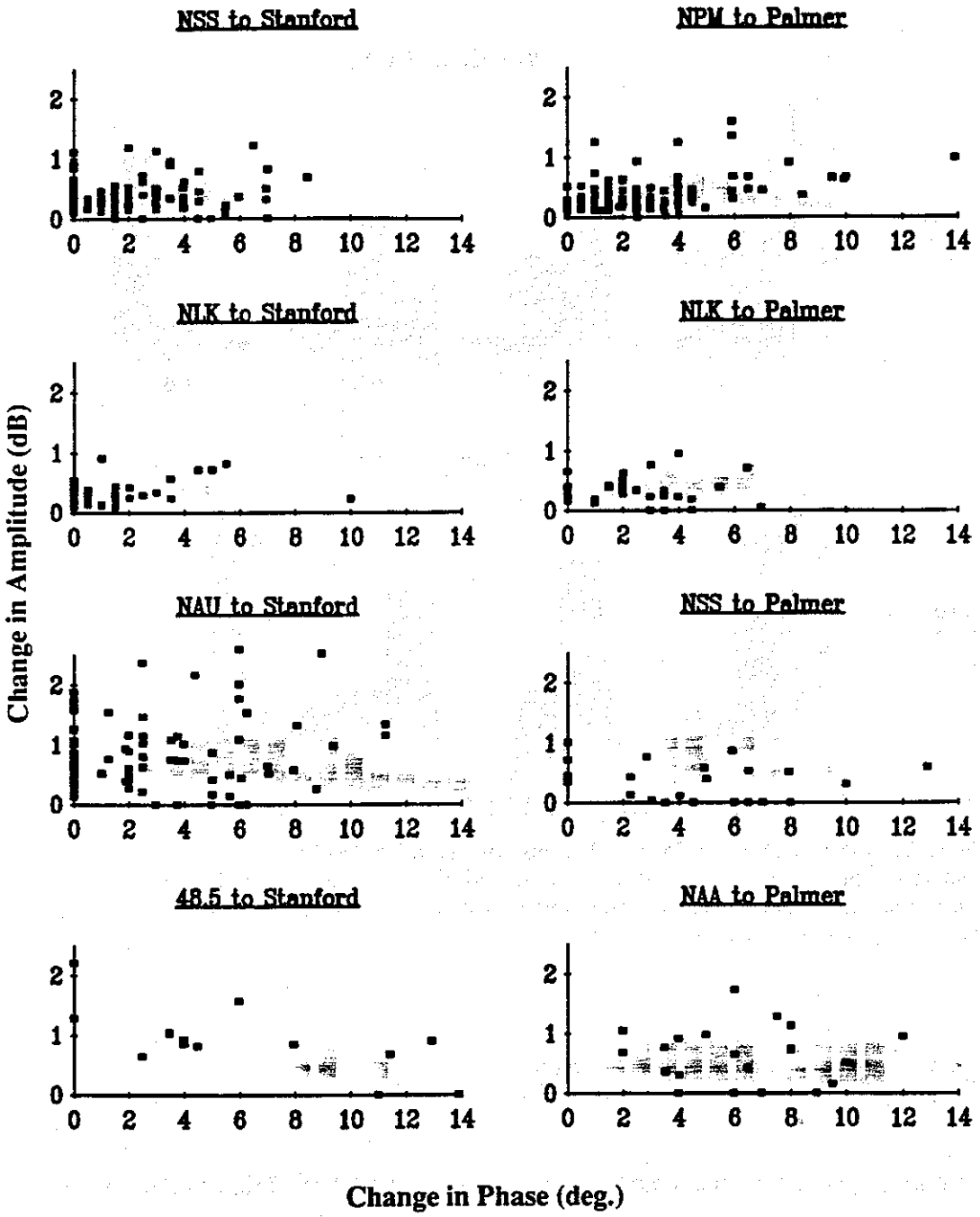

Figure 5-3 Scatter Plot of Amplitude vs. Phase. For each path analyzed, a point is plotted for each event showing the magnitude of the simultaneous amplitude and phase change. For the NPM to Palmer path, only the first 150 events are plotted. A similar plot of all 578 events appears the same, but more cluttered.

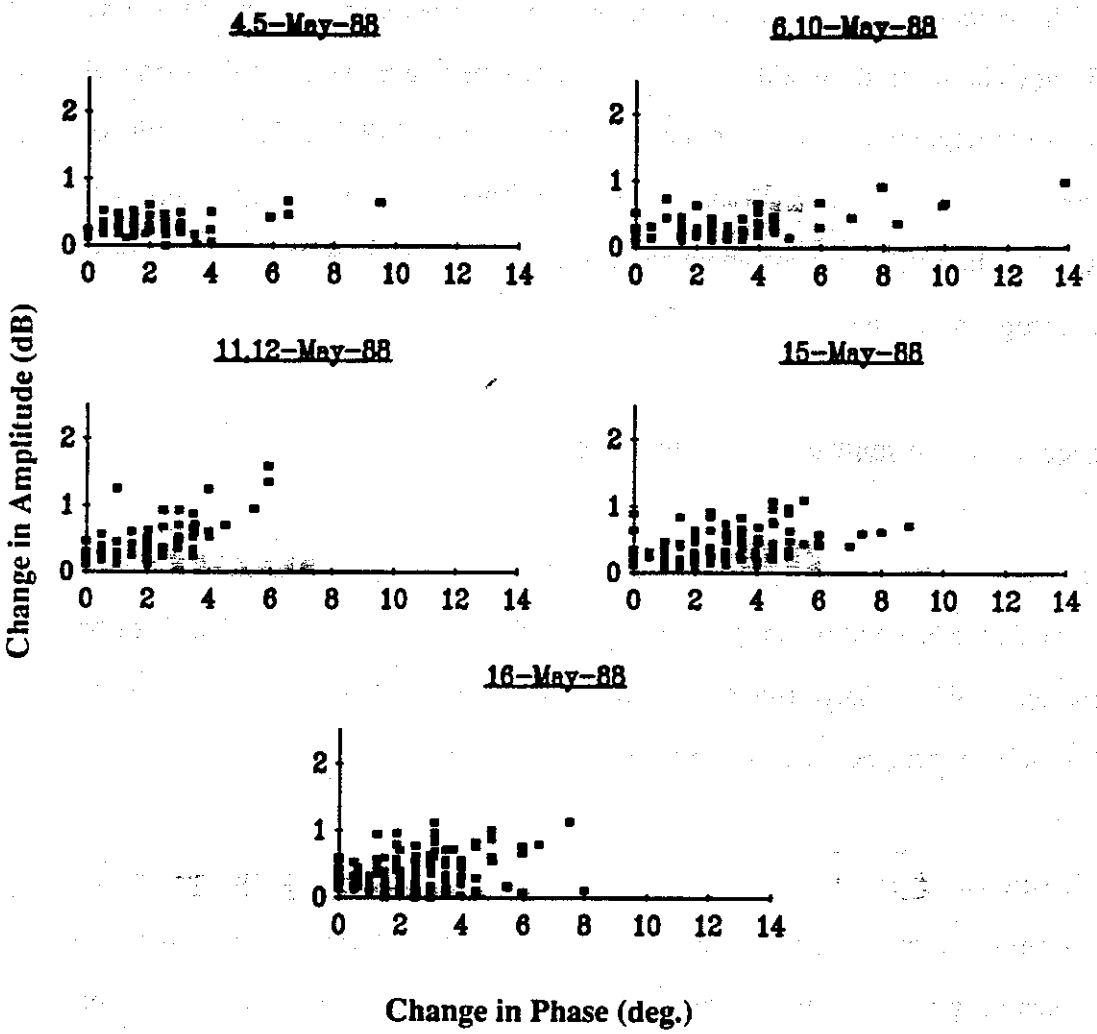

Figure 5-4 Variation with Time of the Scatter Plot. For the NPM - PA path, a scatter plot of ΔA vs. $\Delta\phi$ is shown for each day (or pair of days) for which more than 10 events per day were found.

Figure 5-3 contains scatter plots of $\Delta\phi$ vs. simultaneous ΔA for each of the eight paths investigated. On each graph, a point is plotted for each event investigated, except NPM - PA which had so many events that only the first 150 are plotted (a similar plot of all 578 events appears the same, but more cluttered). It is obvious that no path shows a strong correlation between ΔA and $\Delta\phi$, either directly or inversely. Instead each path has the majority of events in a fairly uniform distribution within a rectangle characterized by some maximum change in amplitude (ΔA_M) and some maximum change in phase ($\Delta\phi_M$).

The size of this rectangle (ΔA_M by $\Delta\phi_M$) varies from path to path, as if it were a property of the path. In order to verify that the size of this rectangle is a property of the path and not randomly varying, similar scatter plots were made for the NPM to Palmer path for each day for which more than ten events were found. These plots, shown in Figure 5-4, demonstrate that the size of the rectangle enclosing the event distribution does not vary significantly from day to day on a single path.

5.1.3 Independence of Amplitude and Phase Events

In addition to the variation in size of this rectangle, these scatter plots (Figure 5-3) reveal the apparent independence of the magnitude of ΔA and the simultaneous $\Delta\phi$. On all paths studied, the rectangle of ΔA_M and $\Delta\phi_M$ is fairly uniformly filled with events, so the magnitudes could, at best, be weakly correlated.

Another illustration of the relatively weak correlation between amplitude and phase events is shown in Figure 5-5. In this figure, the NPM to Palmer events were divided into categories according to the magnitude of ΔA. Within each category, the events are sorted according to the magnitude of $\Delta\phi$, and the number of events in each $\Delta\phi$ range are shown. It is clear from the figure that there is a weak correlation between strong amplitude and strong phase events. While small ΔA (~ 0.1 dB) are most likely to have $\Delta\phi \sim 2^\circ$, large ΔA (~ 0.9 dB) are most likely associated with $\Delta\phi \sim 4^\circ$. This 2° difference may seem significant, but within any given amplitude category, the spread in observed phase changes is $4 - 6^\circ$. Thus, the magnitude of $\Delta\phi$ is only weakly correlated with the magnitude of ΔA.

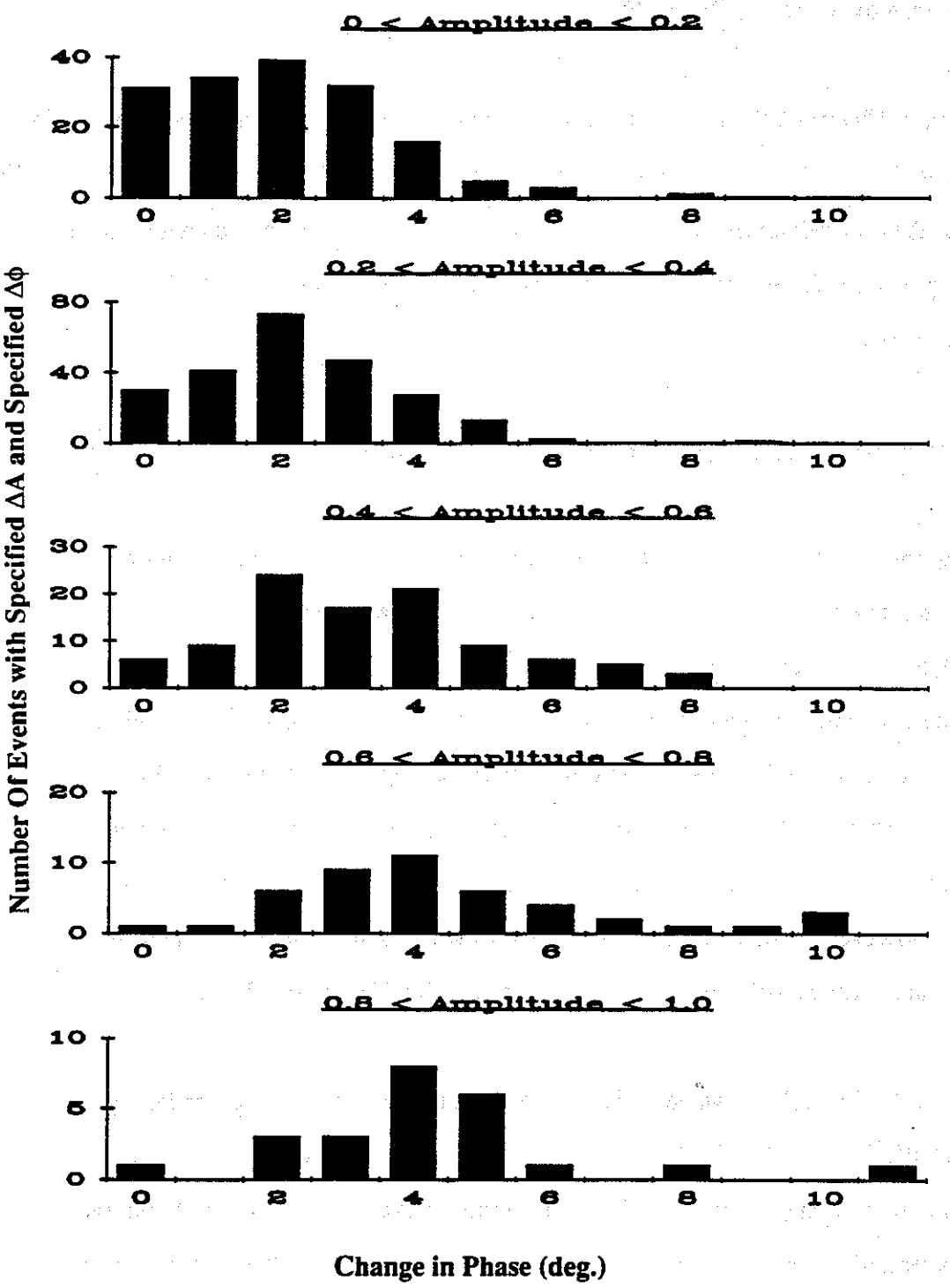

Figure 5-5 Distribution of Δφ as a Function of ΔA. Each panel contains a different range of ΔA (labelled Amplitude and measured in dB), from smallest at the top to largest at the bottom. For each range, the distribution of Δφ is shown. All data are from the NPM to Palmer path.

5.2 Significance of ΔA vs. $\Delta\phi$ Properties

As described in Chapter 2 the precipitation of electrons into the lower ionosphere results in a change in the electron concentration over a range of altitudes. The various simplified models for the consequences of this enhancement, described in that chapter, have different implications for the properties of ΔA vs. $\Delta\phi$, and their applicability to these new observations is discussed below.

5.2.1 Reflection Height Lowering as a Perturbation Mechanism

One consequence of Reflection Height Lowering (RHL) would be the shortening of the path length for the subionospheric signal. This would cause the signal to arrive at the receiver sooner, and would appear as a phase advancement. The fact that nearly all paths observed exhibit a strong preference for phase advancement is consistent with this simple mechanism. Along with RHL, the excess electrons caused by precipitation would lead to an increase in the VLF absorption coefficient in the vicinity of the reflection height, so events would be likely to exhibit simultaneous phase advancement and amplitude attenuation. However, some paths frequently exhibit amplitude enhancement, and many have occasional phase retardation, which cannot be explained by simple RHL.

Since the earth - ionosphere waveguide supports multiple propagating modes, it is usually not sufficient to evaluate the effect of RHL on a single mode signal. Instead the effect on the vector sum of a number of different propagating modes must be considered. Since the attenuation rate for a path depends upon the mode and the surface of the waveguide, the selection of which modes and how many of them to consider can be complicated [Tolstoy et al., 1986]. For long paths over sea water, such as NPM - PA, a single propagating mode is generally considered adequate [Inan and Carpenter, 1987],

and indeed this path exhibits almost entirely phase advances and amplitude attenuations. There is, however, more to the waveguide than this simple picture, since the NLK - PA path which is very similar to NPM - PA (except that NLK - PA crosses the western United States before entering the ocean) has a strong preference for amplitude enhancement.

As discussed by Tolstoy [1982] and in Section 2.4.4, when multiple modes are considered, a wide variety of amplitude and phase changes can result. Using the basic assumption of RHL, that each mode experiences a phase advance, large amplitude changes (either enhancement or attenuation) and large phase changes (either advancement or retardation) could occur when several modes are combined in a destructive manner, as discussed in Section 2.4.4. Under these conditions, each mode experiences a small change, but small changes in the phase of the modes can dramatically change the degree to which they interfere and thus dramatically change the relative magnitude and phase of the received sum. This modal interference situation is consistent with the fact that the path that exhibits the widest swings in ΔA and $\Delta\phi$, 48.5 - SU, is also the one with the high likelihood of phase retardation. Multiple mode interference would also be expected to affect the NLK - SU path, entirely land based and the shortest path, and yet this path has small events (similar in distribution to NPM - PA), only attenuation, and primarily phase advancement - all properties of single mode paths.

Although detailed modal analyses have not been performed on each path, the characteristics of the events such as polarity and magnitude, do not seem to agree well with the path parameters (such as length) that would affect the modal structure. In addition, a single mode picture would suggest that there should be a direct correlation between the magnitude of $\Delta\phi$ and the magnitude of ΔA; the more electrons that are added to the ionosphere, the more the reflection height should lower, and the more absorption that should occur near the reflection height. Such a direct correlation is not apparent in

the data. When multiple modes are considered, the opposite should be true. If the modes interfere destructively, then large phase changes should occur when the net change vector is perpendicular to the original sum vector, and under these circumstances, the amplitude change would be small, as discussed in Chapter 2. Similarly, when the net change is in phase with the original sum, large amplitude changes would occur with small phase changes, as shown in Figure 5-6. This would imply that the scatter plots should contain concentrations of large events near the axes, and few large events off of the axes. This pattern is not apparent in any of the scatter plots.

Thus, while reflection height lowering is an excellent method of visualizing the perturbation, it does not adequately describe the underlying physics, and cannot be successfully applied to all paths, even when multiple propagating modes are considered. Instead alternative methods of explaining the signal properties are required.

5.2.2 Off Axis Scattering as a Perturbation Mechanism

As mentioned in Section 2.4.2, Dowden and Adams [1988] first suggested that rather than lowering the reflection height in a region along the signal path, the mechanism for signal perturbation might be one of scattering. They suggested that the excess ionization might form a diffracting bubble on the bottom of the ionosphere slightly off the path of the propagating signal. This bubble would then act as a scattering center deflecting part of the transmitted signal to the receiver. Thus, when the perturbation occurred, a second signal component deflected to the receiver would be received in addition to the original signal. The vector sum of these two components would then appear as the perturbed signal.

This concept may apply under certain circumstances, but it does not agree with most of the results found here. Assuming, as Dowden and Adams do, that scattering is equally

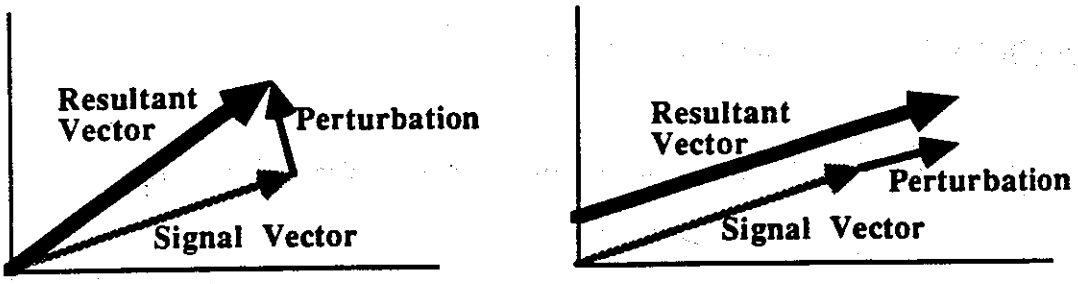

Figure 5-6 Vector Sum of Perturbation Effects. The left panel shows how a vector representing the net change that adds perpendicular to the original signal causes a large phase change and no amplitude change. The right panel shows comparable size vectors with the net change vector in phase with the original vector. In this case, a large amplitude change and no phase change is the result.

effective at a range of distances from the path, phase advancement and retardation as well as amplitude attenuation and enhancement should be equally common, and should not depend upon the particular path being studied, in contradiction with these findings. In particular, the NPM - PA path, a simple single mode path, has almost entirely phase advancement and amplitude attenuation, not the even polarity distribution predicted by Dowden and Adams. In addition, the variation in event magnitude (ΔA_M and $\Delta\phi_M$) with path would not be expected with off axis scattering, where the magnitude is simply a function of the geometry. Finally, as with the multiple mode discussion above, simple vector addition indicates that large phase changes occur when the scattered vector is perpendicular to the original signal vector, implying no amplitude change, and large amplitude changes occur when the vectors are parallel, implying no phase change (similar to Figure 5-6). Thus, the scatter plots should contain concentrations of large events near the axes, with few large events in the center of the plot. This also does not agree with the observations.

Thus, while off axis scattering is an interesting concept and may apply under certain limited conditions, it is not sufficient for obtaining a general understanding of ionospheric perturbations and its consequences on subionospheric signals.

5.2.3 Multi - Dimensional Waveguide Perturbation Analysis

Tolstoy [1982] introduced the use of a detailed computer model of the earth - ionosphere waveguide to analyze the effect of ionospheric perturbations on signal propagation. This model considered the structure of the earth's surface along the path, allowed for variation in ionospheric electron concentration with height and position, and analyzed multiple propagating modes. Tolstoy obtained some interesting results such as on NPM - PA "small amplitude decreases could be produced," while on NLK - PA "... generally produce small increases in the NLK signal amplitude ... small decreases can also occur." Both of these conclusions agree with the observations reported here, but it should be noted that Tolstoy's analysis of the NLK path assumed a transmitter frequency of 18.6 kHz, while the transmitter had switched to 24.8 kHz before any of the current data were collected.

Poulsen et al. [1990] have started the development of a new three dimensional waveguide model. This model uses analytical expressions, provided by Wait [1964], for the wave fields for each propagating mode, utilizing perturbation theory to analyze the effect of a localized ionospheric perturbation. The complex refractive index both for the background ionosphere and for the perturbation are determined numerically, for each mode, based upon ionospheric properties such as electron profile, and other waveguide properties such as earth conductivity [Morfitt and Shellman, 1976]. This new formulation allows for the possibility of the perturbation not being on the great circle path, and of the waveguide not being uniform in the horizontal direction perpendicular to the path. Instead, the perturbation is allowed to occur anywhere in the lower ionosphere, in the vicinity of the path. Although multiple modes have not yet been analyzed with this model, preliminary results indicate that phase advances are common for perturbations near the path, as expected. Also, the location of the perturbation, both position along the path, and its

offset from the path, can cause significant variation in the magnitude and polarity of both ΔA and $\Delta\phi$. Ranges of both ΔA and $\Delta\phi$ magnitude found using this waveguide analysis agree with the observations for simple paths such as NPM - PA [Poulsen et al., 1990].

5.3 Distribution of Event Magnitudes

Since the range of event magnitude appears to be a property of the particular path, the distribution in magnitude for each path was investigated. In order to accomplish this, the data for each path were sorted according to the size of the amplitude change (ΔA) and phase change ($\Delta\phi$). Figure 5-7 contains eight graphs showing the distribution of ΔA for each path, while Figure 5-8 shows the corresponding distributions of $\Delta\phi$. Most of these graphs have similar envelopes resembling log - normal probability distributions [Sachs, 1984]. The distinctive features of these distributions are relatively few events near zero, the number of events rising rapidly to a peak, and then tapering off slowly as the magnitude of the event increases. The location of the peak and the width of the distribution depends upon the path, but the same general shape is apparent in most of the plots.

The fact that all of the plots have similar envelopes suggests that this shape may be a property of the mechanism that causes perturbations. Inan and Carpenter [1986] have reported a correlation between event magnitude and associated whistler intensity, so it would be interesting to establish whether whistler intensities exhibit a similar distribution (many lightning parameters, including return - stroke current have been found to exhibit log - normal distributions [Uman, 1987]). Since the width of the distribution is a property of the path, this is probably determined by the particular waveguide properties of that path (eg. conductivity variation and roughness of the earth's surface along the path) and

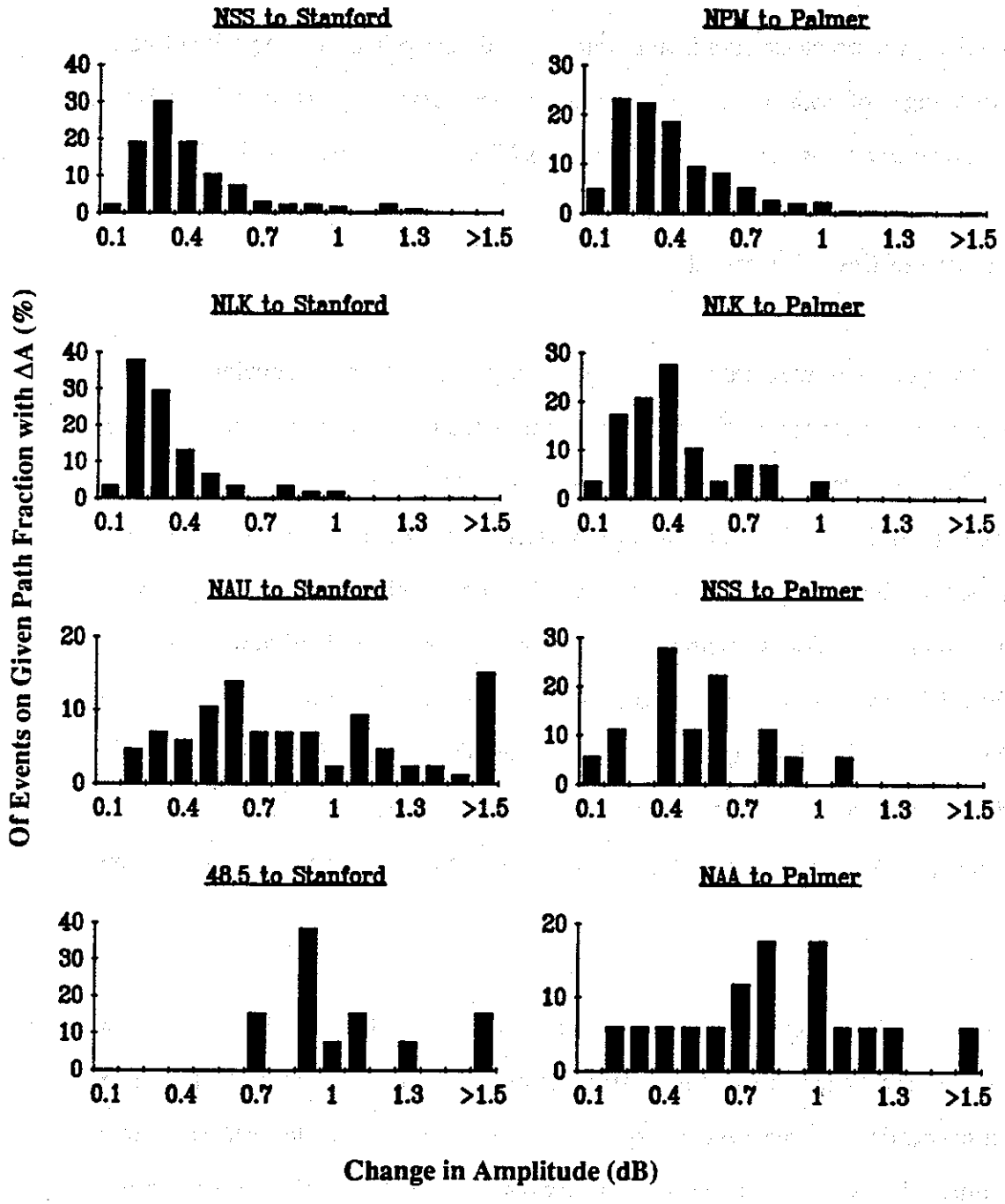

Figure 5-7 Magnitude Distribution for Amplitude Events. For each of the eight paths, histograms show the per cent of events in different ΔA ranges. Only nonzero events are shown here. Events with ΔA ~ 0 are shown in Figure 5-13.

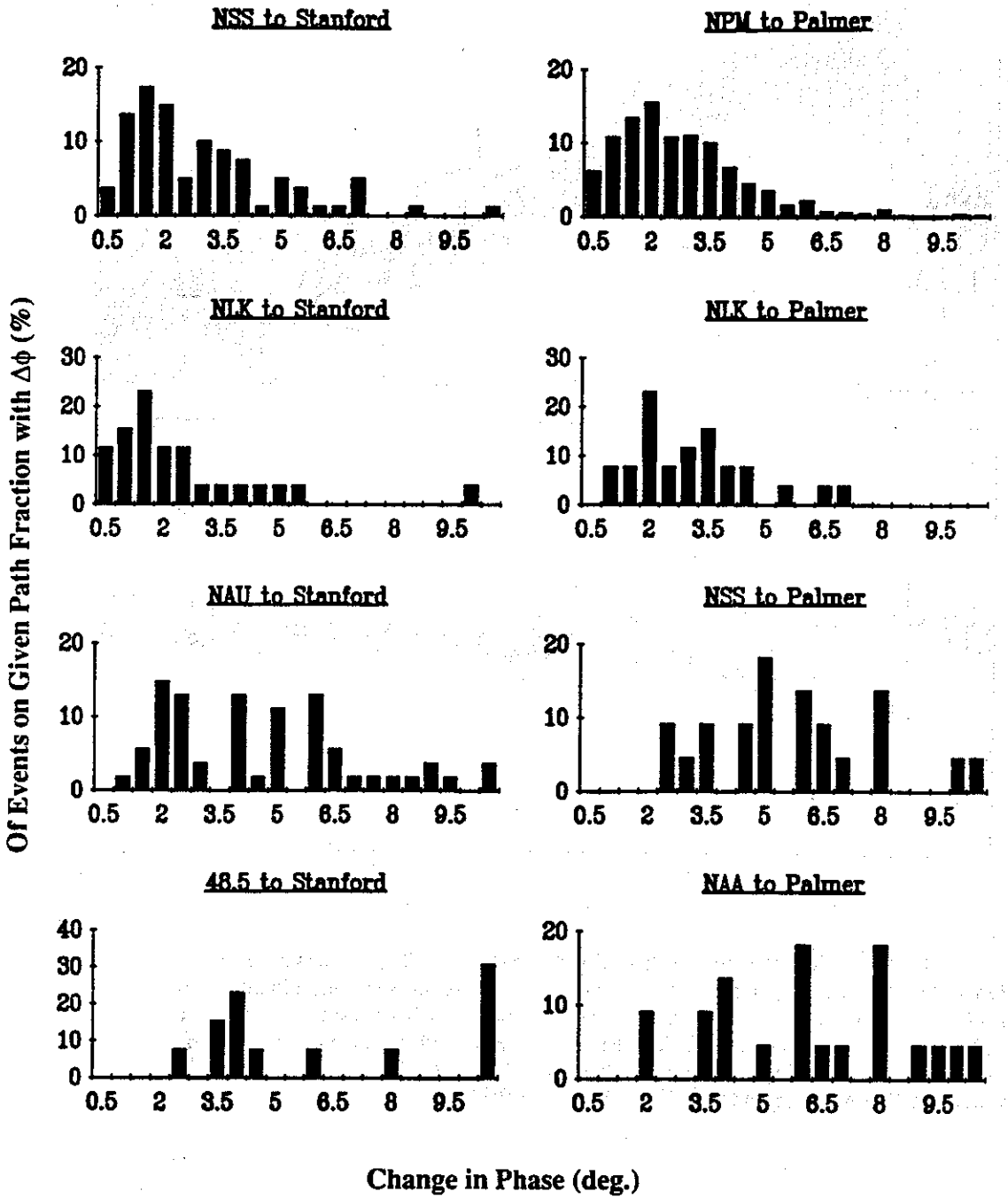

Figure 5-8 Magnitude Distribution for Phase Events. For each of the eight paths, histograms show the per cent of events in different $\Delta\phi$ ranges. Only nonzero events are shown here. Events with $\Delta\phi \sim 0$ are shown in Figure 5-13.

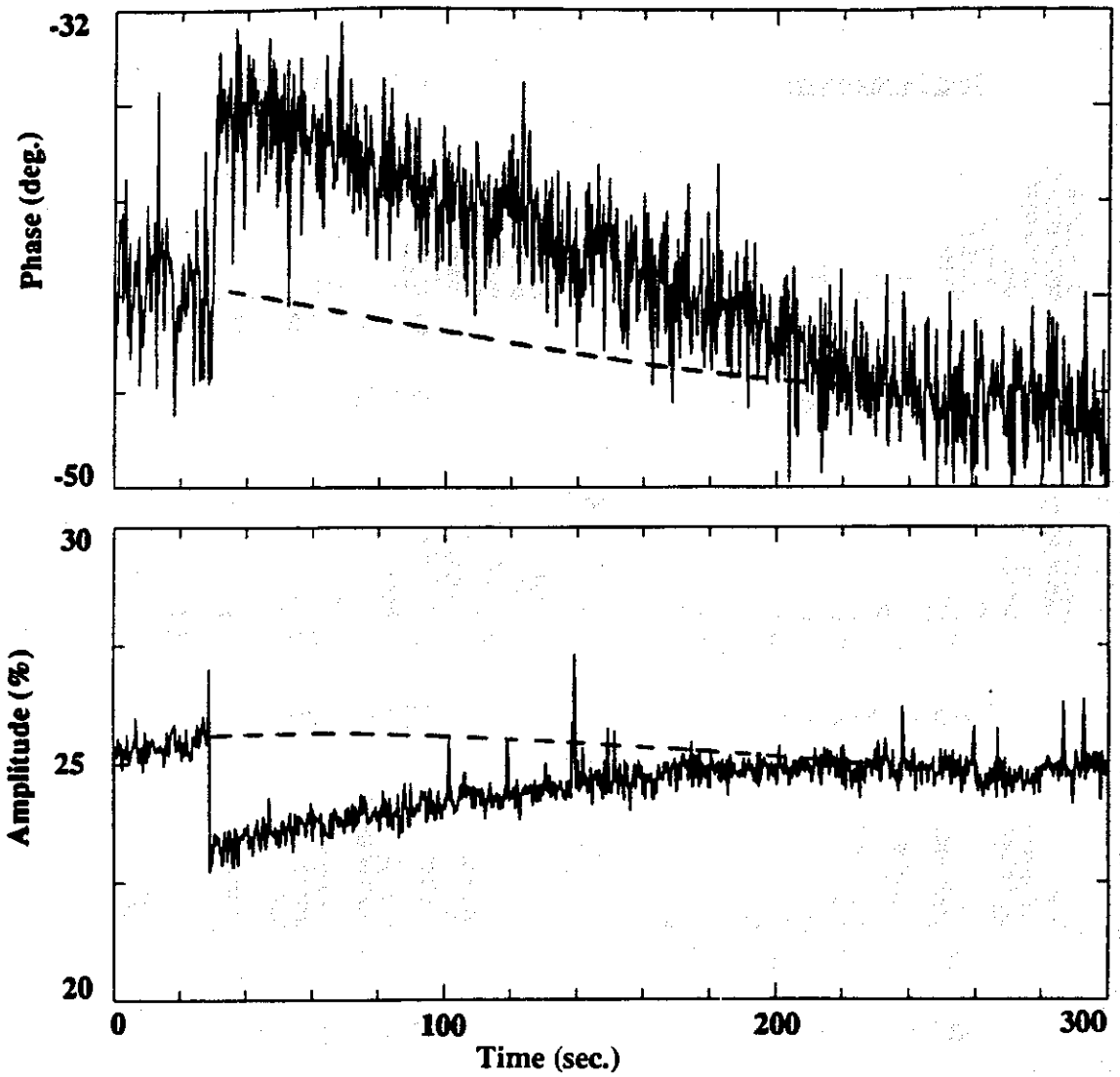

Figure 5-9 High Time Resolution Plot of a Typical Event. The top panel shows the signal phase as a function of time, and the bottom panel contains the simultaneous amplitude. The dashed lines represent the interpolated levels if no event had occurred. Both amplitude and phase have similar sharp onsets and similar recoveries to pre-event levels. 0.32 sec. averaging was applied to these data from the NSS transmitter, observed at Stanford. The plot starts at 02:25 UT on 15 March 1987.

by the number of propagating modes that are dominant for that path. Testing of both of these characteristics should be possible soon, using the new three dimensional model of VLF propagation in the waveguide, currently under development [Poulsen et al., 1990].

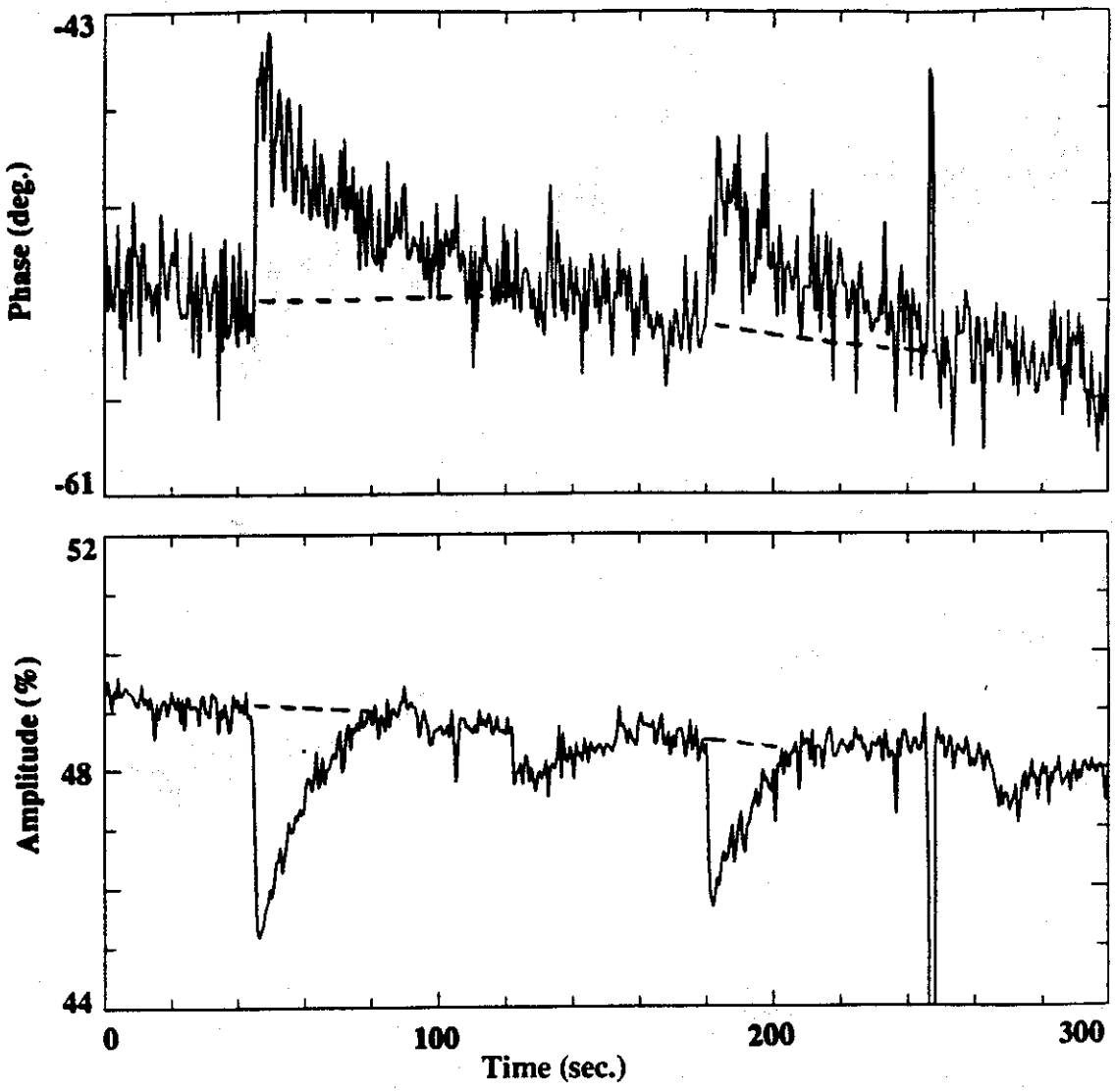

Figure 5-10 High Time Resolution Plot of an Event with a Slow Phase Recovery. Both events shown here have substantially faster amplitude recoveries than phase recoveries. The dashed lines represent the interpolated levels if no event had occurred. 0.64 sec. averaging was applied to these data from the NPM transmitter, observed at Palmer Station. The plot starts at 06:37 UT on 4 May 1988.

5.4 Independence of High Time Resolution Event Signatures

To further investigate the apparent independence between the amplitude and simultaneous phase events, arbitrarily selected events were replotted at higher time resolution. Figure 5-9 shows a typical event where the amplitude and phase recoveries appear quite similar in shape. Figures 5-10 and 5-11 are two similar plots showing events

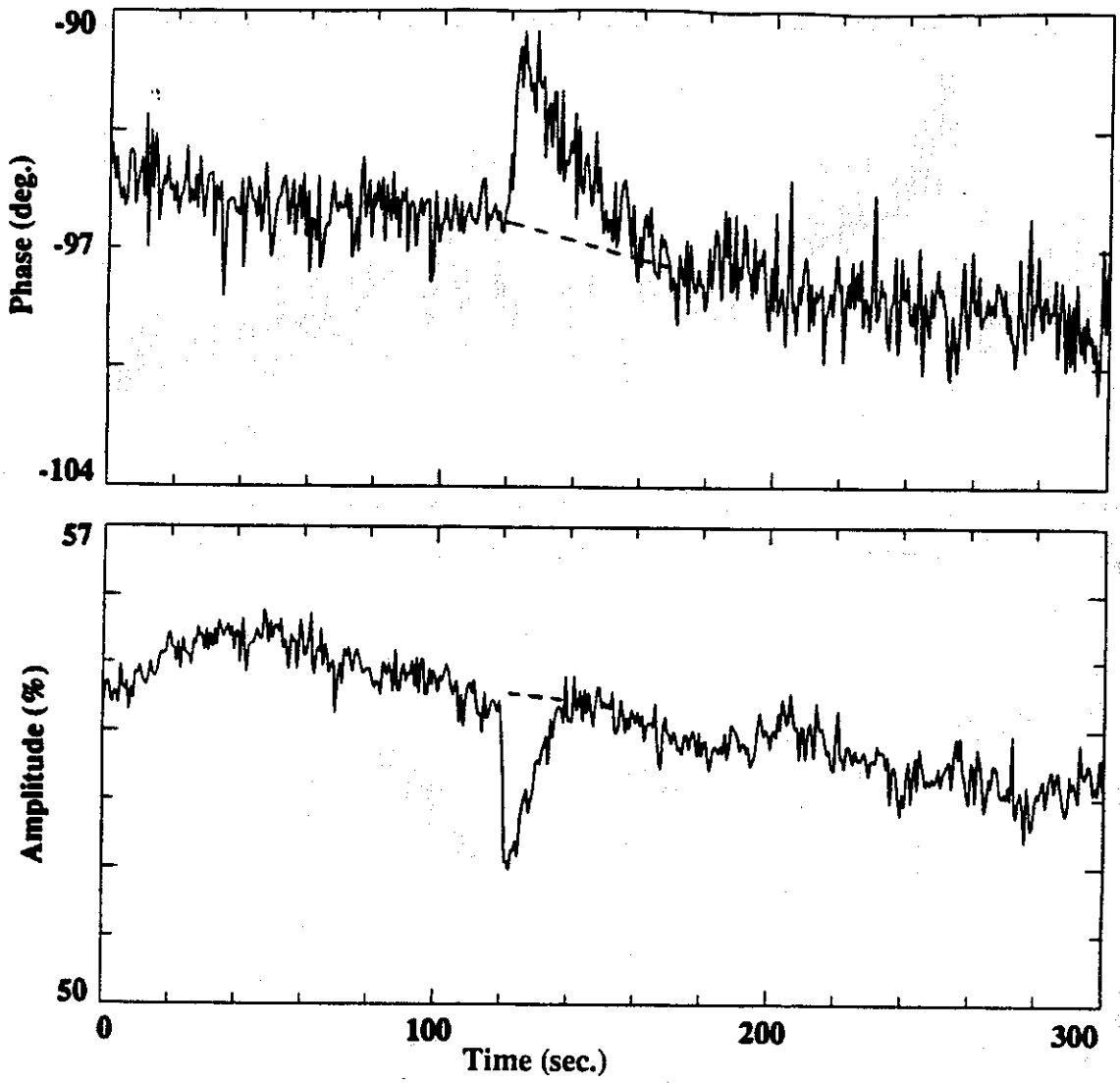

Figure 5-11 Plot of another Event with a Slow Phase Recovery. In this event also, the amplitude recovers substantially faster than the phase of the recorded signal. The dashed lines represent the interpolated levels if no event had occurred. 0.64 sec. averaging was applied to these data from the NPM transmitter, observed at Palmer Station. The plot starts at 08:20 UT on 6 May 1988.

observed on the NPM to Palmer path. In both of these events, and others observed, the phase recovery time appears to be substantially longer than the amplitude recovery.

Figure 5-12 shows another event with very different amplitude and phase signatures. In this event the onset of the phase change appears to be much slower than the onset of the simultaneous amplitude change, and the phase may start to advance before the beginning

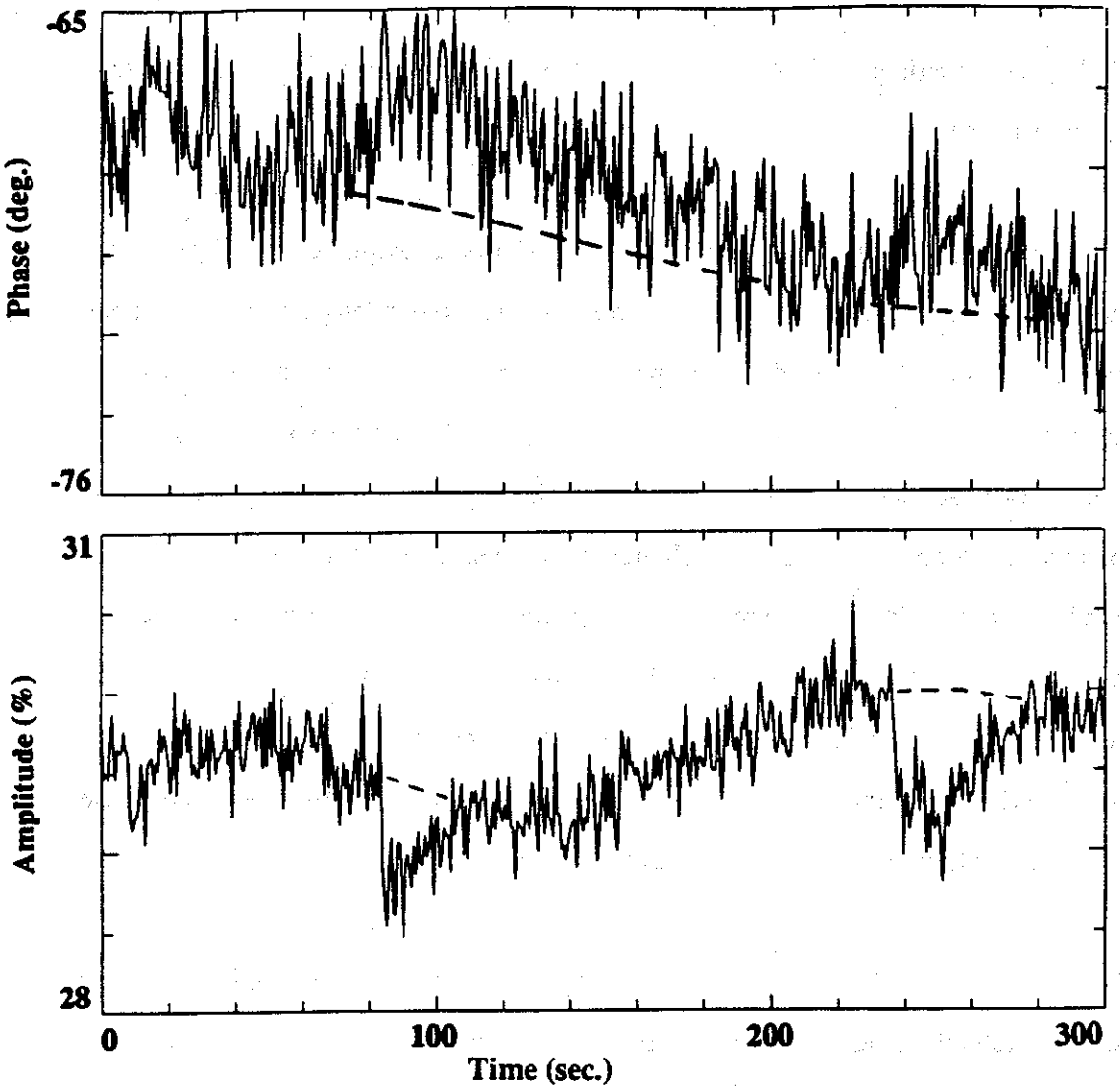

Figure 5-12 Plot of an Event with a Unique Phase Signature. In this event, the amplitude has the characteristic rapid onset and slow recovery, but the simultaneous phase measurement shows a much slower onset. The phase also may start to advance before the amplitude change begins. 0.64 sec. averaging was applied to these data from the NPM transmitter, observed at Palmer Station. The plot starts at 09:15 UT on 5 May 1988.

of the amplitude change. Although the amplitude signature of this event is typical of a Trimpi event, the phase signature is so unusual that a different, as yet undetermined mechanism may be involved. Events with these anomalous signatures are curious, but

occur only rarely (perhaps 1% of events analyzed) and would not affect the statistical analyses presented here.

These observations imply that the perturbation of the ionosphere is affecting the amplitude and phase of the signal independently. While acknowledging that the excess ionization is distributed in altitude, most previous discussions using simple models for the perturbation mechanism have treated the change in the ionosphere as a patch of excess ionization at one altitude, typically near the nighttime reflection height. The perturbation then becomes essentially a change in geometry, that is, the reflection height is lowered, the waveguide has a depression, or an additional scattering center appears. If this single geometric change occurs, and then gradually recovers to normal, the amplitude and phase of the perturbation would be expected to have similar time signatures. The results reported here indicate that not only are the magnitudes of amplitude and phase events independent, but often so are the time signatures.

The most likely explanation for this independence lies in the fact that the excess ionization is actually distributed over a range of altitudes in the lower ionosphere. Collision frequency decreases with increasing altitude in this region, as shown in Figure 2-2 and so does excess ion recombination rate [Gledhill, 1986]. Thus, the excess electrons generated higher up would be expected to persist longer than those lower down. Since total reflection does not occur for VLF signals, some portion of the wave penetrates higher into the ionosphere. Reflection can be represented by an effective reflection coefficient determined by analyzing wave fields throughout the ionosphere above the effective reflection height. As a result, this effective reflection coefficient, and hence the reflected wave component could be sensitive to ionization changes higher up in the ionosphere. Since the most absorbing portions of the ionosphere are low, where the recombination rate is high, it would not be surprising that amplitude changes recover

quickly, while phase changes, which are influenced by electrons higher up, recover more slowly.

The waveguide models [Tolstoy et al., 1986; Poulsen et al., 1990] have utilized a perturbation distributed in altitude, and so more accurately reflect the range and independence of ΔA and $\Delta\phi$ found. In particular, Poulsen et al. [1990] have shown that by varying the energy of the precipitated electrons, and therefore the altitude of the excess ionization, a wide range of ΔA versus $\Delta\phi$ distributions can be obtained. Thus, a range of precipitation events, with a range of electron energies would be expected to produce a scatter plot of ΔA versus $\Delta\phi$ with a fairly uniform distribution, as has been reported here. None of these models currently simulates the time evolution of perturbations, so event recoveries have not been investigated. The faster amplitude recoveries observed here have not been confirmed with computer simulations, however Poulsen [private communication, 1989] has established that precipitation at altitudes as high as 250 km can perturb the subionospheric signal phase and not its amplitude. The slow recovery time at this altitude suggests that an event which deposited excess electrons over a wide range of altitudes could indeed continue to affect phase after the lower portions that influenced amplitude had recovered to normal levels.

Since these results suggest that the altitude profile of the excess ionization is critical in understanding the relationship between amplitude and phase of a subionospheric signal perturbation, it is important that improved models include accurate analysis of the pitch angle distribution of the precipitating electrons. Cyclotron resonance scatters the electron pitch angle by only a few degrees, so only electrons near the loss cone will be precipitated [Inan et al., 1988c]; these precipitating electrons having been near the loss cone initially, enter the ionosphere with pitch angles very near 90°. Based on the ionization profiles shown by Rees [1963], it appears that precipitating electrons with high pitch angles distribute their energy over a wider range of altitude than low pitch angle

electrons of the same energy. For lack of more precise data, previous analyses [Inan et al., 1988a] have used the ionization profiles from Rees [1963] which are for electrons distributed in pitch angle; even the profile shown in Figure 2-9 is for an isotropic pitch angle distribution, not a near 90° distribution. Although useful tools, these profiles are probably not adequate for an understanding of the relationship between amplitude and phase of a given event.

The electrons with large pitch angles are also more likely to backscatter upon reaching the ionosphere rather than precipitate [Berger et al., 1974], so the actual precipitating flux may depend strongly upon pitch angle distribution. This backscattering could add variability to the event rise time, as the onset could be spread over several bounce periods [Chang and Inan, 1985], and it could spread out the pitch angle distribution, since the process of backscattering alters the electron pitch angles [Davidson and Walt, 1977].

5.5 Amplitude - Only and Phase - Only Events

In analyzing the magnitude distribution of events, an unexpected result was uncovered. Not surprisingly, some of the amplitude events had no measurable corresponding phase change ($\Delta\phi < 0.5°$), and similarly, there were phase events with no measurable amplitude change ($\Delta A < 0.1$ dB). However, the relative occurrence rates of these events with $\Delta A \sim 0$ or $\Delta\phi \sim 0$ is a most puzzling finding. For each of the eight paths analyzed, the fraction of the total number of events that exhibited either $\Delta A \sim 0$ or $\Delta\phi \sim 0$ are shown in Figure 5-13.

Although there were some differences between the various paths, approximately 10% of the events observed at Stanford had $\Delta A < 0.1$ dB, while this occurred on more than 20% of the events observed at Palmer. This difference is noticeable, but the difference in

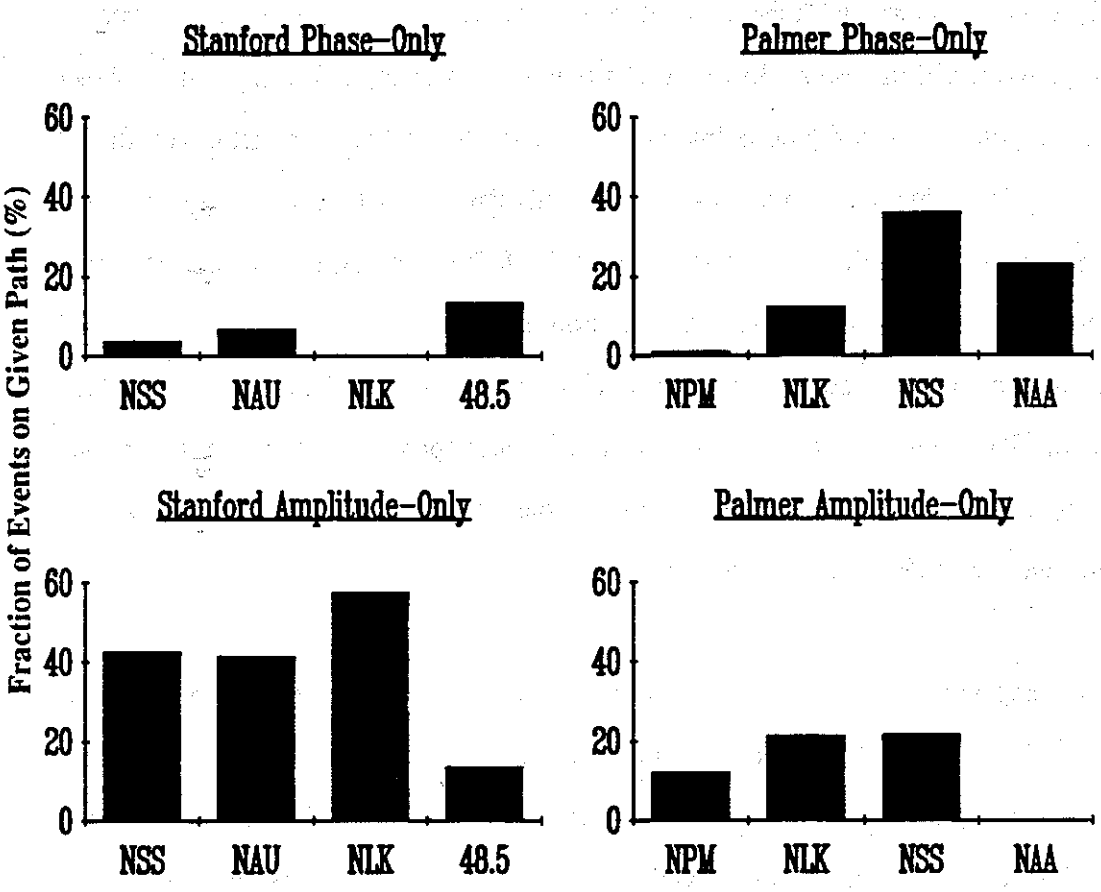

Figure 5-13 Amplitude-Only and Phase-Only Event Occurrence Rates. For each path analyzed, the percent of events for which $\Delta A < 0.1$ dB are shown in the upper panels and the percent of events for which $\Delta\phi < 0.5^\circ$ are shown in the lower panels. The left panels are the Stanford paths and the right panels are the Palmer paths.

Amplitude - Only events is dramatic. The Palmer paths had less than 20% of the events with $\Delta\phi < 0.5^\circ$, while nearly 50% of the events at Stanford exhibited such behavior.

This dramatic difference between Stanford paths and Palmer paths is not predicted by any of the existing models for the perturbation mechanism. In order to speculate on the causes of this difference, it is necessary to identify the differences between the Palmer and Stanford paths. By looking at characteristics of the signal paths, as in Figure 4-8 and Table 2, several differences become apparent. First, all of the Stanford paths are

relatively short, compared with the paths observed at Palmer. This would suggest that the Stanford paths would in general have more propagating modes, and as a result, a wider range of possible ΔA and $\Delta\phi$ combinations. In addition, the Stanford paths are almost entirely over land, including mountains, while the Palmer paths are mostly over sea water. Sea water is smooth and conductive, so at VLF frequencies, it can be treated as a nearly perfect conductor [Wait, 1970]. The mountainous land is rough in shape, and varying in conductivity, so its properties as a waveguide surface are much more complicated. This roughness may allow more mixing and conversion between the various propagating modes, which again would increase the variety in the resultant changes in amplitude and phase [Pappert and Snyder, 1972].

Two other geographic differences can be identified, but their consequences are not clear. First, most of the Stanford paths follow an approximately East - West direction while the Palmer paths are predominantly in a North - South direction. East - West paths traverse regions of relatively constant L value, and hence constant magnetic field strength, while North-South paths cross a wide range of L values. This path orientation might be important if the precipitation regions are not circular in horizontal cross - section. If, for example, the perturbation is elongated in geomagnetic longitude (along lines of constant L), East - West paths would experience a longer perturbation region than North - South paths.

The last geographic difference is more subtle. Lightning is not very common in California, but is quite common in the central and eastern United States. As a result, the ionospheric perturbations are likely to be far from the receiver on Stanford paths. Perturbations observed at Palmer are primarily the result of lightning in the eastern United States causing precipitation in its magnetic conjugate region near Palmer Station [Inan and Carpenter, 1986]. Thus, the ionospheric perturbations observed at Palmer are

primarily located near the receivers at Palmer. If the distance the signal propagates after encountering the ionospheric perturbation affects the perceived signal perturbation, this difference in perturbation location could be significant. This may be particularly significant when there is substantial coupling between waveguide modes along the path. When this occurs, the effect of a distant perturbation may be disseminated among many modes, altering its appearance.

Related to this conjugate precipitation are several magnetospheric differences between the Palmer paths and the Stanford paths. First, as discussed in Section 2.3.4, the Stanford paths should generally be perturbed by direct precipitation, where southbound lightning impulses in the magnetosphere interact with northbound energetic electrons, causing them to precipitate into the northern ionosphere. Palmer path perturbations are primarily the result of mirrored precipitation, where the northbound energetic electrons, after interacting with the southbound lightning impulses are mirrored by the Earth's magnetic field. They then traverse the length of the magnetic field and precipitate into the southern ionosphere. Related to this difference, is the proximity of Palmer Station to the South Atlantic Anomaly. As a result, the magnetic field near the longitude of Palmer is very asymmetric, while near Stanford, it is quite symmetric. The consequences of direct versus mirrored precipitation and of an asymmetric magnetic field are not at all obvious, however two potential differences can be anticipated. In the vicinity of the South Atlantic Anomaly, the energetic electron population near the southern hemisphere loss cone may exceed the population near the northern hemisphere loss cone by two orders of magnitude [Inan et al., 1988c]. In addition, as discussed in Section 5.4, the precipitating electrons have pitch angles near 90°, and so may experience as much as 90% backscattering. The process of backscattering spreads the pitch angle distribution of the electrons, and can also spread their geographic extent to other nearby field lines [Berger et al., 1974]. Thus, the mirrored and backscattered precipitation may have higher flux, wider pitch angle distribution, and larger geographic extent, than the direct precipitation.

Because of the high backscatter rates, the northern hemisphere precipitation is probably not entirely direct precipitation. Significant precipitation would be expected to result from electrons scattered into the southern hemisphere loss cone that mirror in the north and then backscatter in the south, ending up in the northern hemisphere loss cone. These differences in pitch angle distribution, flux, and geographic extent would be expected to alter the altitude profile of the excess ionization, and the horizontal shape of the perturbation, causing different amplitude versus phase distributions for northern and southern hemisphere events.

Chapter 6 - Conclusions and Future Work

6.1 Summary and Conclusions

The Trimpi effect is a characteristic perturbation in the amplitude or phase of a subionospherically propagating radio signal. These perturbations are generally caused by lightning through a sequence of atmospheric interactions. The lightning discharge generates a VLF whistler which propagates along a magnetic field line, into the magnetosphere, where it resonates with energetic electrons. This interaction alters the momentum of these electrons causing them to precipitate into the ionosphere. The secondary ionization in the ionosphere, that results from this precipitation, in turn, alters the character of the earth - ionosphere waveguide, causing a perturbation in the subionospheric signals.

By developing hardware that could make accurate phase and amplitude measurements on multiple signals and deploying this equipment at several receiving sites, it became possible, for the first time, to analyze a comprehensive set of data on Trimpi events. In addition to the size of the data set, this data set is unique in that it consists of simultaneous amplitude and phase measurements on multiple signal paths, received at sites in both the northern and southern hemispheres.

As a result of this analysis, it was found that the existing simplified models for the mechanism of the Trimpi effect are useful primarily as conceptual and qualitative explanations of the phenomenon. They may even accurately describe some individual events, but cannot be generalized to explain the new patterns and features of the Trimpi events revealed in this analysis. Instead, these new features provide an empirical

framework that will guide the evolution of more sophisticated models that are currently being developed.

Among the important new features found, with which new perturbation models must be consistent, are the following:

- Amplitude changes are evenly distributed, overall, between enhancement and attenuation, but individual paths may have strong preferences for one or the other.
- Phase changes show a different character in that almost all paths show a strong preference for phase advancement; phase retardation does occur, but is rare.
- The magnitudes of simultaneous amplitude and phase changes are only weakly correlated.
- The range in size of amplitude and phase events varies from one path to another, but is relatively constant with time for a given path.
- Half of the events observed in the north had no detectable phase change, while less than one fifth of the southern hemisphere events did.

Preliminary analysis of the time signatures of events has also shown that in many events with simultaneous amplitude and phase changes on a given signal, the two changes have different behavior with time. This suggests that not only are the occurrence rate and size of simultaneous amplitude and phase events independent, but so are the time signatures. This independence implies that it is inadequate to treat the ionosphere as an abrupt waveguide boundary with a perturbation in the altitude of this boundary. Instead, the ionosphere must be treated as a continuous, varying medium, forming a gradual boundary, with absorption, reflection, and transmission properties changing with altitude. In addition, the perturbation in the ionosphere, caused by enhanced ionization from the precipitating electrons, must be treated as a three dimensional change in this medium, distributed not only in horizontal extent, but also in altitude. The difference in recovery

times for phase and amplitude may then be indicative of the altitude dependence of the ion recombination rate.

6.2 Suggestions for Future Work

Although this analysis has produced a number of significant new observations, these results can be refined and augmented in a number of ways. Further research can progress in three synergistic directions. Additional data can be analyzed to expand upon the results reported here, new related experiments can be performed to increase the variety of paths for which data are available, and further theoretical modelling can be performed to match the empirical observations to the models.

6.2.1 Analytical Work

At the time this analysis was performed, all available data from the described apparatus were investigated. Since that time, substantial quantities of additional data have been received from Palmer Station and Stanford. Processing of these additional data would increase the statistical reliability of many of the observations. In particular finding more events on the paths for which less than 30 events have been analyzed would greatly increase the reliability of these observations. This larger data set could also be used to eliminate some of the extraneous variables in the original data. For example, the Palmer data processed in this analysis were obtained during a six week period in April and May 1988, while the Stanford data were collected over several years. Continuous Palmer data are now available for over a year, so time of year could be eliminated as a variable in the difference between Stanford and Palmer data.

Further analysis should also be performed in the temporal signature of the events, at high time resolution. This temporal analysis would allow the identification of additional

characteristic parameters of events besides magnitude. The temporal characteristics of onset delay, rise time, and recovery time identified in Chapter 2 contain information about the physics of the interaction and variations in these parameters between paths would provide interesting information.

Increasing the size of the data set would also allow the investigation of the variability of event properties with other parameters. Some of the parameters, for which data are available, that might affect the events include the following:

- Time of Year. Are winter events different from summer events, or are equinoctial events different?
- Path Characteristics. Are long path events different from short path events? Are land paths different from sea paths?
- Lightning Characteristics. Are any event characteristics related to lightning parameters? Do cloud - to - ground and cloud - to - cloud lightning cause different effects?

6.2.2 Empirical Work

Many of the differences between Stanford and Palmer paths can only be eliminated as variables by collecting data on additional paths. For example, long sea paths to Stanford such as NPM (Hawaii) and NWC (Australia) could be compared to long sea paths to Palmer. A short path received at Palmer such as from Omega - Argentina could be compared to a short path received at Stanford such as from Omega - North Dakota.

Other of these variables can be eliminated by adding additional receiving sites. Several new sites in North America have been added, and additional ones are planned. These additional sites can be used to pursue questions such as North - South vs. East - West

paths, Sea vs. Land paths, and Long vs. Short paths. Finally, if data can be obtained from additional southern hemisphere sites, the effect of Palmer Station's proximity to the South Atlantic Anomaly could be determined.

6.2.3 Theoretical Work

The various steps in the physics of the Trimpi events have been studied and modelled on computers, but as yet, these models have not been combined into one integrated model of lightning - associated perturbations in subionospheric VLF propagation. For the wave - particle interaction, pitch angle scattering has been modelled [Inan, 1977], extension of interaction with whistlers off the equator has been studied [Inan et al., 1989], and the difference between direct and mirrored precipitation has been analyzed [Chang and Inan, 1985a; 1985b]. These analyses provide a profile of energy versus electron flux versus time, for the whistler induced precipitation. Given a precipitating electron flux, the production of secondary ionization and backscatter that results can then be computed using sophisticated computer models [Davidson and Walt, 1976]. Alternatively, simpler models using the empirical data from Rees [1963; 1969] have been used to analyze this particular step in the overall process leading to Trimpi events [Inan et al., 1988a]. The perturbation of VLF signals by these ionization changes is modelled by detailed waveguide propagation programs [Tolstoy et al., 1986; Poulsen et al., 1990], and W. Poulsen, as part of his Ph. D. work, is currently integrating these models by using more precisely determined profiles of excess ionization, determined by the models mentioned above, in his waveguide modelling.

As discussed in Chapter 5, the profile of secondary ionization versus altitude is dependent upon the pitch angle distribution of the precipitating electrons [Rees, 1963]. Computer models of the wave - particle interaction have been used to compute the electron pitch angle distribution, integrated over energy and time [Inan et al., 1989], as

well as the energy versus flux versus time distribution of the precipitating electrons [Chang and Inan, 1985a; 1985b], but an accurate profile of secondary ionization requires the addition of pitch angle as a parameter in the computer model, yielding a distribution of pitch angle versus energy versus flux versus time. Existing wave - particle interaction models should be modified to provide such a distribution for whistler - induced precipitation, and combined with an accurate model of the pitch angle dependent production of secondary ionization, to provide an accurate profile of secondary ionization versus altitude. This is particularly important in view of the results presented here which suggest that this excess electron profile versus altitude plays an important role in the distribution of amplitude and phase perturbations. An accurate model of the pitch angle distribution is also critical because mirrored precipitation is thought to consist of those electrons that were not within the northern loss cone, or those that were backscattered in the north, and which therefore have a different pitch angle distribution than direct precipitation. Such differences may be part of the explanation for the substantially higher incidence of amplitude - only events in the northern versus the southern hemispheres.

Appendix A - List of Events Analyzed

"48.5" to Stanford

Date	Time (UT)	Δφ* (deg.)	ΔA† (dB)	Date	Time (UT)	Δφ* (deg.)	ΔA† (dB)
7/26/88	3:13:10	-2.48	-0.64	7/26/88	4:02:50	-3.48	1.03
7/26/88	3:32:09	4.00	0.86	7/26/88	4:11:29	-3.97	-0.85
7/26/88	3:49:39	-12.91	-0.90	7/26/88	4:15:19	0.00	-1.29
7/26/88	3:53:39	-4.47	0.81	7/26/88	4:26:49	-11.42	0.67
7/26/88	3:55:20	-3.48	1.05	7/26/88	4:34:10	-5.96	1.58
7/26/88	3:56:20	-13.90	0.00	7/26/88	4:43:09	0.00	2.21
7/26/88	3:57:00	-7.94	0.85	7/26/88	4:45:10	-11.00	0.00
7/26/88	3:59:40	-3.97	0.93				

NLK to Stanford

Date	Time (UT)	Δφ* (deg.)	ΔA† (dB)	Date	Time (UT)	Δφ* (deg.)	ΔA† (dB)
6/18/88	5:38:49	0.00	-0.54	6/25/88	10:00:29	0.50	-0.19
6/18/88	5:43:00	0.00	-0.26	6/25/88	10:02:50	0.00	-0.16
6/18/88	5:47:10	0.00	-0.34	6/25/88	10:10:09	0.00	-0.34
6/18/88	5:48:39	0.00	-0.16	6/25/88	10:15:10	2.50	-0.29
6/18/88	5:56:49	0.00	-0.10	6/25/88	10:16:45	0.00	-0.16
6/18/88	6:01:30	0.50	-0.29	6/25/88	10:18:19	0.00	-0.16
6/18/88	6:35:30	0.00	-0.26	6/25/88	10:19:39	0.00	-0.12
6/18/88	6:36:44	0.00	-0.27	6/25/88	10:20:40	-0.50	-0.23
6/18/88	6:38:09	0.00	-0.16	6/25/88	10:21:20	3.00	-0.34
6/18/88	6:40:09	0.00	-0.16	6/25/88	10:26:00	0.00	-0.14
6/18/88	7:06:50	0.00	-0.24	6/25/88	10:27:39	0.00	-0.19
6/18/88	7:59:30	0.00	-0.20	6/25/88	10:29:39	-1.50	-0.08
6/18/88	7:15:00	0.00	-0.21	6/25/88	10:33:24	0.00	-0.15
6/18/88	7:36:29	0.00	-0.15	6/25/88	10:37:50	0.00	-0.14
6/23/88	6:53:15	0.00	-0.45	6/25/88	10:41:59	-1.00	-0.11
6/23/88	6:53:39	0.00	-0.35	6/25/88	10:45:20	0.00	-0.09
6/23/88	6:55:00	0.00	-0.26	6/25/88	10:46:19	1.50	-0.25
6/24/88	6:22:59	0.00	-0.33	6/25/88	10:48:40	5.00	-0.72
6/24/88	6:28:09	1.01	-0.91	6/25/88	10:52:59	4.50	-0.71
6/25/88	7:11:00	0.00	-0.20	6/25/88	11:00:10	1.01	-0.13
6/25/88	7:15:00	-2.01	-0.24	6/25/88	11:03:09	-0.50	-0.13
6/25/88	7:19:19	0.00	-0.48	6/25/88	11:04:29	1.51	-0.25
6/25/88	7:21:59	-1.51	-0.43	6/25/88	11:06:20	0.00	-0.18
6/25/88	7:38:39	1.01	-0.13	6/25/88	11:13:44	1.00	-0.12
6/25/88	7:54:20	0.00	-0.16	6/25/88	11:[illegible]10	5.50	-0.82
6/25/88	7:57:29	0.00	-0.19	6/25/88	11:[illegible]59	3.50	0.57
6/25/88	7:58:40	0.00	-0.39	6/25/88	11:22:09	1.50	-0.31
6/25/88	8:03:19	-0.50	-0.38	6/25/88	11:26:19	3.52	-0.24
6/25/88	8:03:40	0.00	-0.25	6/25/88	11:30:00	1.51	-0.16
6/25/88	8:33:40	0.00	-0.24	6/25/88	11:35:00	2.01	-0.42

NLK to Stanford

Date	Time (UT)	Δφ* (deg.)	ΔA† (dB)
6/25/88	11:46:49	10.00	-0.22

NAU to Stanford

Date	Time (UT)	Δφ* (deg.)	ΔA† (dB)	Date	Time (UT)	Δφ* (deg.)	ΔA† (dB)
3/24/87	3:15:01	0.00	-0.43	3/27/87	9:33:40	6.25	-1.54
3/24/87	3:23:00	0.00	-0.40	3/27/87	9:44:30	2.50	-1.03
3/24/87	3:23:30	0.00	-0.29	3/27/87	9:48:49	5.00	0.16
3/24/87	3:27:21	0.00	-0.57	3/27/87	9:50:40	1.88	0.39
3/24/87	3:33:40	0.00	-0.43	4/22/87	3:32:11	5.00	-0.87
3/24/87	3:37:30	0.00	-0.31	4/22/87	3:36:31	7.00	-0.64
3/24/87	3:43:21	0.00	-0.56	4/22/87	3:42:01	5.00	-0.87
3/24/87	3:55:30	2.48	-0.21	4/22/87	3:53:30	4.00	-0.74
3/24/87	5:44:40	0.00	0.67	4/22/87	4:01:59	4.38	-2.16
3/24/87	5:57:20	3.52	0.75	4/22/87	4:06:59	1.25	-0.76
3/24/87	6:05:20	1.99	0.48	4/22/87	4:13:29	0.00	-1.25
3/24/87	6:09:41	2.98	0.00	4/22/87	4:18:39	1.88	-0.94
3/24/87	6:18:20	0.00	0.53	4/22/87	4:27:40	2.50	-1.47
3/24/87	6:19:41	0.00	0.38	4/22/87	4:31:19	0.00	-1.75
3/24/87	6:22:40	-0.99	0.53	4/22/87	4:34:50	0.00	-1.58
3/24/87	7:06:44	0.00	-0.61	4/22/87	4:49:50	1.25	-1.55
3/27/87	5:07:00	0.00	-0.44	4/22/87	5:01:39	5.96	-2.59
3/27/87	5:13:30	0.00	-0.82	4/22/87	5:10:00	2.48	-2.37
3/27/87	5:19:40	0.00	-0.49	4/22/87	5:30:10	0.00	-0.52
3/27/87	5:28:21	0.00	-0.74	4/22/87	5:33:39	-1.99	-0.60
3/27/87	5:44:51	4.97	0.00	4/22/87	5:34:59	8.94	-2.52
3/27/87	5:54:21	5.96	0.00	4/22/87	5:38:09	0.00	-1.27
3/27/87	5:56:30	0.00	-0.74	4/22/87	5:42:20	0.00	-0.59
3/27/87	6:07:19	0.00	1.08	4/22/87	5:46:19	7.94	-0.58
3/27/87	6:49:29	5.96	1.09	4/22/87	5:49:39	0.00	-1.05
3/27/87	7:07:59	0.00	-1.05	4/22/87	5:53:30	0.00	-1.01
3/27/87	8:01:30	0.00	-1.88	4/22/87	5:59:20	0.00	-1.65
3/27/87	8:04:39	11.25	1.15	4/22/87	6:01:00	0.00	-0.67
3/27/87	8:14:09	11.25	-1.33	4/22/87	6:08:30	0.00	0.87
3/27/87	8:19:29	5.63	-0.50	4/22/87	6:25:30	2.50	-1.15
3/27/87	8:24:29	9.38	-0.98	4/22/87	6:45:41	5.00	-2.70
3/27/87	8:27:49	8.75	0.26	4/22/87	7:01:59	3.97	-1.02
3/27/87	8:38:20	5.63	-0.14	4/22/87	7:06:10	1.99	-1.17
3/27/87	8:40:49	3.75	0.00	4/22/87	7:11:40	-2.98	0.00
3/27/87	9:04:29	3.75	-0.73	4/22/87	7:18:40	5.96	-2.01
3/27/87	9:10:30	0.00	-0.69	4/22/87	7:23:20	5.96	-1.76
3/27/87	9:12:49	2.50	-0.63	4/22/87	7:28:49	3.52	-1.08
3/27/87	9:14:49	6.25	0.00	4/22/87	7:33:10	8.06	-1.32
3/27/87	9:18:40	2.50	-0.80	4/22/87	7:36:50	1.01	0.51
3/27/87	9:24:19	3.75	-1.15	4/22/87	7:37:00	6.04	0.45
3/27/87	9:26:50	0.00	-0.55	4/22/87	7:41:10	7.05	0.51

NAU to Stanford

Date	Time (UT)	Δφ* (deg.)	ΔA† (dB)	Date	Time (UT)	Δφ* (deg.)	ΔA† (dB)
5/24/87	4:35:31	0.00	0.15	5/24/87	9:16:30	-2.00	0.89
5/24/87	5:04:19	0.00	-0.13	5/24/87	9:24:50	-2.00	-0.40
5/24/87	6:02:39	0.00	0.21	5/24/87	9:30:00	-5.00	-0.41
5/24/87	6:13:10	0.00	-0.36	5/25/87	7:37:19	-2.00	-0.28
5/24/87	6:16:39	0.00	-0.25	5/25/87	7:53:39	0.00	-0.59

NSS to Stanford

Date	Time (UT)	Δφ* (deg.)	ΔA† (dB)	Date	Time (UT)	Δφ* (deg.)	ΔA† (dB)
11/17/86	3:35:00	1.48	-0.42	2/5/87	11:46:40	1.50	0.11
11/17/86	3:46:40	0.00	-0.30	2/5/87	11:50:21	1.50	-0.08
11/17/86	3:53:11	0.00	-0.26	2/5/87	11:52:51	0.00	-0.15
11/17/86	4:23:40	1.51	0.00	2/5/87	12:18:30	0.00	-0.16
11/17/86	4:37:00	1.00	-0.46	2/5/87	12:29:39	0.99	-0.33
11/17/86	4:42:40	0.00	-0.54	2/5/87	12:41:00	0.00	-0.20
2/5/87	6:13:49	0.00	-0.33	2/5/87	13:28:40	3.50	0.33
2/5/87	6:34:59	0.00	-0.25	2/14/87	4:41:29	15.89	-0.73
2/5/87	6:48:39	0.50	-0.34	2/14/87	5:15:10	8.44	0.67
2/5/87	6:53:29	0.00	-0.30	3/13/87	7:33:15	2.00	1.18
2/5/87	7:03:39	0.00	-0.21	3/13/87	7:55:01	0.00	0.47
2/5/87	7:22:19	0.00	-0.29	3/13/87	7:58:50	1.50	0.37
2/5/87	7:25:20	0.00	-0.29	3/13/87	8:12:30	0.00	0.16
2/5/87	7:41:49	0.00	-0.22	3/13/87	8:18:49	-1.97	0.21
2/5/87	7:52:00	0.00	0.14	3/13/87	8:21:39	0.00	0.22
2/5/87	8:16:09	0.00	0.31	3/13/87	8:27:39	-0.99	0.27
2/5/87	8:39:59	0.00	0.19	3/13/87	8:31:59	0.00	0.26
2/5/87	8:53:39	0.00	0.52	3/15/87	1:52:01	4.00	0.61
2/5/87	9:06:45	0.00	-0.30	3/15/87	2:25:19	7.00	-0.82
2/5/87	9:18:40	0.00	0.52	3/15/87	2:37:49	2.50	0.00
2/5/87	9:19:29	0.00	-0.44	3/15/87	2:42:00	7.00	0.00
2/5/87	9:29:49	0.00	-0.32	3/15/87	2:47:39	4.00	-0.19
2/5/87	9:51:50	2.98	-0.42	3/15/87	2:49:39	4.50	0.00
2/5/87	9:52:59	0.00	-0.21	3/15/87	4:54:21	-1.01	-0.37
2/5/87	9:56:29	1.99	-0.52	3/15/87	4:57:10	0.00	-0.30
2/5/87	10:07:59	0.00	-0.41	3/15/87	5:01:39	0.00	-0.51
2/5/87	10:09:55	0.00	0.10	3/15/87	5:06:30	0.00	-0.38
2/5/87	10:11:10	0.00	0.21	3/15/87	8:24:00	0.00	0.29
2/5/87	10:17:20	0.00	0.21	3/15/87	8:29:20	1.49	0.21
2/5/87	10:20:40	0.00	0.16	3/15/87	8:42:51	3.48	-0.34
2/5/87	10:32:10	0.00	-0.21	3/15/87	9:06:50	0.00	0.85
2/5/87	10:36:10	0.00	0.21	3/16/87	3:06:51	3.00	-0.19
2/5/87	10:39:59	-0.50	0.16	3/16/87	3:29:41	0.00	-0.19
2/5/87	10:43:40	1.49	-0.29	3/16/87	3:37:40	1.00	-0.26
2/5/87	11:07:40	0.00	0.13	3/16/87	3:46:46	0.00	0.21
2/5/87	11:09:50	0.00	0.27	3/16/87	3:48:40	0.00	-0.10
2/5/87	11:36:50	0.00	-0.14	3/16/87	3:53:00	0.00	-0.19

NSS to Stanford

Date	Time (UT)	Δφ* (deg.)	ΔA† (dB)	Date	Time (UT)	Δφ* (deg.)	ΔA† (dB)
3/16/87	4:00:10	0.99	-0.38	3/17/87	7:22:10	2.00	0.42
3/16/87	4:08:09	1.49	-0.26	3/17/87	7:23:39	0.00	0.21
3/16/87	4:09:55	1.99	-0.13	3/17/87	7:26:20	0.00	0.59
3/16/87	4:11:20	2.98	-0.50	3/17/87	7:28:00	0.00	0.24
3/16/87	5:05:00	0.00	-0.58	3/17/87	7:29:39	0.00	0.44
3/16/87	5:20:05	0.50	-0.27	3/17/87	7:30:59	0.00	0.35
3/16/87	5:23:11	3.50	-0.95	3/17/87	7:35:10	-2.50	0.61
3/16/87	5:33:15	1.00	-0.12	3/17/87	7:36:39	0.00	0.66
3/16/87	5:34:00	1.00	-0.15	3/17/87	7:38:39	-3.00	1.12
3/16/87	5:47:51	2.00	-0.21	3/17/87	7:42:49	-1.50	0.54
3/16/87	6:43:25	2.52	-0.39	3/17/87	7:45:50	0.00	0.36
3/16/87	7:12:40	3.97	-0.51	3/17/87	7:47:10	-3.50	0.88
3/16/87	7:14:49	3.97	-0.28	3/17/87	7:52:00	-2.50	0.72
3/16/87	7:18:59	3.97	0.17	3/17/87	7:55:09	-3.00	0.15
3/16/87	7:22:49	0.00	1.11	3/17/87	7:59:20	-6.50	1.21
3/16/87	7:56:34	-0.50	0.17	3/17/87	8:03:19	-4.53	0.79
3/16/87	8:00:25	6.95	-0.49	3/17/87	8:08:20	-4.53	0.45
3/16/87	8:23:51	-1.49	0.47	3/17/87	8:12:09	-3.02	0.42
3/16/87	8:30:00	5.96	-0.36	3/17/87	8:20:00	-3.02	0.49
3/16/87	8:40:11	-1.99	0.40	3/17/87	8:23:14	-4.53	0.29
3/16/87	8:43:40	-0.99	0.29	3/17/87	8:43:19	-3.02	0.36
3/16/87	8:53:26	-1.49	0.47	3/17/87	8:54:40	-2.01	0.22
3/16/87	9:08:49	0.00	0.32	3/26/87	7:17:00	-5.46	-0.06
3/16/87	9:15:39	0.00	0.35	3/26/87	7:38:30	-0.99	0.15
3/16/87	9:17:50	0.00	0.20	3/26/87	7:57:01	-1.99	-0.17
3/16/87	9:53:49	-1.49	-0.35	3/26/87	8:16:40	-1.51	-0.32
3/16/87	10:33:09	6.95	-0.31	3/26/87	8:23:49	0.00	-0.17
3/17/87	3:45:52	-1.00	0.25	3/26/87	8:26:35	-1.01	-0.26
3/17/87	4:10:12	-3.00	0.39	3/26/87	8:33:19	-1.01	-0.29
3/17/87	6:17:30	-1.99	0.34	4/13/87	8:07:11	-3.97	0.35
3/17/87	6:20:00	-1.99	0.25	4/13/87	8:43:50	-2.98	-0.27
3/17/87	6:50:30	-5.46	-0.13	4/13/87	9:13:40	0.00	-0.21
3/17/87	6:54:40	-4.97	0.00	4/13/87	10:06:50	0.00	-0.91
3/17/87	7:03:50	-5.50	-0.22				

NAA to Palmer

Date	Time (UT)	Δφ* (deg.)	ΔA† (dB)	Date	Time (UT)	Δφ* (deg.)	ΔA† (dB)
4/18/88	3:06:10	7.50	1.28	4/18/88	4:21:39	9.50	0.15
4/18/88	3:18:19	10.00	0.51	4/18/88	4:45:50	8.00	1.13
4/18/88	3:23:29	12.00	0.95	4/18/88	4:50:10	6.00	1.73
4/18/88	3:28:09	4.00	0.30	4/24/88	7:19:35	1.99	-0.68
4/18/88	3:31:39	8.00	0.75	4/24/88	7:23:20	4.97	-0.98
4/18/88	3:35:20	8.00	0.71	4/24/88	7:24:40	1.99	-1.04
4/18/88	3:42:40	6.00	0.64	4/24/88	7:28:00	6.46	0.42
4/18/88	3:44:00	3.50	0.36	4/26/88	0:31:49	3.48	0.76

NAA to Palmer

Date	Time (UT)	Δφ* (deg.)	ΔA† (dB)	Date	Time (UT)	Δφ* (deg.)	ΔA† (dB)
4/26/88	0:33:39	3.97	0.91	4/28/88	3:13:00	8.94	0.00
4/28/88	3:07:30	6.95	0.00	4/28/88	3:15:00	5.96	0.00
4/28/88	3:09:39	5.96	0.00	4/28/88	3:16:45	3.97	0.00

NSS to Palmer

Date	Time (UT)	Δφ* (deg.)	ΔA† (dB)	Date	Time (UT)	Δφ* (deg.)	ΔA† (dB)
4/18/88	3:38:49	-4.03	0.10	4/28/88	4:08:09	5.00	-0.39
4/18/88	3:45:49	-3.02	-0.04	4/28/88	4:09:20	0.00	0.72
4/18/88	6:03:50	0.00	0.35	4/28/88	4:10:00	6.00	0.00
4/28/88	3:15:00	0.00	0.38	4/28/88	4:11:49	8.00	0.00
4/28/88	3:19:30	0.00	0.37	4/28/88	4:14:40	6.50	0.00
4/28/88	3:24:09	2.27	0.43	4/28/88	4:16:39	7.00	0.00
4/28/88	3:28:40	-2.84	0.76	4/28/88	4:24:00	6.50	0.53
4/28/88	3:52:10	4.54	0.00	4/28/88	4:47:50	-10.00	0.31
4/28/88	3:54:00	0.00	0.46	4/28/88	4:57:49	4.50	0.00
4/28/88	3:55:09	2.27	-0.13	4/28/88	6:01:59	8.00	0.00
4/28/88	3:56:29	4.54	0.00	4/28/88	6:19:19	12.91	0.59
4/28/88	3:57:20	0.00	1.01	4/28/88	6:21:30	7.94	0.51
4/28/88	4:00:19	6.00	0.00	4/28/88	7:45:00	5.92	0.86
4/28/88	4:06:35	3.50	0.00	4/28/88	7:46:59	4.93	0.58

NLK to Palmer

Date	Time (UT)	Δφ* (deg.)	ΔA† (dB)	Date	Time (UT)	Δφ* (deg.)	ΔA† (dB)
5/6/88	3:45:10	2.47	-0.33	5/6/88	8:37:09	3.48	0.32
5/6/88	3:52:20	0.99	0.12	5/6/88	8:41:59	1.99	0.37
5/6/88	3:54:09	3.45	0.24	5/6/88	8:52:59	2.98	0.22
5/6/88	4:28:40	2.01	0.62	5/6/88	8:53:09	3.97	0.22
5/6/88	8:02:29	0.00	0.65	5/6/88	8:53:24	1.99	0.31
5/6/88	8:03:30	1.99	0.45	5/6/88	9:00:50	2.00	0.35
5/6/88	8:05:09	0.00	0.32	5/6/88	9:02:29	0.00	0.16
5/6/88	8:14:20	0.00	0.30	5/6/88	9:04:10	1.50	0.41
5/6/88	8:22:00	6.46	0.70	5/6/88	9:12:09	1.00	0.19
5/6/88	8:26:19	0.00	0.17	5/6/88	9:18:30	1.50	0.39
5/6/88	8:27:39	5.46	0.38	5/6/88	9:19:39	0.00	0.24
5/6/88	8:29:30	6.95	0.04	5/6/88	9:21:20	2.00	0.28
5/6/88	8:30:04	4.47	0.00	5/6/88	9:26:19	3.00	0.76
5/6/88	8:30:39	2.98	0.00	5/6/88	10:28:40	0.00	0.40
5/6/88	8:31:19	3.48	0.00	5/6/88	10:48:30	4.00	0.95
5/6/88	8:34:29	3.48	0.00	5/6/88	11:22:09	1.99	0.50
5/6/88	8:35:19	4.47	0.18				

NPM to Palmer

Date	Time (UT)	Δϕ* (deg.)	ΔA† (dB)	Date	Time (UT)	Δϕ* (deg.)	ΔA† (dB)
5/1/88	5:19:39	0.50	-0.13	5/4/88	9:27:59	1.24	-0.11
5/1/88	5:27:40	2.00	-0.23	5/5/88	9:16:20	2.50	-0.25
5/1/88	5:46:29	0.00	-0.10	5/5/88	9:19:00	1.50	-0.21
5/1/88	5:52:30	0.99	-0.12	5/5/88	9:20:30	0.50	-0.30
5/1/88	7:53:19	0.99	-0.11	5/5/88	9:26:59	1.00	-0.18
5/2/88	6:21:00	0.99	-0.40	5/5/88	9:36:00	4.00	-0.06
5/2/88	6:24:39	1.49	-0.62	5/5/88	9:48:39	0.50	-0.52
5/2/88	6:55:29	0.00	-0.09	5/5/88	10:00:30	0.00	-0.20
5/4/88	4:54:19	1.99	-0.31	5/5/88	10:01:30	0.00	-0.23
5/4/88	5:18:39	3.00	-0.49	5/5/88	10:04:00	0.49	-0.20
5/4/88	5:26:34	2.50	-0.37	5/5/88	10:07:00	0.99	-0.26
5/4/88	5:28:10	0.50	-0.17	5/5/88	10:08:59	0.99	-0.47
5/4/88	5:30:00	1.50	-0.35	5/5/88	10:09:59	0.00	-0.24
5/4/88	5:55:30	2.98	-0.27	5/5/88	10:10:15	0.99	-0.28
5/4/88	5:57:30	0.99	-0.30	5/5/88	10:13:25	1.48	-0.30
5/4/88	6:00:09	0.00	-0.24	5/5/88	10:16:55	2.47	-0.38
5/4/88	6:01:49	1.50	-0.21	5/5/88	10:28:00	5.92	-0.42
5/4/88	6:08:39	0.00	-0.12	5/5/88	10:29:40	1.97	-0.22
5/4/88	6:11:20	0.00	-0.24	5/5/88	10:33:09	3.45	-0.16
5/4/88	6:23:49	0.50	-0.32	5/5/88	10:41:20	1.48	-0.13
5/4/88	6:26:59	1.50	-0.45	5/5/88	11:03:39	2.52	-0.15
5/4/88	6:37:50	9.50	-0.65	5/5/88	11:06:00	2.52	0.00
5/4/88	6:40:00	6.50	-0.46	5/5/88	11:15:49	3.52	-0.02
5/4/88	6:47:59	1.50	-0.15	5/5/88	11:17:49	2.01	-0.22
5/4/88	6:48:39	6.50	-0.66	5/5/88	11:23:39	0.00	-0.14
5/4/88	7:11:19	1.50	-0.33	5/5/88	11:26:40	1.51	-0.21
5/4/88	7:20:00	1.00	-0.31	5/5/88	11:29:00	0.50	-0.35
5/4/88	7:27:00	2.00	-0.25	5/5/88	11:30:20	1.01	-0.37
5/4/88	7:30:09	3.00	-0.26	5/6/88	3:17:50	0.99	0.73
5/4/88	7:34:09	2.50	-0.32	5/6/88	7:02:30	0.00	0.52
5/4/88	7:36:19	3.00	-0.29	5/6/88	7:09:39	2.48	-0.33
5/4/88	7:37:19	2.00	-0.60	5/6/88	7:11:29	0.00	-0.13
5/4/88	7:46:40	1.00	-0.32	5/6/88	7:13:09	0.00	0.14
5/4/88	7:48:00	2.00	-0.45	5/6/88	7:16:29	2.98	0.13
5/4/88	7:49:10	1.00	-0.22	5/6/88	7:16:59	3.48	-0.12
5/4/88	7:50:10	1.00	-0.27	5/6/88	7:18:19	4.47	-0.30
5/4/88	7:57:49	1.00	-0.22	5/6/88	7:20:20	3.48	-0.27
5/4/88	7:59:49	4.00	-0.50	5/6/88	7:21:20	2.48	-0.36
5/4/88	8:02:29	1.49	-0.51	5/6/88	7:22:00	1.99	-0.21
5/4/88	8:16:49	2.00	-0.21	5/6/88	7:23:30	1.99	-0.22
5/4/88	8:32:00	3.00	-0.19	5/6/88	7:25:20	3.97	-0.18
5/4/88	8:46:09	3.97	-0.23	5/6/88	7:29:40	4.97	-0.14
5/4/88	8:46:45	3.00	-0.33	5/6/88	7:31:49	2.48	-0.11
5/4/88	8:47:49	2.00	-0.25	5/6/88	7:33:09	2.48	-0.14
5/4/88	8:50:30	3.00	-0.32	5/6/88	7:34:09	3.97	-0.21
5/4/88	8:56:20	1.50	-0.19	5/6/88	7:35:09	3.97	-0.24
5/4/88	9:10:49	2.48	-0.46	5/6/88	7:36:45	5.96	-0.67
5/4/88	9:21:10	1.86	-0.17	5/6/88	7:38:19	4.47	-0.41

NPM to Palmer

Date	Time (UT)	Δϕ* (deg.)	ΔA† (dB)	Date	Time (UT)	Δϕ* (deg.)	ΔA† (dB)
5/6/88	7:39:59	4.47	-0.46	5/11/88	3:51:59	3.97	-1.24
5/6/88	7:40:39	7.94	-0.91	5/11/88	3:54:39	5.92	1.35
5/6/88	7:44:10	2.48	-0.44	5/11/88	3:56:40	5.92	-1.58
5/6/88	7:46:40	0.99	-0.44	5/11/88	4:00:30	1.00	-1.25
5/6/88	7:47:00	1.49	-0.46	5/11/88	4:05:20	2.50	-0.93
5/6/88	7:48:30	0.50	-0.32	5/11/88	4:46:00	3.97	-0.61
5/6/88	7:49:54	0.50	-0.30	5/11/88	4:47:00	5.46	-0.95
5/6/88	7:51:00	0.50	-0.14	5/11/88	4:51:20	1.99	-0.33
5/6/88	7:51:50	0.50	-0.30	5/11/88	4:52:59	0.00	-0.26
5/6/88	7:53:15	0.00	-0.21	5/11/88	4:54:59	2.48	-0.33
5/6/88	8:02:19	2.00	-0.21	5/11/88	4:59:49	3.48	-0.66
5/6/88	8:21:59	4.50	-0.34	5/11/88	5:30:50	1.49	-0.37
5/6/88	8:29:10	3.00	-0.33	5/11/88	5:33:20	2.98	-0.46
5/6/88	8:31:20	1.50	-0.30	5/11/88	5:37:00	3.48	-0.87
5/6/88	9:50:49	9.93	-0.62	5/11/88	5:53:20	0.50	-0.28
5/6/88	9:51:39	1.99	-0.63	5/11/88	5:53:40	3.50	-0.58
5/6/88	9:53:09	2.48	-0.25	5/11/88	5:56:30	3.00	-0.52
5/6/88	9:53:49	2.48	-0.15	5/11/88	5:58:20	3.00	-0.71
5/6/88	10:27:00	3.97	-0.38	5/11/88	6:03:09	3.02	-0.48
5/6/88	10:29:10	13.90	-0.98	5/11/88	6:03:39	3.52	-0.72
5/6/88	10:32:59	1.49	-0.23	5/11/88	6:06:09	4.53	-0.70
5/6/88	10:33:25	3.48	-0.43	5/11/88	6:09:19	3.52	-0.66
5/6/88	10:34:19	3.97	-0.53	5/11/88	6:11:20	0.50	-0.25
5/6/88	10:43:30	1.49	-0.32	5/11/88	6:20:20	2.01	-0.63
5/6/88	10:45:00	3.97	-0.66	5/11/88	6:26:35	0.00	-0.46
5/6/88	10:49:00	2.98	-0.19	5/11/88	6:30:19	3.02	-0.93
5/6/88	10:56:49	8.44	-0.37	5/11/88	7:29:40	2.50	-0.36
5/6/88	11:01:39	4.00	-0.34	5/11/88	7:38:39	4.00	-0.52
5/6/88	11:02:59	3.00	-0.21	5/11/88	7:43:50	2.50	-0.24
5/6/88	11:03:15	4.50	-0.41	5/11/88	7:47:30	2.00	-0.10
5/6/88	11:06:44	7.00	-0.44	5/11/88	7:50:10	0.00	0.24
5/6/88	11:39:59	3.00	-0.12	5/11/88	8:01:59	2.48	-0.24
5/6/88	11:42:59	2.00	-0.29	5/11/88	8:06:44	2.48	-0.23
5/6/88	11:53:10	0.00	-0.29	5/11/88	8:09:54	0.00	0.17
5/10/88	6:24:59	1.48	-0.16	5/11/88	8:21:49	1.99	-0.18
5/10/88	6:28:19	0.49	-0.14	5/11/88	8:33:40	3.48	-0.23
5/10/88	6:29:39	0.00	-0.09	5/11/88	8:43:15	2.98	-0.38
5/10/88	6:32:19	0.49	-0.13	5/11/88	9:16:20	0.00	-0.16
5/10/88	6:33:29	1.97	-0.17	5/11/88	9:18:30	0.00	-0.23
5/10/88	6:37:20	1.97	-0.21	5/11/88	9:21:20	1.99	-0.25
5/10/88	6:41:20	0.00	-0.16	5/11/88	9:22:59	0.99	-0.16
5/10/88	6:42:20	1.50	-0.24	5/11/88	9:29:29	0.00	-0.16
5/10/88	6:44:20	3.50	-0.23	5/11/88	9:33:50	1.49	-0.24
5/10/88	6:47:39	10.00	-0.66	5/11/88	9:36:00	0.00	-0.30
5/10/88	6:52:49	4.50	-0.23	5/11/88	9:48:39	1.99	-0.17
5/10/88	7:08:19	2.48	-0.13	5/11/88	9:59:20	0.00	-0.25
5/10/88	7:57:29	5.96	-0.30	5/11/88	10:02:50	1.50	-0.37
5/10/88	8:19:59	1.51	-0.10	5/11/88	10:13:15	0.50	-0.22

NPM to Palmer

Date	Time (UT)	Δφ* (deg.)	ΔA† (dB)	Date	Time (UT)	Δφ* (deg.)	ΔA† (dB)
5/11/88	10:16:09	0.50	-0.39	5/14/88	5:13:40	0.74	-0.16
5/11/88	10:21:40	1.50	-0.32	5/14/88	5:33:24	2.22	-0.68
5/11/88	10:29:00	2.50	-0.67	5/14/88	5:34:30	1.48	-0.26
5/11/88	10:34:39	1.50	-0.42	5/14/88	5:44:39	1.48	-0.15
5/12/88	4:39:29	2.96	-0.36	5/14/88	5:50:10	1.48	-0.36
5/12/88	4:42:10	1.97	-0.17	5/14/88	5:50:50	0.00	-0.21
5/12/88	4:46:20	1.97	-0.22	5/14/88	5:53:20	0.00	-0.21
5/12/88	5:31:30	1.99	-0.29	5/15/88	6:01:39	0.00	-0.11
5/12/88	5:33:14	1.99	-0.35	5/15/88	6:02:59	0.00	-0.30
5/12/88	5:33:50	1.99	-0.36	5/15/88	6:03:29	0.99	-0.35
5/12/88	5:36:10	1.49	-0.34	5/15/88	6:04:39	0.00	-0.22
5/12/88	5:38:59	1.49	-0.40	5/15/88	7:11:09	6.00	-0.57
5/12/88	5:43:39	3.48	-0.52	5/15/88	7:13:19	5.00	-0.26
5/12/88	5:51:40	0.99	-0.21	5/15/88	7:32:49	6.00	-0.44
5/12/88	5:55:00	0.00	-0.18	5/15/88	7:39:29	2.00	-0.29
5/12/88	5:55:50	0.99	-0.25	5/15/88	7:42:50	1.00	-0.20
5/12/88	6:33:15	0.99	-0.45	5/15/88	7:44:30	0.00	-0.16
5/12/88	6:36:10	1.99	-0.43	5/15/88	7:46:10	2.50	-0.18
5/12/88	6:37:40	0.00	-0.29	5/15/88	7:46:40	1.00	-0.09
5/12/88	6:44:40	1.99	-0.52	5/15/88	7:49:20	2.50	-0.20
5/12/88	6:51:19	1.49	-0.60	5/15/88	7:51:20	3.00	-0.28
5/12/88	6:55:19	1.49	-0.36	5/15/88	7:52:00	5.00	-0.33
5/12/88	6:57:20	0.00	-0.25	5/15/88	7:53:19	4.00	-0.48
5/12/88	7:22:20	1.49	-0.30	5/15/88	7:54:09	5.50	-0.43
5/12/88	7:25:00	0.99	-0.30	5/15/88	7:56:35	3.50	-0.46
5/12/88	7:28:50	0.00	-0.26	5/15/88	7:56:59	2.50	-0.37
5/12/88	7:33:09	1.99	-0.32	5/15/88	7:58:29	2.50	-0.18
5/12/88	7:35:09	0.99	-0.45	5/15/88	8:00:19	3.45	-0.24
5/12/88	7:36:35	1.49	-0.27	5/15/88	8:02:59	1.97	-0.30
5/12/88	7:37:09	0.50	-0.29	5/15/88	8:06:40	2.47	-0.32
5/12/88	7:39:45	0.00	-0.26	5/15/88	8:24:59	1.97	-0.18
5/12/88	7:44:20	2.98	-0.36	5/15/88	8:29:54	2.96	-0.21
5/12/88	7:53:39	1.99	-0.35	5/15/88	8:33:00	3.95	-0.31
5/12/88	7:56:29	0.99	-0.29	5/15/88	8:33:50	2.96	-0.31
5/12/88	7:56:45	3.48	-0.33	5/15/88	8:36:10	3.45	-0.26
5/12/88	8:08:00	0.00	-0.18	5/15/88	8:43:19	2.96	-0.23
5/12/88	8:09:00	0.50	-0.57	5/15/88	8:46:35	8.88	-0.71
5/12/88	8:18:49	2.00	-0.35	5/15/88	8:50:00	3.95	-0.24
5/12/88	8:25:19	0.50	-0.18	5/15/88	8:53:20	7.40	-0.59
5/12/88	8:35:00	0.00	-0.16	5/15/88	8:54:10	2.96	-0.24
5/12/88	8:41:49	0.00	-0.15	5/15/88	8:54:40	1.97	-0.16
5/12/88	8:42:59	0.50	-0.17	5/15/88	8:56:20	0.99	-0.32
5/12/88	8:44:19	1.00	-0.24	5/15/88	8:56:50	2.96	-0.23
5/12/88	8:45:09	1.00	-0.27	5/15/88	8:58:20	1.97	-0.16
5/12/88	8:47:29	2.50	-0.34	5/15/88	8:59:10	4.44	-0.23
5/12/88	8:52:10	0.00	-0.18	5/15/88	9:01:09	3.00	-0.31
5/12/88	9:01:59	0.99	-0.11	5/15/88	9:02:59	3.50	-0.20
5/12/88	9:07:09	0.00	-0.11	5/15/88	9:03:19	3.00	-0.23

NPM to Palmer

Date	Time (UT)	Δφ* (deg.)	ΔA† (dB)	Date	Time (UT)	Δφ* (deg.)	ΔA† (dB)
5/15/88	9:04:19	2.00	-0.25	5/15/88	10:28:40	0.00	-0.19
5/15/88	9:06:45	7.00	-0.40	5/15/88	10:32:49	0.00	-0.17
5/15/88	9:07:49	3.00	-0.11	5/15/88	10:33:39	5.00	-0.91
5/15/88	9:08:49	2.00	-0.13	5/15/88	10:33:59	0.00	-0.34
5/15/88	9:09:59	1.50	-0.20	5/15/88	10:34:59	2.00	-0.28
5/15/88	9:10:19	2.50	-0.13	5/15/88	10:35:29	5.50	-1.09
5/15/88	9:10:29	1.50	-0.09	5/15/88	10:35:59	4.00	-0.50
5/15/88	9:14:30	2.50	-0.16	5/15/88	10:36:45	3.50	-0.56
5/15/88	9:15:10	3.00	-0.14	5/15/88	10:37:39	4.50	-0.77
5/15/88	9:15:50	3.00	-0.18	5/15/88	10:39:55	2.00	-0.53
5/15/88	9:20:20	4.00	-0.13	5/15/88	10:40:29	4.50	-0.96
5/15/88	9:22:10	4.00	-0.11	5/15/88	10:41:50	2.50	-0.84
5/15/88	9:23:39	4.50	-0.22	5/15/88	10:43:24	3.00	-0.73
5/15/88	9:24:09	0.00	-0.18	5/15/88	10:44:50	1.50	-0.83
5/15/88	9:24:19	3.50	-0.20	5/15/88	10:48:40	0.00	-0.88
5/15/88	9:25:59	5.00	-0.31	5/15/88	10:51:00	0.00	-0.63
5/15/88	9:26:39	2.00	-0.07	5/15/88	10:52:20	3.50	-0.65
5/15/88	9:27:59	4.00	-0.18	5/15/88	10:53:19	1.50	-0.43
5/15/88	9:28:19	4.50	-0.31	5/15/88	10:56:59	2.00	-0.26
5/15/88	9:28:49	4.50	-0.38	5/15/88	10:57:19	4.50	-0.43
5/15/88	9:30:29	4.50	-0.20	5/15/88	10:58:29	0.50	-0.23
5/15/88	9:35:20	0.00	-0.11	5/15/88	11:00:39	0.00	-0.26
5/15/88	9:39:54	1.00	-0.15	5/15/88	11:02:19	2.52	-0.24
5/15/88	9:42:40	6.00	-0.41	5/15/88	11:03:50	3.52	-0.37
5/15/88	9:43:24	3.00	-0.26	5/15/88	11:05:00	3.02	-0.60
5/15/88	9:46:19	8.00	-0.62	5/15/88	11:06:10	5.03	-0.48
5/15/88	9:46:59	1.00	-0.19	5/15/88	11:07:50	3.02	-0.48
5/15/88	9:49:59	1.00	-0.39	5/15/88	11:09:40	4.53	-0.74
5/15/88	9:50:59	1.00	-0.17	5/15/88	11:15:00	5.03	-0.63
5/15/88	9:51:15	2.00	-0.55	5/15/88	11:16:45	4.03	-0.68
5/15/88	9:52:39	2.00	-0.27	5/15/88	11:20:05	4.03	-0.52
5/15/88	9:53:19	1.00	-0.20	5/15/88	11:26:50	3.02	-0.53
5/15/88	9:54:59	2.00	-0.22	5/15/88	11:29:50	4.03	-0.44
5/15/88	9:59:30	3.00	-0.57	5/15/88	11:32:50	3.52	-0.63
5/15/88	10:01:50	2.00	-0.47	5/15/88	11:33:40	1.51	-0.39
5/15/88	10:03:40	3.50	-0.82	5/15/88	11:34:00	3.52	-0.35
5/15/88	10:06:10	5.00	-0.97	5/15/88	11:37:20	1.01	-0.46
5/15/88	10:09:59	2.00	-0.59	5/15/88	12:01:59	0.00	-0.11
5/15/88	10:10:59	4.50	-1.07	5/15/88	12:06:59	1.00	-0.16
5/15/88	10:13:19	0.50	-0.31	5/15/88	12:17:10	0.00	-0.17
5/15/88	10:14:59	2.50	-0.91	5/15/88	12:19:20	0.00	-0.11
5/15/88	10:16:45	2.00	-0.63	5/16/88	4:33:39	1.88	-0.96
5/15/88	10:17:59	3.50	-0.55	5/16/88	4:34:59	1.88	-0.79
5/15/88	10:20:04	2.00	-0.46	5/16/88	4:36:35	0.63	-0.15
5/15/88	10:20:50	2.00	-0.57	5/16/88	4:40:19	0.63	-0.31
5/15/88	10:21:50	2.50	-0.63	5/16/88	4:40:39	2.50	-0.54
5/15/88	10:24:00	0.00	-0.32	5/16/88	4:45:40	3.13	-0.69
5/15/88	10:25:00	0.00	-0.31	5/16/88	4:47:10	2.50	-0.61

NPM to Palmer

Date	Time (UT)	Δϕ* (deg.)	ΔA† (dB)	Date	Time (UT)	Δϕ* (deg.)	ΔA† (dB)
5/16/88	4:48:40	2.50	-0.77	5/16/88	6:17:30	0.50	-0.19
5/16/88	4:50:20	0.63	-0.44	5/16/88	6:19:50	1.49	-0.38
5/16/88	4:51:40	2.50	-0.52	5/16/88	6:20:40	2.98	-0.53
5/16/88	4:53:19	0.00	-0.41	5/16/88	6:25:19	0.99	-0.21
5/16/88	4:54:39	1.25	-0.94	5/16/88	6:26:19	4.47	-0.76
5/16/88	4:55:19	0.00	-0.59	5/16/88	6:26:59	2.98	-0.64
5/16/88	4:56:29	0.00	-0.57	5/16/88	6:27:59	0.99	-0.31
5/16/88	4:56:55	0.00	-0.34	5/16/88	6:29:19	1.99	-0.70
5/16/88	4:58:29	0.00	-0.39	5/16/88	6:30:19	1.99	-0.40
5/16/88	5:33:40	0.00	-0.43	5/16/88	6:32:09	4.97	-1.00
5/16/88	5:36:50	3.72	-0.71	5/16/88	6:33:50	1.49	-0.38
5/16/88	5:38:19	3.10	-1.11	5/16/88	6:35:20	0.50	-0.32
5/16/88	5:40:39	0.62	-0.35	5/16/88	6:38:00	0.50	-0.18
5/16/88	5:41:19	0.00	-0.22	5/16/88	6:39:40	1.49	-0.59
5/16/88	5:41:59	1.24	-0.43	5/16/88	6:40:30	0.50	-0.52
5/16/88	5:42:59	0.62	-0.18	5/16/88	7:45:20	2.48	-0.21
5/16/88	5:43:39	3.10	-0.85	5/16/88	7:48:00	1.49	-0.26
5/16/88	5:44:19	3.10	-0.93	5/16/88	7:48:50	0.50	-0.18
5/16/88	5:44:59	4.97	-0.88	5/16/88	7:50:10	3.48	-0.25
5/16/88	5:45:49	3.10	-0.82	5/16/88	7:52:00	2.98	-0.11
5/16/88	5:46:19	1.24	-0.55	5/16/88	7:53:29	1.99	-0.26
5/16/88	5:46:45	1.86	-0.40	5/16/88	7:54:29	2.48	-0.11
5/16/88	5:47:19	3.10	-0.82	5/16/88	7:56:35	2.98	-0.17
5/16/88	5:48:39	3.10	-0.97	5/16/88	7:58:19	0.99	-0.08
5/16/88	5:49:40	0.62	-0.31	5/16/88	7:59:09	1.49	-0.09
5/16/88	5:51:00	1.24	-0.57	5/16/88	8:00:19	3.97	-0.19
5/16/88	5:52:50	1.24	-0.51	5/16/88	8:01:59	2.48	-0.13
5/16/88	5:53:20	1.86	-0.48	5/16/88	8:02:59	2.48	-0.15
5/16/88	5:53:40	1.24	-0.36	5/16/88	8:05:10	3.48	-0.11
5/16/88	5:55:30	1.86	-0.56	5/16/88	8:13:00	2.48	-0.07
5/16/88	5:56:10	1.86	-0.46	5/16/88	8:20:39	-2.98	0.00
5/16/88	5:56:40	0.00	-0.15	5/16/88	8:21:19	2.48	0.00
5/16/88	5:57:10	0.62	-0.23	5/16/88	8:21:59	3.97	-0.02
5/16/88	5:58:40	1.24	-0.35	5/16/88	8:23:19	3.48	-0.09
5/16/88	5:59:40	3.10	-0.61	5/16/88	8:23:59	1.99	-0.07
5/16/88	6:01:09	1.49	-0.39	5/16/88	8:25:59	5.96	-0.07
5/16/88	6:03:29	1.49	-0.34	5/16/88	8:28:20	1.99	-0.07
5/16/88	6:03:59	4.97	-0.87	5/16/88	8:29:30	4.47	-0.07
5/16/88	6:04:39	4.47	-0.82	5/16/88	8:30:40	5.46	-0.17
5/16/88	6:05:19	5.96	-0.76	5/16/88	8:32:30	4.47	-0.29
5/16/88	6:06:35	1.99	-0.39	5/16/88	8:33:10	3.48	-0.07
5/16/88	6:06:59	2.48	-0.54	5/16/88	8:34:20	4.47	-0.09
5/16/88	6:07:59	3.48	-0.70	5/16/88	8:38:29	1.99	-0.14
5/16/88	6:09:19	-0.99	-0.19	5/16/88	8:39:49	1.49	-0.19
5/16/88	6:10:19	0.50	-0.17	5/16/88	8:40:49	3.97	-0.56
5/16/88	6:12:40	1.49	-0.36	5/16/88	8:41:19	3.97	-0.31
5/16/88	6:15:30	0.99	-0.19	5/16/88	8:42:49	3.97	-0.45
5/16/88	6:16:34	0.99	-0.23	5/16/88	8:44:59	2.98	-0.48

NPM to Palmer

Date	Time (UT)	Δϕ* (deg.)	ΔA† (dB)	Date	Time (UT)	Δϕ* (deg.)	ΔA† (dB)
5/16/88	8:46:29	1.99	-0.33	5/16/88	10:03:24	1.48	-0.16
5/16/88	8:46:49	3.48	-0.33	5/16/88	10:03:40	1.97	-0.14
5/16/88	8:48:19	5.96	-0.66	5/16/88	10:04:40	1.48	-0.09
5/16/88	8:50:40	2.98	-0.53	5/16/88	10:08:19	3.45	-0.36
5/16/88	8:52:00	4.97	-0.61	5/16/88	10:10:09	3.45	-0.43
5/16/88	8:53:00	1.49	-0.24	5/16/88	10:18:50	2.96	-0.26
5/16/88	8:53:20	0.00	-0.31	5/16/88	10:21:20	3.45	-0.26
5/16/88	8:54:40	3.48	-0.48	5/16/88	10:23:20	5.00	-0.40
5/16/88	8:57:20	3.48	-0.56	5/16/88	10:26:10	3.50	-0.34
5/16/88	8:58:20	0.00	-0.28	5/16/88	10:27:00	3.00	-0.23
5/16/88	8:59:54	2.98	-0.48	5/16/88	10:29:20	3.00	-0.17
5/16/88	9:00:09	3.00	-0.39	5/16/88	10:34:39	3.00	-0.03
5/16/88	9:01:39	2.50	-0.44	5/16/88	10:36:39	2.00	0.00
5/16/88	9:02:49	2.50	-0.38	5/16/88	10:37:49	2.00	-0.09
5/16/88	9:03:25	0.00	-0.13	5/16/88	10:39:39	3.00	-0.09
5/16/88	9:03:39	1.50	-0.23	5/16/88	10:40:09	5.50	-0.21
5/16/88	9:04:59	2.50	-0.28	5/16/88	10:41:09	2.50	-0.03
5/16/88	9:06:49	1.50	-0.15	5/16/88	10:42:20	5.00	-0.15
5/16/88	9:07:59	6.50	-0.79	5/16/88	10:43:40	2.00	-0.15
5/16/88	9:09:19	-8.00	-0.10	5/16/88	10:45:10	3.00	-0.09
5/16/88	9:10:05	0.00	-0.16	5/16/88	10:46:40	3.00	-0.06
5/16/88	9:11:20	2.00	-0.21	5/16/88	10:50:10	2.50	-0.03
5/16/88	9:12:10	7.50	-1.13	5/16/88	10:55:19	2.00	-0.11
5/16/88	9:13:10	2.50	-0.44	5/16/88	10:56:35	5.00	-0.32
5/16/88	9:14:30	4.00	-0.44	5/16/88	10:58:39	3.00	-0.23
5/16/88	9:15:50	3.00	-0.52	5/16/88	11:00:05	6.41	-0.57
5/16/88	9:16:40	1.50	-0.11	5/16/88	11:01:09	1.97	-0.08
5/16/88	9:18:40	0.50	-0.11	5/16/88	11:02:09	6.90	-0.56
5/16/88	9:19:50	2.00	-0.10	5/16/88	11:03:15	3.45	-0.30
5/16/88	9:21:30	2.50	-0.13	5/16/88	11:05:40	0.99	-0.13
5/16/88	9:24:39	2.00	-0.10	5/16/88	11:06:50	4.93	-0.40
5/16/88	9:27:59	2.50	-0.10	5/16/88	11:08:40	7.89	-0.50
5/16/88	9:36:10	0.00	0.26	5/16/88	11:10:20	7.40	-0.52
5/16/88	9:39:30	1.50	0.00	5/16/88	11:11:40	1.48	-0.20
5/16/88	9:44:20	5.50	-0.15	5/16/88	11:13:00	2.96	-0.23
5/16/88	9:46:39	3.50	-0.10	5/16/88	11:18:19	3.45	-0.38
5/16/88	9:49:29	3.50	-0.13	5/16/88	11:23:29	1.48	-0.32
5/16/88	9:51:29	2.00	-0.16	5/16/88	11:23:59	2.96	-0.49
5/16/88	9:52:09	4.00	-0.32	5/16/88	11:25:19	0.49	-0.23
5/16/88	9:52:59	1.00	-0.21	5/16/88	11:27:20	1.48	-0.35
5/16/88	9:53:39	2.50	-0.29	5/16/88	11:28:00	2.47	-0.35
5/16/88	9:57:40	5.00	-0.56	5/16/88	11:29:00	0.49	-0.19
5/16/88	9:58:20	3.00	-0.35	5/16/88	11:[illegible]:50	0.49	-0.19
5/16/88	9:59:50	5.00	-0.54	5/16/88	11:[illegible]:40	1.97	-0.32
5/16/88	10:00:20	1.97	-0.23	5/16/88	11:35:00	0.00	-0.14
5/16/88	10:00:50	1.48	-0.23	5/16/88	11:35:34	0.00	-0.21
5/16/88	10:01:20	3.45	-0.32	5/16/88	11:39:55	1.48	-0.12
5/16/88	10:02:40	1.48	-0.09	5/16/88	11:42:59	1.48	-0.24

NPM to Palmer

Date	Time (UT)	$\Delta\phi^*$ (deg.)	$\Delta A^\dagger$ (dB)
5/16/88	11:44:59	3.45	-0.33
5/16/88	11:47:09	0.99	-0.14

* Negative phase events indicate phase retardation.

† Negative amplitude events indicate attenuation.

Appendix B - Phase Correcting Program - Source Listing

```
/*  FILE: CORRECT.C */

#include "global2.h"
#include "external.h"
#include "this_sys.h"

#ifdef QUICKC
   #include <conio.h>     /*kbhit(), getch()*/
#endif

#include <string.h>

#define NO 'N'
#define SMALL_NO 'n'

short main(int argc,char *argv[])
{
    long i;
    short j, in_data;
    char shift_flag;
    char filename[50];
/*
 * Loop until input says stop the program.
 */
    while(get_file() == 0)
    {
/*
 * Get all the operating parameters
 */
        get_times();
        get_processing_parameters();
        get_output_file(DEFAULT_OUTPUT_DATAFILE, "wb");
/*
 * Skip through the data file up to the first data of interest.
 */
        if (!repos_data(skip_size))
        {
            printf("Done skipping data\n");
            printf("Reading %ld samples\n", read_size);
/*
 * Change the header block, by modifying the start time, and by adding
 * the processing parameters used. Then, write it to the output file.
 */
            write_header();
            in_data = shift_initialize();
/*
 * Loop over the number of samples to be processed
 */
            for (i = 0; ((i <= read_size )&& !feof(file_pointer));
                    i++)
            {
/*
 * Output the sample.
 */
                write_data(in_data);
```

```
/*
 * Get the next sample.
 */
                in_data = read_shift();
            }
            if (feof(file_pointer))
            {
                printf("End of File encountered while ");
                printf("reading data\n");
            }
            fclose(out_pointer);
        }
        else printf("EOF encountered while skipping data\n");
        fclose(file_pointer);
    }
    return(0);
}

/*  FILE: GET_FILE.C  */

#include "this_sys.h"
#include "global2.h"
#include "external.h"

#include <string.h>  /* strncmp(), strtok(), strcpy(), strlen() */

#define INPUT_SIZE 50
#define DEFAULT_FLAG "\n\0"
#define STOP_FLAG "QUIT\n\0"

/*
 * An array containing the input filename. It is static so that the same
 * filename can be the default for the next pass through the program.
 */
static char in_filename[INPUT_SIZE] = DEFAULT_FLAG;
/*
 * Function to query the operator for a filename, open the file, and read
 * the header block.
 *
 * The function returns a value of 0 if the file is opened
 * successfully, 1 if EOF is encountered while reading the header,
 * and -1 if the STOP_FLAG value was entered for a filename.
 */
short get_file(void)
{
    short flag, i;
    char input_string[INPUT_SIZE];
    long start_msec;

    for(i = 0; i <= (INPUT_SIZE - 1); i++) input_string[i] = in_filename[i];
/*
 * Try to Open the File
 * Loop until a valid file is opened.
 */
    do{
        printf("Enter the filename of the data file (or Enter for");
        printf(" default):\n");
        printf("Default is same as last time. Enter QUIT to end ");
        printf("program\n");
        fgets(input_string, INPUT_SIZE, stdin);
```

```
/*
 * Check for end of program string.
 */

        if (flag = (strncmp(input_string, STOP_FLAG, strlen(STOP_FLAG))
                == 0))break;
/*
 * If not default string, strip off "\n", then use this as the file name.
 */
        if (strncmp(input_string, DEFAULT_FLAG, strlen(DEFAULT_FLAG))
                != 0)
        {
            strtok(input_string,"\n");
            strcpy(in_filename, input_string);
        }
/*
 * If using the default, use the previous file name if it exists.
 * If not, use the established default.
 */
        else if (strncmp(in_filename, DEFAULT_FLAG, strlen(DEFAULT_FLAG)
                ) == 0)strcpy(in_filename, DEFAULT_FILENAME);
    }while ((file_pointer = fopen(in_filename, "rb")) == NULL);
    if (!flag)
/*
 * If not quitting, Get the Header Record
 */
    {
        if (!read_header())
/*
 * File appears to be good, return a 0.
 */
            flag = 0;
/*
 * EOF encountered while trying to read header.
 * Close the file and return a 1.
 */
        else{
            flag = 1;
            fclose(file_pointer);
        }
    }
/*
 * Ending the program, return a -1
 */
    else flag = -1;
    return (flag);
}

/*  FILE: GET_HDR.C  */

#include "global2.h"
#include "external.h"

#include <stdlib.h>   /* atoi() */

/*
   * required for QUICK C on IBM PC *
#include <memory.h>  / * memcmp() * /
*/

#define NO 'N'
#define SMALL_NO 'n'
```

```
const char label[LABELSIZE]=LABEL;

/*
 * Function to read the header record from the file and extract the
 * required information
 */
short read_header(void)
{
    int i, j, numhdrs, flag;
    char swap_flag, in_data;
    long start_msec;
/*
 * Get the First Header Record
 */

/*
 * guess at the block size
 */
    this_file.block_size = ASSUMED_HEADER_SIZE;
    do{
        rewind(file_pointer);
/*
 * Read the entire header structure.
 */
        fread(&datafilehdr, sizeof(char), this_file.block_size,
            file_pointer);
        if (!(flag = feof(file_pointer)))
        {
/*
 * Is this a Header record ?
 */
            if (memcmp(datafilehdr.labelstring, label, LABELSIZE)
                == 0)
            {
                printf("%s\n",datafilehdr.abbrev);
                printf("%s\n",datafilehdr.title);
                printf("Recorded on %s/%s/%s at %s:%s:%s.%s\n",
                    datafilehdr.month, datafilehdr.day,
                    datafilehdr.year,
                    datafilehdr.hours, datafilehdr.minutes,
                    datafilehdr.seconds, datafilehdr.msec);
                printf("Data recorded with sampling period of");
                printf(" %s\n", datafilehdr.sampling_period);
                printf("Data stored with %s bits",
                        datafilehdr.samplebits);
                printf(" and %s bytes per sample\n",
                        datafilehdr.wordsize);

/*
 * Convert some of the string fields from the record to numeric variables
 */
                this_file.numhdrs = atoi(datafilehdr.totalhdrs);
                this_file.start_time.hrs =
                        atoi(datafilehdr.hours);
                this_file.start_time.min =
                        atoi(datafilehdr.minutes);
                this_file.start_time.sec =
                        atoi(datafilehdr.seconds);
                this_file.start_time.msec =
                        atoi(datafilehdr.msec);
                this_file.start_date.mon =
                        atoi(datafilehdr.month);
                this_file.start_date.dat =
                        atoi(datafilehdr.day);
```

```
                this_file.start_date.yr =
                        atoi(datafilehdr.year);
                this_file.period = (float)
                    atof(datafilehdr.sampling_period);
                this_file.block_size =
                    atoi(datafilehdr.recordsize);
                this_file.cycle_size =
                    atoi(datafilehdr.cycle_size);
                this_file.swap = datafilehdr.swapping;
            }
            else{
                printf("File does not contain a Header Block\n"
                        );
                this_file.numhdrs = 0;
                this_file.block_size = ASSUMED_HEADER_SIZE;
/*
 * If no header in the file, get the necessary information from
 * the operator.
 */
                start_msec = parse_time(
                    "Start Time of the File", "[0:0:0.0]");
/*
 * If default, assume file starts at 0.
 */
                if (start_msec == -1) start_msec = 0;
                msec_to_time(&this_file.start_time, start_msec);
                printf("Enter the sampling period ");
                printf("(in seconds)[.02]: ");
                this_file.period = parse_real((float)0.02);
                printf("Is the data swapped (low byte first)");
                printf(" ([Y] or N)?");
/*
 * Use the last character before the '\n' character as the response.
 */
                while((in_data = (char)getchar()) != '\n')
                        swap_flag = in_data;
                if ((swap_flag != NO) &&
                        (swap_flag != SMALL_NO))
                        this_file.swap = SWAPPED;
                else this_file.swap = UNSWAPPED;
            }
        }
/*
 * If block size is different, try again with correct block size.
 */
    } while (this_file.block_size != ASSUMED_HEADER_SIZE);
    if (flag)
        printf ("End of File encountered while reading headers\n");
    else printf("Done reading header\n");
    return (flag);
}


/*  FILE: GET_TIME.C */

#include "global2.h"
#include "external.h"

#define NO 'N'
#define SMALL_NO 'n'
```

```
/*
 * Function to input the times required for the program.
 */
short get_times(void)
{
    long start_size;
/*
 * First find where to start looking at data.
 */
    start_size = parse_time("Start Time", "[beginning of file]");
    if (start_size < 0) skip_size = 0;
/*
 * Compute the number of data samples to skip over.
 */
    else skip_size = (long)((start_size
                - time_to_msec(this_file.start_time))
                / (this_file.period * (float)1000.));
/*
 * Then, how much data to look at.
 */
    read_size = parse_time("Total Amount of Data to Read", "[0:30:0.0]");
    if (read_size <= 0) read_size = 1800000;
/*
 * Compute the number of data samples to read.
 */
    read_size /= (this_file.period * 1000.);
    return(0);
}

/*  FILE: GET_PARA.C    */

#include "global2.h"
#include "external.h"

#define NO 'N'
#define SMALL_NO 'n'

/*
 * Function to get other processing parameters.
 * These include the size of one cycle of phase data, the averaging
 * size for processing averages, and the dynamic limiter size.
 */
short get_processing_parameters(void)
{
    char shift_flag, in_data;
    short default_cycle;

    printf("Should the data be shifted to a single cycle ([Y] or N)?");
/*
 * Use the last character before the '\n' character as the response.
 */
    while((in_data = (char)getchar()) != '\n') shift_flag = in_data;
    if ((shift_flag != NO) && (shift_flag != SMALL_NO))
    {
/*
 * If not contained in the data file, get the cycle size.
 */
        if (this_file.cycle_size <> 0)
            default_cycle = this_file.cycle_size;
        else default_cycle = FULL_SCALE / 2;
        printf("Enter the size of one cycle in raw data [%d]: ",
                            default_cycle);
```

```
            this_file.cycle_size = parse_int(0, FULL_SCALE, default_cycle);
            printf("Shifting data to cover one cycle of %d units.\n",
                                this_file.cycle_size);
        }
        else this_file.cycle_size = 0;
        if(this_file.cycle_size != 0)
        {
            printf("Enter the rise time of the data (sec) [0.1]: ");
/*
 * Figure out how many samples are required to make a transition.
 */
            this_file.transition_size = round(parse_real((float)0.1)
                                / this_file.period);
            printf("Enter the fraction of a cycle considered to be a ");
            printf("transition (%%) [50]:");
            this_file.transition_level = (short)(parse_int(5, 100, 50)
                * (long)this_file.cycle_size / 100);
            wrap_value = this_file.cycle_size;
        }
        else{
            this_file.proc_average = 0;
            wrap_value = FULL_SCALE / 2;
            this_file.transition_size = TRANSITION_SIZE;
        }
        printf("Enter the Processing Averaging Time (sec) [300.]:");
/*
 * Convert this to the number of samples in the processing average.
 */
        this_file.proc_average = round(parse_real((float)300.)
                                / this_file.period);
        printf("Enter the dynamic limiter threshold (deg) ");
        printf("(enter 0 if no limiting is to be done) [0]: ");
/*
 * Convert this from degrees to size in sample units.
 */
        this_file.clip_level = (short)(parse_int(0, 180, 0)
                        * (long)wrap_value / 180);

        printf("Enter the maximum data slope (deg. per 0.1 sec.)");
        printf("(enter 0 if no limiting is to be done) [0]: ");
/*
 * Convert this from degrees per 0.1 sec. to sample units per two samples.
 */
        this_file.slope_level = (short)(parse_int(0, 180, 0) * (float)wrap_value
                                * this_file.period / 78.);
        return(0);
}

/*  FILE: GET_OUT.C  */

#include "this_sys.h"
#include "global2.h"
#include "external.h"

#include <string.h>   /* strncmp(), strtok(), strcpy(), strlen() */

#define INPUT_SIZE 50
#define DEFAULT_FLAG "\n\0"
```

```
/*
 * The output filename. This is a static variable, so that the name can
 * be used as the default on the next pass through the program.
 */
static char out_filename[INPUT_SIZE] = DEFAULT_FLAG;

/*
 * function to open the output file.
 *
 * as arguments, it takes a string containing the name of the default
 * output filename, and one describing the type of access required, this
 * would normally be "w" or "wb".
 */
short get_output_file(char default_name[], char access[])
{
    short flag, i;
    char input_string[INPUT_SIZE];

    for(i = 0; i <= (INPUT_SIZE - 1); i++)
        input_string[i] = out_filename[i];
/*
 * Try to Open the File
 * Loop until a valid file is opened.
 */
    do{
        printf("Enter the filename of the output file (or Enter for ");
        printf("default):\nDefault is same as last time.\n");
        fgets(input_string, INPUT_SIZE, stdin);
/*
 * If not default string, strip off "\n", then use this as the file name.
 */
        if (strncmp(input_string, DEFAULT_FLAG, strlen(DEFAULT_FLAG))
                != 0)
        {
            strtok(input_string,"\n");
            strcpy(out_filename, input_string);
        }
/*
 * If using the default, use the previous file name if it exists.
 * If not, use the established default.
 */
        else if (strncmp(out_filename, DEFAULT_FLAG,
                strlen(DEFAULT_FLAG)) == 0)
                    strcpy(out_filename, default_name);
    }while (NULL == (out_pointer =
#ifdef QUICKC
                fopen(out_filename, access)));
#endif
#ifndef QUICKC
            fopen(out_filename, access,"rfm=fix","mrs=512")));
#endif
    return(0);
}

/*  FILE: FILE_HND.C */

#include "global2.h"
#include "this_sys.h"
```

```
/*
 * Function to read one data value from the file
 *
 * The function returns the data value read from the file.
 */
short read_data(void)
{
    int data_value;

/*
 * Read each byte, and combine them as appropriate, depending upon
 * the swap flag.
 */
    data_value = getc(file_pointer);
    if (this_file.swap == SWAPPED)
        data_value += getc(file_pointer) * 256;
    else data_value = data_value * 256 + getc(file_pointer);
/*
 * If an End of File is found, set the data to flag this fact.
 */
    if (feof(file_pointer)) data_value = EOF_FLAG;
    return(data_value);
}


/*
 * Function to write one data value to the file
 *
 * The function returns the data value written to the file.
 */
short write_data(short data_value)
{
/*
 * Write each byte, Least Significant first
 */
    putc((data_value % 256), out_pointer);
    putc((data_value / 256), out_pointer);
    return(data_value);
}


/*
 * Function to Reposition the File to a specified point
 *
 * As an argument, the function takes a long integer telling how many
 * samples to skip over.
 * It returns a logical value that is true if an End of File was
 * encountered while skipping data, and false if the skip was successful.
 */
short repos_data(long skip_samples)
{
    short flag;
    long i;
/*
 * Start at the beginning
 */
    rewind(file_pointer);
/*
 * First skip over any headers
 */
#ifdef QUICKC
    fseek(file_pointer, (long) this_file.numhdrs * this_file.block_size,
        SEEK_SET);
```

```
#else
    for(i = 1; i <= this_file.numhdrs * this_file.block_size; i++)
        getc(file_pointer);
#endif
/*
 * Compute the number of bytes to skip
 */
    skip_samples *= 2;
    printf("Skipping %ld bytes\n",skip_samples);
/*
 * Skip over all the bytes except the last one which will be read to
 * check for End of File
 */
#ifdef QUICKC
    if (skip_samples >= 2)
        fseek(file_pointer, (skip_samples - 1), SEEK_CUR);
    if (skip_samples >= 1) getc(file_pointer);
#else
    for(i = 1; i <= skip_samples; i++)
        getc(file_pointer);

#endif
    if (flag = feof(file_pointer))
        printf("End of File encountered while skipping data\n");
    return(flag);
}


/*  FILE: PUT_HDR.C  */


#include "global2.h"
#include "external.h"

#include <stdlib.h>
#include <string.h>

   char *my_itoa(short value, char string[], short radix, short width)
   {
    if (radix == 8) sprintf(string, "%0*o", width, value);
    else if (radix == 16) sprintf(string, "%0*x", width, value);
    else sprintf(string, "%0*d", width, value);
    return(&string[0]);
   }

/*
 * Function to adjust the start time parameters in the file header, and
 * write a new header block. This block also contains the processing
 * parameters.
 */
short write_header(void)
{
   struct time skip_time;
   short i;
/*
 * If this file did not have a header, we are going to give it one.
 */
   if (this_file.numhdrs == 0)
   {
    memset(datafilehdr.labelstring, '\0', ASSUMED_HEADER_SIZE);
    strcpy(datafilehdr.labelstring, LABEL);
    my_itoa(1, datafilehdr.totalhdrs, 10, 2);
    my_itoa(ASSUMED_HEADER_SIZE, datafilehdr.recordsize, 10, 5);
    gcvt(this_file.period, 6, datafilehdr.sampling_period);
```

```
    }
/*
 * First compute the data start time and date.
 * Then put it in the file header structure, as strings.
 */
    msec_to_time(&skip_time,
        lround(skip_size * this_file.period * (float)1000.));
    add_times(&this_file.start_time, &skip_time, &this_file.start_date);
    my_itoa(this_file.start_date.mon, datafilehdr.month, 10, 2);
    my_itoa(this_file.start_date.dat, datafilehdr.day, 10, 2);
    my_itoa(this_file.start_date.yr, datafilehdr.year, 10, 4);
    my_itoa(this_file.start_time.hrs, datafilehdr.hours, 10, 2);
    my_itoa(this_file.start_time.min, datafilehdr.minutes, 10, 2);
    my_itoa(this_file.start_time.sec, datafilehdr.seconds, 10, 2);
    my_itoa(this_file.start_time.msec, datafilehdr.msec, 10, 3);
    my_itoa(this_file.cycle_size, datafilehdr.cycle_size, 10, 4);
    my_itoa(this_file.clip_level, datafilehdr.clip_level, 10, 4);
    my_itoa(this_file.slope_level, datafilehdr.slope_level, 10, 4);
    my_itoa(this_file.transition_size, datafilehdr.transition_size, 10, 2);
    my_itoa(this_file.transition_level, datafilehdr.transition_level, 10, 4);
    my_itoa(this_file.proc_average, datafilehdr.proc_average, 10, 4);
    datafilehdr.swapping = SWAPPED;
/*
 * Now write the header to the output file.
 */
#ifdef QUICKC
    fwrite(&datafilehdr, sizeof(char), this_file.block_size, out_pointer);
#endif
#ifndef QUICKC
    fwrite(&datafilehdr, this_file.block_size, 1,out_pointer);
#endif
/*
 * Also copy over any other header blocks.
 */
    for (i = 2; i <= this_file.numhdrs; i++)
    {
    fread(&datafilehdr, sizeof(char), this_file.block_size, file_pointer);
#ifdef QUICKC
    fwrite(&datafilehdr, sizeof(char), this_file.block_size, out_pointer);
#endif
#ifndef QUICKC
        fwrite(&datafilehdr, this_file.block_size, 1,out_pointer);
#endif
    }
    return(0);
}


/*  FILE: FIX_DATA.C  */


#include "global2.h"
#include "external.h"

#include <stdlib.h>   /* atoi(), abs() */

#define MY_TRUE 1
#define MY_FALSE 0
```

```
/*
 * These arrays contain the next few data values, so that the program
 * look for trends in the data and decide on the validity of upcoming can
 * data points.
 */
static short buffer[TRANSITION_SIZE + 1],  /*Array of the next few data
                                             values. The current data is
                                             taken from buffer[0]. */
       flag[TRANSITION_SIZE + 1];       /*Array of flag bits
                                          corresponding to the data in
                                          buffer[]. */
/*
 * These three variables contain thresholds used in deciding how to
 * correct or shift the data around. They are stored as static variables to
 * avoid recomputing each time they are used.
 */
static short one_fourth_range,      /*variable containing one fourth of the
                                      maximum data value allowed after
                                      processing.*/
       three_fourths_range,    /*variable containing three fourths of
                                      the maximum data value allowed after
                                    processing.*/
       full_scale;          /*variable containing the maximum data
                              value allowed after processing.*/
static short slope_flag;       /*a flag indicating that an excessive
                                 slope has been found in the data.
                                 As long as this flag is set, data
                                     will be considered bad. It is cleared
                                 when a data value falls within normal
                                 limits. */


/*
 * First shift the data through the storage buffer.
 *
 * The data and flag buffers are shifted down one, the new value passed
 * as data_value is put in the top of the buffer, and the oldest value [0]
 * is returned as the current data, using the function return value.
 */
short buffer_shift(short data_value)
{
    short i, current_buffer, current_flag, future_buffer;

    current_buffer = buffer[0];
    current_flag = flag[0];
/*
 * Shift the buffer down one.
 */
    for (i = 0; i <= (this_file.transition_size - 1); i++)
    {
        buffer[i] = buffer[i + 1];
        flag[i] = flag[i + 1];
    }
/*
 * Put the new data at the top of the buffer
 */
    future_buffer = buffer[this_file.transition_size]
                        = data_value & DATA_MASK;
    flag[this_file.transition_size] = data_value - future_buffer;
    return(current_buffer + current_flag);
}
```

```
/*
 * This function detects when the slope of the data over the next two
 * samples exceeds a specified threshold. If it does, those two samples are
 * marked as invalid, and a flag is set. As long as the flag is set, all
 * subsequent data will be considered invalid, until a data point falls
 * within normal limits, as determined by the function clipper().
 *
 * The current data value is passed to this function as an argument, and
 * returned as the function return value. Only a flag bit in it can be
 * changed.
 */
short slope_limit(short data_value)
{
    short current_buffer, current_flag, next_data, next_next_data;

    current_buffer = data_value & DATA_MASK;
    current_flag = data_value - current_buffer;
    if(this_file.slope_level != 0)
    {
        next_data = buffer[0] & DATA_MASK;
        next_next_data = buffer[1] & DATA_MASK;
/*
 * If the flag is set, mark this sample as bad data.
 */
        if (slope_flag == MY_TRUE) current_flag |= SLOPE_FLAG;
/*
 * If this sample is good data, and the slope exceeds a threshold, then
 * mark the next two points as bad, and set the flag.
 */
        if ((current_flag & (BAD_FLAG + SLOPE_FLAG)) == 0)
        {
            if (((current_buffer - next_data)
                > this_file.slope_level)
                && ((next_data - next_next_data)
                > this_file.slope_level))

            {
                buffer[0] |= SLOPE_FLAG;
                buffer[1] |= SLOPE_FLAG;
                slope_flag = MY_TRUE;
            }
            else if (((current_buffer - next_data)
                < -this_file.slope_level)
                && ((next_data - next_next_data)
                < -this_file.slope_level))

            {
                buffer[0] |= SLOPE_FLAG;
                buffer[1] |= SLOPE_FLAG;
                slope_flag = MY_TRUE;
            }
        }
    }
    return(current_buffer + current_flag);
}


/*
 * Function to look for values that are in transition between two
 * equivalent points, one cycle apart. These must be stripped out before
 * any shifting is done, as the shifting will obscure the fact that these
 * were transition points. This is done by setting the BAD bit of the flag
 * nibble. This test can only be done if no EOF or BOF has been
 *  encountered.
```

```
 *
 * The current data value is passed as an argument, and returned as the
 * function return value. It does not get changed.
 */
short transition_check(short data_value)
{
    short current_buffer, current_flag, i, future_buffer, future_flag;

    current_buffer = data_value & DATA_MASK;
    current_flag = data_value - current_buffer;
    if(this_file.cycle_size != 0)
    {
        future_buffer = buffer[this_file.transition_size];
        future_flag = flag[this_file.transition_size];

        if (future_flag != EOF_FLAG && current_flag != BOF_FLAG)
        {
/*
 * If the difference between data points spaced transition_size apart
 * exceeds the specified threshold, mark all points between them as bad.
 */
            if (abs(current_buffer - future_buffer)
                >= this_file.transition_level)
            {
                for (i = 1; i <= (this_file.transition_size - 1)
                        ; i++)
                    flag[i] |= BAD_FLAG;
            }
        }
    }
    return(data_value);
}


/*
 * Function to shift data down to a single cycle and add hysterisis to
 * avoid jumping back and forth.
 * This function decides, for each data point, whether to shift the data
 * up or down by wrap_value, in order to keep the data reasonably
 * smooth. This is done by looking at a long term average called
 * running_average and keeping the data close to the long term average.
 *
 * The current data is passed to the function as an argument, and the
 * shifted data is returned as the function return value.
 */
short cycle_shift(short data_value)
{
    char translate;         /* a flag indicating whether the data has
                               been translated. */
    short current_buffer, current_flag, i, future_buffer, future_flag;

    current_buffer = data_value & DATA_MASK;
    current_flag = data_value - current_buffer;
    if(this_file.cycle_size != 0)
    {
        future_buffer = buffer[this_file.transition_size];
        future_flag = flag[this_file.transition_size];
```

```
/*
 * always translate down to useable range
 */
        if (current_buffer >= full_scale)
        {
            current_buffer = current_buffer % wrap_value;
            translate = MY_TRUE;
        }
        else translate = MY_FALSE;
/*
 * Now apply hysterisis.
 * First if running average is in upper quarter, translate data up
 * to top half of range.
 */
        if (running_average > three_fourths_range)
        {
            if (current_buffer <= wrap_value)
            {
                current_buffer = current_buffer + wrap_value;
                translate = MY_TRUE;
            }
        }
/*
 * Second, if running average is in bottom quarter, translate data down
 * to bottom half of plot
 */
        else if (running_average < one_fourth_range)
        {
            if (current_buffer >= wrap_value)
            {
                current_buffer = current_buffer - wrap_value;
                translate = MY_TRUE;
            }
        }
/*
 * Finally, if running average is in middle half, translate data up
 * or down to move data within half of range, centered on the average.
 */
        else
        {
            if (current_buffer >=
                    (running_average + one_fourth_range))
            {
                current_buffer = current_buffer - wrap_value;
                translate = MY_TRUE;
            }
            else if (current_buffer <=
                    (running_average - one_fourth_range))
            {
                current_buffer = current_buffer + wrap_value;
                translate = MY_TRUE;
            }
        }
/*
 * If the data has been moved around, set the flag bit.
 */
        if (translate == MY_TRUE) current_flag |= SHIFT_FLAG;
    }
    return(current_buffer + current_flag);
}
```

```
/*
 * Function to update the running average, if this is not bad data.
 * This average is a little bit complicated in order to avoid round_off
 * errors due to the bit size of the computer. Two variables are
 * maintained. The first is running_average, which is the current best
 * approximation to the long term average, given that it must be an
 * integer. The second variable is accumulated_error, which is essentially
 * the fractionalpart of the running_average, indicating how far off the
 * actual long term average the running_average is. Every time
 * accumulated_error exceeds the averaging size (proc_average), it is
 * decreased by that amount, and running_average is incremented.
 * The equation for the running_average is essentially:
 * (old_value)*(proc_average - 9)/proc_average + new_value
 *
 * the current data value is passed to the function as an argument, and
 * there is no return value.
 */
short processing_average(short data_value)
{
    short current_buffer, current_flag;

    current_buffer = data_value & DATA_MASK;
    current_flag = data_value - current_buffer;
/*
 * If this is good data, use it to update the average.
 */
    if ((current_flag & (BAD_FLAG + SLOPE_FLAG + LIMIT_FLAG)) == 0)
    {
        accumulated_error = (short)((((long)accumulated_error
            * (this_file.proc_average - 9))
            + ((long)(current_buffer - running_average) * 9 *
            this_file.proc_average)) / this_file.proc_average);
        while(accumulated_error >= this_file.proc_average)
        {
            accumulated_error -= this_file.proc_average;
            running_average++;
        }
        while(accumulated_error <= -this_file.proc_average)
        {
            accumulated_error += this_file.proc_average;
            running_average--;
        }
    }
    return(0);
}
/*
 * Now establish the region of the data we are currently using. If the
 * average up to this point is at the bottom of the chart, and this point
 * is near the middle, reset the average to the middle of the chart, to
 * force data to be translated into the middle region. Conversely, if the
 * average is at the top, and the new data is near the middle, reset the
 * average to the middle, to force data to be translated into the middle
 * region.
 */
short shift_average(short data_value)
{
    short current_buffer, current_flag;

    current_buffer = data_value & DATA_MASK;
    current_flag = data_value - current_buffer;
```

```
/*
 * If this is good data, use it to update the average.
 */
    if ((current_flag & (BAD_FLAG + SLOPE_FLAG)) == 0)
    {
        if (running_average < one_fourth_range && current_buffer
            > (one_fourth_range + running_average))
        {
            running_average += wrap_value;
        }
        else if (running_average > three_fourths_range &&
            current_buffer < (running_average - one_fourth_range))
        {
            running_average -= wrap_value;
        }
    }
    return(0);
}
/*
 * This function clips the data at a specified level on either side of
 * the running_average. It assures that a single bad sample cannot
 * significantly affect the averages.
 *
 * The current data value is passed as an argument, and the function
 * return value is the clipped data value.
 */
short clipper(short data_value)
{
    short current_buffer, current_flag, temp;

    current_buffer = data_value & DATA_MASK;
    current_flag = data_value - current_buffer;
    if (this_file.clip_level != 0)
    {
        if (current_buffer
            > (temp = running_average + this_file.clip_level))
        {
            current_buffer = temp;
/*
 * just to make sure that we cannot end up with all flags set, if this
 * data point has the SLOPE_FLAG set, do not also set the LIMIT_FLAG.
 */
            if ((current_flag & SLOPE_FLAG) == 0)
                current_flag |= LIMIT_FLAG;
        }
        else if (current_buffer
            < (temp = running_average - this_file.clip_level))
        {
            current_buffer = temp;
/*
 * just to make sure that we cannot end up with all flags set, if this
 * data point has the SLOPE_FLAG set, do not also set the LIMIT_FLAG.
 */
            if ((current_flag & SLOPE_FLAG) == 0)
                current_flag |= LIMIT_FLAG;
        }
/*
 * If the data is within acceptable limits, then clear the slope_flag, to
 * say that the data is back to normal.
 */
        else slope_flag = MY_FALSE;
    }
```

```
    else slope_flag = MY_FALSE;
    return(current_buffer + current_flag);
}


/*
 * Function to read one data value from the file and massage it
 */
short read_shift(void)
{
    short data, current_buffer, current_flag;

/*
 * First get the new data, and shift it through the buffer.
 * Then, check for transitions between points a cycle apart.
 * Next look for excessive slopes.
 */
    data = slope_limit(transition_check(buffer_shift(read_data())));
/*
 * Shift the data down to a single cycle.
 */
    data = cycle_shift(data);
/*
 * lastly, update the running_average, and clip the data to limits around
 * the running_average.
 */
    shift_average(data);
    data = clipper(data);
    processing_average(data);
    return (data);
}


/*
 * Function to initialize the shift data buffer, by stuffing it full of the
 * first TRANSITION_SIZE samples read from the current file location.
 * This function also sets up thresholds, and initializes flags for the
 * shifting routine.
 * This function must be called before any of the functions above can be
 * used reliably.
 *
 * The function returns the first data value to be used.
 */
short shift_initialize(void)
{
    short i;
    long running_total;

/*
 * Compute various thresholds and start flags out right.
 */
    full_scale = wrap_value * 2;
    one_fourth_range = wrap_value / 2;
    three_fourths_range = full_scale - one_fourth_range;
    slope_flag = MY_FALSE;
/*
 * Stuff the buffer full of BOT flags.
 */
    for (i = 0; i <= this_file.transition_size; i++)
    {
        buffer[i] = 0;
        flag[i] = BOF_FLAG;
    }
```

```
/*
 * Start the running_average at something reasonable (midscale).
 */
    running_average = wrap_value;
    accumulated_error = 0;
/*
 * Start reading in data to fill up the buffer, and massage the data as
 * needed.
 */
    for (i = 0; i <= this_file.transition_size; i++)
        cycle_shift(slope_limit(transition_check(buffer_shift(
            read_data()))));
/*
 * Now, set the running_average to the average of the first few data
 * values.
 */
    running_total = 0;
    for (i = 0; i <= this_file.transition_size; i++)
        running_total += buffer[i];
    running_average = running_total / (this_file.transition_size + 1);
    accumulated_error = 0;
/*
 * Finally, get the first real data value to return.
 */
    return (cycle_shift(slope_limit(transition_check(buffer_shift(
        read_data())))));
}


/*  FILE: PARSING.C  */


#include <stdio.h>    /* fgets(), printf() */
#include <stdlib.h>   /* atof(), atoi() */
#include <string.h>   /* strncmp(), strtok(), strlen() */
#include "datafile.h"

#define DEFAULT_FLAG "\n\0"
#define INPUT_SIZE 50
#define MSEC_IN_DAY 86400000

const short days_in_month[13] = {0,31,28,31,30,31,30,31,31,30,31,30,31};

/*
 * functions to round a float variable to the nearest integer.
 */
short round(float x)
{
    return((short)(x + (float)0.5));
}
long lround(float x)
{
    return((long)(x + (float)0.5));
}


/*
 * Function to convert a time structure to milliseconds.
 */
long time_to_msec(struct time skip)
{
return((long) ((skip.hrs * 60 + skip.min) * 60 + skip.sec) * 1000
            + skip.msec);
}
```

```
/*
 * Function to convert total milliseconds to a time structure
 * (hr, min, sec, msec).
 */
short msec_to_time(struct time *skip, long msec)
{
    long temp, temp1;
    if (msec >= 0)
    {
        (*skip).msec = (short)(msec - 1000 * (temp = msec / 1000));
        (*skip).sec = (short)(temp - 60 * (temp1 = temp / 60));
        (*skip).hrs = (short)temp1 / (short)60;
        (*skip).min = (short)temp1 - (short)60 * (*skip).hrs;
    }
    else (*skip).hrs = (*skip).min = (*skip).sec = (*skip).msec = 0;
    return (0);
}

short increment_date(struct date *source_date)
{
   (*source_date).dat++;
   if ((*source_date).dat > days_in_month[(*source_date).mon])
   {
    (*source_date).dat = 1;
    (*source_date).mon++;
    if ((*source_date).mon > 12)
    {
        (*source_date).mon = 1;
        (*source_date).yr++;
    }
   }
   return(0);
}

short add_times(struct time *source, struct time *increment,
    struct date *source_date)
{
   long msec;

   msec = time_to_msec(*source) + time_to_msec(*increment);
   while (msec >= MSEC_IN_DAY)
   {
    msec -= MSEC_IN_DAY;
    increment_date(source_date);
   }
   msec_to_time(source, msec);
   return(0);
}

/*
 * Function to get a float input value.
 * It allows for the setting of a default value if none is input
 */
float parse_real(float default_value)
{
    char input_string[INPUT_SIZE];
    float value;
    fgets(input_string, INPUT_SIZE, stdin);
```

```
/*
 * If no data, set to default value.
 */
    if (strncmp(input_string, DEFAULT_FLAG, strlen(DEFAULT_FLAG)) == 0)
            value = default_value;
    else value = (float)atof(input_string);
    return (value);
}


/*
 * Function to get an integer input value.
 * It checks the input and makes sure it is between a specified maximum
 * and minimum value. It also allows a default value to be set if no
 * number is input.
 */
short parse_int(short minimum, short maximum, short default_value)
{
    char input_string[INPUT_SIZE];
    short flag, value;
/*
 * Loop until valid values are obtained.
 */
    do{
        fgets(input_string, INPUT_SIZE, stdin);
/*
 * If no data, set to default value.
 */
        if (strncmp(input_string, DEFAULT_FLAG, strlen(DEFAULT_FLAG))
            == 0) value = default_value;
        else value = atoi(input_string);
/*
 * Check for valid range.
 */
        if (flag = (value < minimum || value > maximum))
            printf("Invalid value, please reenter: ");
    }while (flag);
    return (value);
}


/*
 * Function to input a specified time in the form of hours, minutes,
 * seconds and milliseconds, seperated by appropriate delimiters.
 * The arguments are strings, the first describes the time being asked for,
 * and the second describes the default value to be used.
 * The value returned is the total milliseconds corresponding to the time
 * specified. It will be -1 if the default is chosen.
 */
/*
 * Possible delimiters in time string.
 */
const char *delimiters = " :./";

long parse_time(char description[], char default_string[])
{
    char flag, input_string[INPUT_SIZE], item_string[3], *token;
    long value;
    struct time new_time;

    printf(" Enter the %s (hh:mm:ss.mmm), %s: ",description,
            default_string);
    fgets(input_string, INPUT_SIZE, stdin);
```

```
    if (strncmp(input_string, DEFAULT_FLAG, strlen(DEFAULT_FLAG)) == 0)
                value = -1;
    else {
/*
 * break the string into tokens for the various time fields.
 */
        token = strtok(input_string, delimiters);
        if (token == NULL) new_time.hrs = 0;
        else new_time.hrs = atoi(token);
        token = strtok(NULL, delimiters);
        if (token == NULL) new_time.min = 0;
        else new_time.min = atoi(token);
        token = strtok(NULL, delimiters);
        if (token == NULL) new_time.sec = 0;
        else new_time.sec = atoi(token);
        token = strtok(NULL, delimiters);
        if (token == NULL) new_time.msec = 0;
        else new_time.msec = atoi(token);
        value = time_to_msec(new_time);
    }
    return(value);
}

/*  FILE: GLOBAL2.C  */

#include <stdio.h>
#include "datafile.h"

struct file_data this_file;
struct header1 datafilehdr;
FILE *file_pointer, *out_pointer;
long skip_size, read_size;
short running_average, accumulated_error, wrap_value;

/*  FILE: THIS_SYS.H  */

#define DEFAULT_FILENAME "scratch:npm-p-6.dat"
#define OUT_FILENAME "scratch:transit.dat"
#define DEFAULT_OUTPUT_LISTFILE "scratch:data.spl"
#define SHIF_FILENAME "scratch:shif_dat.dat"
#define DEFAULT_OUTPUT_DATAFILE "scratch:update.dat"

/*  FILE: DATAFILE.H  */

/*
 * datafile.h -- header format for standard digitized data files.
 */

/*
 * set the block size for Header records
 */
#define ASSUMED_HEADER_SIZE 512

/*
 * this defines the assumed label for the first header record
 * and the size of the label field
 */
#define LABELSIZE 8
```

```
#define LABEL "DATA"

/*
 * Set the assumed full scale data value
 */
#define FULL_SCALE 4096

/*
 * Set the assumed cycle size for each station
 */
#define PALMER_CYCLE 2085
#define STANFORD_CYCLE 1988

/*
 * Set the number of samples required to make a response to a step
 * input. ie., the filter rise time, in samples.
 */
#define TRANSITION_SIZE 10

/*
 * Set the possible flags used to mark massaged data. These are powers
 * of two from 1 to 8. A massaged data byte will contain the data value
 * plus 0 to 15 times the maximum data value. The number from 0 to 15
 * is the sum of all flags that are set.
 */
#define BAD_FLAG (8 * FULL_SCALE)
#define LIMIT_FLAG (4 * FULL_SCALE)
#define SLOPE_FLAG (2 * FULL_SCALE)
#define SHIFT_FLAG (1 * FULL_SCALE)
#define DATA_MASK (FULL_SCALE - 1)

/*
 * Set the value returned for data when an EOF is encountered
 */
#define EOF_FLAG (short)(15 * FULL_SCALE)
#define BOF_FLAG (short)(15 * FULL_SCALE)

/*
 * these define possible values for the typemark field of the
 * header.
 */
#define AMPLITUDE    'A'
#define PHASE        'P'
#define REFERENCE    'R'
#define SPECIAL      'S' /* special or unknown */
#define DUMMY        ' '  /* invalid data! */
#define NOINFO       '\0' /* no information -- data possibly
                             from some old version of software
                             or from stripped-down software...*/
/*
 * swapping types
 */
#define SWAPPED      'S'
#define UNSWAPPED    'U'

/*
 * signing types
 */
#define SIGNED       'S'
#define UNSIGNED     'U'
```

```
/*
 * calibration types
 *
 * If uncalibrated all other calibration-related fields are to be
 * ignored and may contain garbage.  If either max or min values
 * are calibrated then the corresponding field should be a reasonable
 * floating point number.
 */
#define CALIBRATED      'C'
#define UNCALIBRATED    'U'
#define ONLYMINCALIBRATED  'N'
#define ONLYMAXCALIBRATED 'X'

/*
 * For portability (and type-ability) the header is made up entirely
 * of ascii bytes.  For ease of reading with scanf all strings are
 * null-terminated.  All numbers, including floating point numbers,
 * are written as null terminated strings, e.g. "0.401".
 *
 * If a field is incompletely filled by characters or digits, the rest
 * of the field is to be filled with nulls ('\0').
 *
 * There are some single-character fields.  These are not read as
 * strings and thus do not have null-termination.
 *
 * The "DATA\0\0\0\0" identifier in the beginning is for programs
 * which read these files to know that this file has a header.
 *
 * The option for additional headers is application-specific.  Standard
 * programs should be able to skip over any additional headers without
 * breaking.  Additional headers might simply contain text to explain
 * the following data in greater detail.  Some programs might wish
 * to allow the user to add explanation headers after looking at the
 * data.
 */

struct header1
{
    char labelstring[8],        /* identifier, should be "DATA\0\0\0\0" */
      totalhdrs[3],         /* total number of headers
                               incl. this one. (null-terminated ascii) */
      abbrev[8],          /* 7 char abbreviation for title if any */
      stationcode[3],   /* Receiving Station I.D. Code */
      title[82],        /* where the recording was made/title */
      month[3],     /* numeric WITH ZERO PLACEHOLDER,
                       e.g. 03 = march, 10 = october, etc. */
      day[3],         /* numeric with zero placeholder */
      year[5],        /* full year, eg 1987 */
      hours[3],       /* numeric with zero placeholder */
      minutes[3],       /* numeric with zero placeholder */
      seconds[3],       /* numeric with zero placeholder */
      msec[4],      /* milliseconds later than above time,
                       again with zero placeholders */
      sampling_period[15],    /* floating point number in Hz */
      samplebits[3],        /* BITS per data sample (e.g., "12") --
                               this establishes min/max values */
      wordsize[2],      /* bytes reserved per data sample("1","2"...)*/
      typemark,         /* see data type #defines above */
      swapping,         /* see swapping type #defines */
      signing,      /* see signing type #defines */
      caltype,      /* see calibration type #defines */
      calmin[15],       /* floating point min value if calibrated */
      calmax[15],       /* floating point max value if calibrated */
      calunits[40],     /* null-terminated units string (eg "volts") */
```

```
    recordsize[6],          /* bytes to get in single read, usually 512 */
    cycle_size[5],  /* size of one cycle of phase data in raw samples*/
    clip_level[5],     /* dynamic limiter threshold */
    slope_level[5],   /* maximum slope threshold */
    transition_size[3],   /* number of samples required to make
                             transitions */
    transition_level[5],  /* size of transition needed to count it */
    proc_average[6],    /* number of samples in processing average */
    fill[(ASSUMED_HEADER_SIZE - 254)];    /* round out header total.
                                             This region should not be filled with
                                             anything but nulls, so that later
                                             versions of this header will be
                                             compatible.  Any text comments should
                                             be placed in additional headers. */
};

struct time
{
    int hrs, min, sec, msec;
};

struct date
{
    int mon, dat, yr;
};

struct file_data
{
    int numhdrs;          /*number of header records in the file*/
    float period;         /*the sampling period for the data*/
    struct time start_time; /*the start time of the data (hrs,min,sec,msec)*/
    struct date start_date; /*the starting date of the data (mon,day,yr) */
    short block_size,       /*the block size of this file*/
    cycle_size,       /*the size of one cycle of phase data in samples*/
    clip_level,
    slope_level,
    transition_size,
    transition_level,
    proc_average;
    char swap,            /*flag to indicate whether data is byte
                            swapped*/
    station_code[3]; /*two letter station identification*/
};


/*  FILE: EXTERNAL.H*/


extern long time_to_msec(struct time);
extern long parse_time(char [], char[]);
extern short parse_int(short, short, short);
extern float parse_real(float);
extern short round(float);
extern long lround(float);
extern short msec_to_time(struct time *, long);
extern short add_times(struct time *, struct time *, struct date *);
extern short get_file(void);
extern short get_output_file(char [], char []);
extern short get_times(void);
extern short get_processing_parameters(void);
extern short skipping_data(void);
extern short shift_initialize(void);
extern short read_shift(void);
extern short read_header(void);
```

```
extern short read_data(void);
extern short write_header(void);
extern short repos_data(long);


/*  FILE: GLOBAL2.H  */


#include <stdio.h>
#include "datafile.h"

extern struct file_data this_file;
extern struct header1 datafilehdr;
extern FILE *file_pointer, *out_pointer;
extern long skip_size, read_size;
extern short running_average, accumulated_error, wrap_value;
```

List of References

Barish, F. D., and R. E. Wiley, "World Contours of Conjugate Mirror Locations", *Journal of Geophysical Research*, Vol. 75, pp. 6342-6347, November 1970.

Berger, M. J., S. M. Seltzer, and K. Maeda, "Some New Results on Electron Transport in the Atmosphere", *Journal of Atmospheric and Terrestrial Physics*, Vol. 36, pp. 591-617, 1974.

Born, M. and E. Wolf, Principles of Optics, 3rd ed., Pergamon Press, Oxford, 1965.

Brice, N., "Fundamentals of Very Low Frequency Emission Generation Mechanisms", *Journal of Geophysical Research*, Vol. 69, pp. 4515-4522, November 1964.

Budden, K. G., The Propagation of Radio Waves, Cambridge University Press, Cambridge, 1985.

Budden, K. G., The Wave - Guide Mode Theory of Wave Propagation, Logos Press, London, 1961.

Burgess, W. C. and U. S. Inan, "Simultaneous Disturbance of Conjugate Ionospheric Regions in Association with Individual Lightning Flashes", submitted to *Geophysical Research Letters*, 1990.

Carlson, A. B., Communication Systems, McGraw - Hill, New York, 1986.

Carlson, C. R., R. A. Helliwell, and D. L. Carpenter, "Variable Frequency VLF Signals in the Magnetosphere: Associated Phenomena and Plasma Diagnostics", *Journal of Geophysical Research*, Vol. 90, pp. 1507-1521, February 1985.

Carpenter, D. L., and J. W. Labelle, "A Study of Whistlers Correlated with Bursts of Electron Precipitation Near L = 2", *Journal of Geophysical Research*, Vol. 87, pp. 4427-4434, June 1982.

Carpenter, D. L., and U. S. Inan, "Seasonal, Latitudinal and Diurnal Distributions of Whistler - Induced Electron Precipitation Events", *Journal of Geophysical Research*, Vol. 92, pp. 3492-3435, April 1987.

Carpenter, D. L., C. G. Park, J. F. Arens, and D. J. Williams, "Position of the Plasmapause during a Stormtime Increase in Trapped Energetic (E > 280 keV) Electrons", *Journal of Geophysical Research*, Vol. 76, pp. 4669-4673, July 1971.

Carpenter, D. L., U. S. Inan, E. W. Paschal, and A. J. Smith, "A New VLF Method for Studying Burst Precipitation Near the Plasmapause", *Journal of Geophysical Research*, Vol. 90, pp. 4383-4388, May 1985.

Carpenter, D. L., U. S. Inan, M. L. Trimpi. R. A. Helliwell, and J. P. Katsufrakis, "Perturbations of Subionospheric LF and MF Signals Due to Whistler - Induced Electron Precipitation Bursts", *Journal of Geophysical Research*, Vol. 89, pp. 9857-9862, November 1984.

Chang, D. C. D., and R. A. Helliwell, "VLF Pulse Propagation in the Magnetosphere", *IEEE Transactions on Antennas and Propagation*, Vol. AP-28, pp. 170-176, March 1980.

Chang, H. C., and U. S. Inan, "A Theoretical Model Study of Observed Correlations between Whistler Mode Waves and Energetic Electron Precipitation Events in the Magnetosphere", *Journal of Geophysical Research*, Vol. 88, pp. 10053-10058, December 1983.

Chang, H. C., and U. S. Inan, "Lightning Induced Energetic Electron Precipitation from the Magnetosphere", *Journal of Geophysical Research*, Vol. 90, pp. 1531-1541, February 1985a.

Chang, H. C., and U. S. Inan, "Test Particle Modeling of Wave - Induced Energetic Electron Precipitation", *Journal of Geophysical Research*, Vol. 90, pp. 6409-6418, July 1985b.

Chang, H. C., U. S. Inan, and T. F. Bell, "Energetic Electron Precipitation due to Gyroresonant Interactions in the Magnetosphere Involving Coherent VLF Waves with Slowly Varying Frequency", *Journal of Geophysical Research*, Vol. 88, pp. 7037-7050, September 1983.

Chen, F. F., Introduction to Plasma Physics and Controlled Fusion, Vol. 1, Plenum Press, New York, 1984.

Davidson, G. and M. Walt, "Loss Cone Distributions of Radiation Belt Electrons", *Journal of Geophysical Research*, Vol. 82, pp. 48-54, January 1977.

Davies, K., Ionospheric Radio Propagation, U. S. Government Printing Office, Washington D. C., 1965.

DeRosa, L. A. (ed.), Reference Data for Radio Engineers, 6th ed., H. W. Sams & Co., Indianapolis, 1968.

Dingle, B., Burst Precipitation of Energetic Electrons from the Magnetosphere, Ph. D. Dissertation, Stanford University, Stanford, 1977.

Doolittle, J. H., Modification of the Ionosphere by VLF Wave - Induced Electron Precipitation, Ph. D. Dissertation, Stanford University, Stanford, 1982.

Dowden R. L., and C. D. D. Adams, "Phase and Amplitude Perturbations on the NWC Signal at Dunedin from Lightning - Induced Electron Precipitation", *Journal of Geophysical Research*, Vol. 94, pp. 497-503, January 1989.

Dowden, R. L., and C. D. D. Adams, "Phase and Amplitude Perturbations on Subionospheric Signals Explained in Terms of Echoes from Lightning - Induced Electron Precipitation Ionization Patches", *Journal of Geophysical Research*, Vol. 93, pp. 11543-11550, October 1988.

Edgar, B. C., "The Upper and Lower - Frequency Cutoffs of Magnetospherically Reflected Whistlers", *Journal of Geophysical Research*, Vol. 81, pp. 205-211, January 1976.

Field, E. C. Jr., and M. Lewinstein, "Amplitude - Probability Distribution Model for VLF/ELF Atmospheric Noise", *IEEE Transactions on Communications*, Vol. COM-26, pp. 83-87, January 1978.

Foley, G., I. C. Wand, and T. B. Jones, "Studies of the Modal Parameters of VLF Radiowaves Propagated below the Night - time Ionosphere", *Journal of Atmospheric and Terrestrial Physics*, Vol. 35, pp. 2111-2122, 1973.

Fraser - Smith, A. C., "Centered and Eccentric Geomagnetic Dipoles and their Poles, 1600 - 1985", *Reviews of Geophysics*, Vol. 25, pp. 1-16, February 1987.

Furgeson, J. A., and F. P. Snyder, "Approximate VLF/LF Waveguide Mode Conversion Model", *Naval Ocean Systems Center Technical Document*, No. 400, San Diego, November 1980.

Gledhill, J. A., "The Effective Recombination Coefficient of Electrons in the Ionosphere between 50 and 150 km", *Radio Science*, Vol. 21, pp. 399-408, June 1986.

Helliwell, R. A., and S. B. Mende, "Correlations between λ4278 Optical Emmisions and VLF Wave Events Observed at L ~ 4 in the Antarctic", *Journal of Geophysical Research*, Vol. 85, pp. 3376-3386, July 1980.

Helliwell, R. A., D. L. Carpenter, and T. R. Miller, "Power Threshold for Growth of Coherent VLF Signals in the Magnetosphere", *Journal of Geophysical Research*, Vol. 85, pp. 3360-3366, July 1980.

Helliwell, R. A., J. P. Katsufrakis, and M. L. Trimpi, "Whistler - Induced Amplitude Perturbations in VLF Propagation", *Journal of Geophysical Research*, Vol. 78, pp. 4679-4688, August 1973.

Helliwell, R. A., J. P. Katsufrakis, and P. A. Bernhardt, "Modification of the Propagation Characteristics of the Ionosphere (and the Magnetosphere) by the Injection into the Magnetosphere of Whistler - Mode Waves", AGARD Conference Proceedings on Artificial Modification of Propagation Media, H. J. Albrecht (ed.), NATO, Vol. 11-1, 1976.

Helliwell, R. A., Whistlers and Related Ionospheric Phenomena, Stanford University Press, Stanford, 1965.

Helliwell, R. A., "Very Low Frequency Magnetospheric Research in the Antarctic", Research in the Antarctic, American Association for the Advancement of Science, Washington, D. C., 1971.

Ho, D., and D. L. Carpenter, "Outlying Plasmasphere Structure Detected by Whistlers", *Planetary and Space Science*, Vol. 24, pp. 987-994, 1976.

Hurren, P. J., A. J. Smith, D. L. Carpenter, and U. S. Inan, "Burst Precipitation - Induced Perturbations on Multiple VLF Propagation Paths in Antarctica", *Annales Geophysicae*, Vol. 4, pp. 311-318, 1986.

Inan, U. S., and D. L. Carpenter, "Lightning - Induced Electron Precipitation Events Observed at L ≈ 2.4 as Phase and Amplitude Perturbations on Subionospheric VLF Signals", *Journal of Geophysical Research*, Vol. 92, pp. 3293-3303, April 1987.

Inan, U. S., and D. L. Carpenter, "On the Correlation of Whistlers and Associated Subionospheric VLF/LF Perturbations", *Journal of Geophysical Research*, Vol. 91, pp. 3106-3116, March 1986.

Inan, U. S., D. C. Shafer, W. Y. Yip, and R. E. Orville, "Subionospheric VLF Signatures of Nighttime D Region Perturbations in the Vicinity of Lightning Discharges", *Journal of Geophysical Research*, Vol. 93, pp. 11455-11472, October 1988b.

Inan, U. S., D. L. Carpenter, R. A. Helliwell, and J. P. Katsufrakis, "Subionospheric VLF/LF Phase Perturbations Produced by Lightning - Whistler Induced Particle Precipitation", *Journal of Geophysical Research*, Vol. 90, pp. 7457-7469, August 1985.

Inan, U. S., F. A. Knifsend, and J. V. Rodriguez, "Subionospheric VLF 'Imaging' of Lightning - Induced Electron Precipitation from the Magnetosphere", Eos, Vol. 69, p. 1392, November 1988d.

Inan, U. S., M. Walt, H. D. Voss, and W. L. Imhof, "Energy Spectra and Pitch Angle Distributions of Lightning - Induced Electron Precipitation: Analysis of an Event Observed on the S81-1 (SEEP) Satellite", *Journal of Geophysical Research*, Vol. 94, pp. 1379-1401, February 1989.

Inan, U. S., Non-Linear Gyroresonant Interactions of Energetic Particles and Coherent VLF Waves in the Magnetosphere, Ph. D. Dissertation, Stanford University, Stanford, 1977.

Inan, U. S., T. F. Bell, and H. C. Chang, "Particle Precipitation Induced by Short - Duration VLF Waves in the Magnetosphere", *Journal of Geophysical Research*, Vol. 87, pp. 6243-6264, August 1982.

Inan, U. S., T. G. Wolf, and D. L. Carpenter, "Geographic Distribution of Lightning - Induced Electron Precipitation Observed as VLF/LF Perturbation Events", *Journal of Geophysical Research*, Vol. 93, pp. 9841-9853, September 1988c.

Inan, U. S., W. C. Burgess, T. G. Wolf, D. C. Shafer, and R. E. Orville, "Lightning - Associated Precipitation of MeV Electrons from the Inner Radiation Belt", *Geophysical Research Letters*, Vol. 15, pp. 172-175, February 1988a.

Jackson, J. D., Classical Electrodynamics, 2nd ed., John Wiley and Sons, New York, 1975.

Jacobs, J. A., Geomagnetic Micropulsations, Springer - Verlag, New York, 1970.

Jensen, D. C., and J. C. Cain, "An Interim Geomagnetic Field", *Journal of Geophysical Research*, Vol. 67, pp. 3568-3569, August 1962.

Leyser, T. B., U. S. Inan, D. L. Carpenter, and M. L. Trimpi, "Diurnal Variation of Burst Precipitation Effects on Subionospheric VLF/LF Signal Propagation Near L = 2", *Journal of Geophysical Research*, Vol. 89, pp. 9139-9143, October 1984.

Lohrey, B., and A. B. Kaiser, "Whistler - Induced Anomalies in VLF Propagation", *Journal of Geophysical Research*, Vol. 84, pp. 5122-5130, September 1979.

Lyons, L. R., and D. J. Williams, Quantitative Aspects of Magnetospheric Physics, D. Reidel Publishing Co., Dordrecht, 1984.

Lyons, L. R., and R. M. Thorne, "Equilibrium Structure of Radiation Belt Electrons", *Journal of Geophysical Research*, Vol. 78, pp. 2142-2149, May 1973.

Mallinckrodt, A. J., Relation of the Ionosphere to the Propagation of Atmospherics, Engineer Thesis, Stanford University, Stanford, 1949.

Morfitt, D. G., and C. H. Shellman, "MODESRCH", An Improved Computer Program for Obtaining ELF/VLF/LF Mode Constants in an Earth - Ionosphere Waveguide, Interim Report No. 77T, Propagation Technology Division, Naval Electronics Laboratory Center, San Diego, October 1976.

Olson, W. P., and K. A. Pfitzer, "A Quantitative Model of the Magnetospheric Magnetic Field", *Journal of Geophysical Research*, Vol. 79, pp. 3739-3748, September 1974.

Papoulis, A., Probability, Random Variables, and Stochastic Processes, McGraw - Hill, New York, 1965.

Pappert, R. A. and F. P. Snyder, "Some Results of a Mode - Conversion Program for VLF", *Radio Science*, Vol. 7, pp. 913-923, October 1972.

Park, C. G., and D. L. Carpenter, "Very Low Frequency Radio Waves in the Magnetosphere", Upper Atmosphere Research in Antarctica, Antarctic Research Series Vol. 29, pp. 72-99, American Geophysical Union, 1978.

Poulsen, W. L., T. F. Bell, and U. S. Inan, "3 - D Modeling of Subionospheric VLF Propagation in the Presence of Localized D - Region Perturbations Associated with Lightning", submitted to *Journal of Geophysical Research*, 1990.

Ramo, S., J. R. Whinnery, and T. Van Duzer, Fields and Waves in Communication Electronics, John Wiley & Sons, New York, 1965.

Ratcliffe, J. A., An Introduction to the Ionosphere and Magnetosphere, Cambridge University Press, Cambridge, 1972.

Ratcliffe, J. A., The Magneto - Ionic Theory and its Applications to the Ionosphere, Cambridge University Press, Cambridge, 1959.

Rees, M. H., Physics and Chemistry of the Upper Atmosphere, Cambridge University Press, Cambridge, 1989.

Rees, M. H., "Auroral Electrons", *Space Science Reviews*, Vol. 10, pp. 413-441, December 1969.

Rees, M. H., "Auroral Ionization and Excitation by Incident Energetic Electrons", *Planetary and Space Science*, Vol. 11, pp. 1209-1218, 1963.

Rishbeth, H., and O. K. Garriott, Introduction to Ionospheric Physics, Academic Press, New York, 1969.

Roederer, J. G., Dynamics of Geomagnetically Trapped Radiation, Springer - Verlag, New York, 1970.

Rosenberg, T. J., J. C. Siren, and L. J. Lanzerotti, "High Time Resolution Riometer and X - ray Measurements of Conjugate Electron Precipitation from the Magnetosphere", *Nature*, Vol. 283, pp. 278-280, January 1980.

Sachs, L., Applied Statistics, Springer - Verlag, New York, 1984.

Schulz, M., and L. J. Lanzerotti, Particle Diffusion in the Radiation Belts, Springer - Verlag, Berlin, 1974.

Shafer, D. C., Trimpi Data System - Software Users Guide, STAR Laboratory, Stanford University, 1988.

Smith, J., Modern Communication Circuits, McGraw - Hill, New York, 1986.

Tolstoy, A., T. J. Rosenberg, and D. L. Carpenter, "The Influence of Localized Precipitation - Induced D - Region Ionization Enhancements on Subionospheric VLF Propagation", *Geophysical Research Letters*, Vol. 9, pp. 563-566, May 1982.

Tolstoy, A., T. J. Rosenberg, U. S. Inan, and D. L. Carpenter, "Model Predictions of Subionospheric VLF Signal Perturbations Resulting from Localized, Electron Precipitation - Induced Ionization Enhancement Regions", *Journal of Geophysical Research*, Vol. 91, pp. 13473-13482, December 1986.

Turtle J. P., E. C. Field, Jr., C. R. Warber, and P. R. McGill, "Low - Frequency Transverse Electric Atmospheric Noise: Measurement and Theory", *Radio Science*, Vol. 24, pp. 325-329, May 1989.

Uman, M. A., Lightning, Dover Publications, New York, 1969.

Uman, M. A., The Lightning Discharge, Academic Press, Orlando, 1987.

Uman, M. A., "Lightning", *Reviews of Geophysics and Space Physics*, Vol. 21, pp. 992-997, June 1983.

Voss, H. D., W. L. Imhof, M. Walt, J. Mobilia, E. E. Gaines, J. B. Reagan, U. S. Inan, R. A. Helliwell, D. L. Carpenter, J. P. Katsufrakis, and H. C. Chang, "Lightning - Induced Electron Precipitation", *Nature*, Vol. 312, pp. 740-742, December 1984.

Wait, J. R. and K. P. Spies, "Characteristics of the Earth - Ionosphere Waveguide for VLF Radio Waves", *NBS Technical Note*, No. 300, U. S. Government Printing Office, Washington, D. C., December 1964.

Wait, J. R., Electromagnetic Waves in Stratified Media, Pergamon Press, Oxford, 1970.

Wait, J. R., "On Phase Changes in Very - Low - Frequency Propagation Induced by an Ionospheric Depression of Finite Extent", *Journal of Geophysical Research*, Vol. 69, pp. 441-445, February 1964.

Wolf, T. G., VLF Phase Receiver Preliminary Operating and Service Manual, STAR Laboratory, Stanford University, 1988.